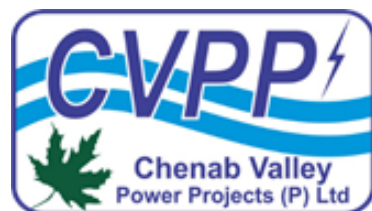




**0390801-INF-BB-LT3.3-0001
FEM ANALYSIS REPORT**

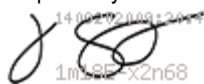
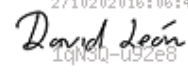


CHANGE CONTROL

MODIFICATION INDEX

Revision	Date	Section Modified	Observations
A	07-07-2020	-	Original Version
B	17-09-2020	3.2.1, 3.2.2, Table 10	Update based on the requests presented in letter no CPP/GM/Design/2020/503 dated 18.08.2020.
C	04-11-2020	5.2, 5.6 and 6.2	Update based on the requests presented in letter no. CVPP/GM/Design/2020/663 dated 14.10.2020

REVIEW AND APPROVAL

TECHNICAL MANAGEMENT	Prepared by:  J. Tello 27.10.2020  D. León 27-10-2020	Reviewed by:  C. Phillips 27.10.2020	Reviewed by:  C. Marulanda E 29-10-2020
	VoBo. Execution Engineer	VoBo. Department Director	VoBo.TM Director

PROJECT	Approved by:  C. Marulanda E 29-09-2020	Approved by:  A. Marulanda E 04-11-2020
	VoBo. Task Manager	VoBo. Project Director

TABLE OF CONTENTS

1. SUMMARY	9
2. BACKGROUND	9
3. INTRODUCTION	10
4. STATIC FINITE ELEMENT ANALYSIS: STRESSES AND DEFORMATIONS IN THE CONCRETE FACE	11
4.1. MECHANISMS INVOLVED IN THE RESPONSE OF THE CONCRETE FACE	11
4.2. MAIN CHARACTERISTICS OF PAKAL DUL CFRD	12
4.3. OTHER CFRD'S WITH THICK OVERBURDEN LAYERS UNDER THE TOE PLINTH	13
4.4. OVERVIEW OF 3D STATIC FE ANALYSIS	14
4.5. GEOMETRY	14
4.5.1. Face-slab thickness	15
4.5.2. Finite element mesh	16
4.6. MATERIALS	18
4.6.1. Rockfill materials	18
4.6.2. Alluvial materials	21
4.6.3. Curb	21
4.6.4. Concrete	22
4.6.5. Reinforcement Steel	24
4.6.6. Foundation	25
4.7. INTERFACES	25
4.7.1. Compressible joints behavior	26
4.8. STAGED CONSTRUCTION AND IMPOUNDMENT	27
4.9. RESULTS AND ANALYSIS OF THREE DIMENSIONAL STATIC ANALYSIS	28
4.9.1. Settlements and construction moduli	28
4.9.2. Deformation of the concrete face under impoundment	29
4.9.3. Stresses and strains in the concrete face	30
4.9.5. Inter-slab and perimeter joint behavior	35
4.9.6. Limitation of crack width	36
4.10. RESULTS INTERPRETATION	40
5. DYNAMIC FINITE ELEMENT ANALYSIS	42
5.1. GEOMETRY	42
5.2. MATERIALS	44
5.2.1. Rockfill material	44
5.2.2. Alluvial deposit	48
5.2.3. Bedrock	50
5.3. MODAL ANALYSIS	50
5.4. DAMPING	51

5.5. BIDIMENSIONAL (2D) MODEL	53
5.5.1. Rockfill damping calibration	54
5.5.2. Accelerations	55
Figure 54. Acceleration time history IT Roorkee input motion - 2D model	57
5.5.3. Permanent deformation due to earthquake	57
5.5.4. Dynamic stability from two dimensional analysis	60
5.6. THREE-DIMENSIONAL (3D) MODEL	62
5.6.1. Acceleration	63
5.6.2. Permanent deformation due to earthquake	65
5.6.3. Dynamic stability from three dimensional analysis	67
6. CONCLUSIONS	70
6.1. STATIC FINITE ELEMENT ANALYSIS	70
6.2. DYNAMIC FINITE ELEMENT ANALYSIS	71
7. REFERENCES	72

LIST OF FIGURES

Figure 1. Vertical projections of various concrete faces from dams around the world.

Figure 2. Assembly for finite element model (exploded view).

Figure 3. Concrete face geometry for finite element model, consisting of 15 m - wide slabs, with thickness varying according to Equation 1

Figure 4. Finite Element Mesh of Pakal Dul CFRD

Figure 5. Finite element mesh of the concrete face

Figure 6. Zonification for Finite Element Analysis

Figure 7. Modified Drucker Prager Cap yield surface. On the vertical axis, t is a measure of deviatoric stress, which reduces to the Von Mises Stress for $K = 1$, where K is the flow stress ratio.

Figure 8. Cap hardening curve for Modified Drucker Prager Cap Model for rockfill material. Material termed $E_{rc} = 70$ MPa corresponds to the best fit to the triaxial test data for the 80 mm Quarry Material. Materials termed $E_{rc} = 120$ MPa and 200 MPa correspond to more compacted materials, necessary to reduce rockfill deformations under impoundment as described in Section 2.9.

Figure 9. Deviatoric stress in MPa vs axial strain for triaxial tests in comparison with the predictions of the Drucker Prager Cap model.

Figure 10. Volumetric strain vs axial strain for triaxial tests comparison with the predictions of the Drucker Prager Cap model for 80 mm quarry material.

Figure 11. Tension/Compression Behavior for Concrete Using Design Strength Parameters from Fib Model Code (see Table 6).

Figure 12. Distribution of reinforcement layers in the slab. Bands 6 and 6 feature two layers of reinforcement, each with nominal cover of 8 cm. In bands 5, 6 and 7, the starting slabs feature the same reinforcement details as each band across the width of the concrete face.

Figure 13. Frictional contact interfaces between concrete face slabs.

Figure 14. Frictional contact interface between articulated plinth and concrete face.

Figure 15. "Softened" pressure-overclosure relationship for considering the effect of a 2 cm layer of wood ($p_0 = 10$ MPa) at the perimeter joint, and rubber ($p_0 = 150$ MPa) for compressible joints

Figure 16. Settlements (m) at the end of construction for rockfill material (Section 2.3.1. Rockfill material), exhibiting a maximum of 1,5 m at an elevation of 1627 m.a.s.l. Section cut through abscisa 0+250.

Figure 17. Concrete face deformation (m) under impoundment.

Figure 18. Stresses in the dam axis direction (horizontal), in MPa on the top and bottom surfaces of the slab. Positive/negative values indicate tension/compression.

Figure 19. Stresses in the direction of the slope on the top and bottom surfaces of the slab. Positive/negative values indicate tension/compression.

Figure 20. Dam axis-wise (total) strains on top and bottom fibers under impoundment to 1700 m.a.s.l.

Figure 21. Slope-wise strains on top and bottom fibers of slab under impoundment to 1700 m.a.s.l.

Figure 22. Status of joints in the concrete face. The majority of joints will be under compression, while those with the potential to open are indicated in the Figure.

Figure 23. Opening of perimeter joint

Figure 24. Uniaxial stresses in the top longitudinal reinforcement layer in bands 6 and 7 (EL. 1559 m.a.s.l to EL. 1604 m.a.s.l.). The small localized grey zone presents stresses of between 60 and 140 MPa.

Figure 25. Uniaxial stresses in the bottom longitudinal reinforcement layer in bands 6 and 7 (EL. 1559 m.a.s.l. to EL. 1604 m.a.s.l.). The small localized grey zone presents stresses of between 60 and 90 MPa. The black region represents stresses between -10 and -76 MPa in compression.

Figure 26. Uniaxial stresses in the bottom longitudinal reinforcement layer in bands 1-5 (EL. 1604 m.a.s.l. to EL. 1704 m.a.s.l.). The small localized grey zone presents stresses of between 60 and 90 MPa. The black region represents stresses between -10 and -97 MPa in compression.

Figure 27. Uniaxial stresses in the top axial reinforcement layer in bands 6-7 (EL. 1559 m.a.s.l. to EL. 1604 m.a.s.l.). The grey zones represent stresses between 60 MPa and 83 MPa while the black region represents stresses of between -50 and -197 MPa in compression.

Figure 28. Uniaxial stresses in the bottom axial reinforcement layer in bands 6-7 (EL. 1559 m.a.s.l. to EL. 1604 m.a.s.l.). The grey zones represent local regions of tensile stresses of between 60 and 149 MPa while the black zones represent regions of between -50 and -182 MPa in compression.

Figure 29. Uniaxial stresses in the single axial reinforcement layer in bands 1-5 (EL. 1604 m.a.s.l. to EL. 1704 m.a.s.l.).

Figure 30. Dynamic model geometry

Figure 31. Dynamic model - Mesh

Figure 32. Mesh detail - Alluvial deposit and rockfill

Figure 33. Strain-stress relationship in a triaxial compression test with the modified Mohr-Coulomb model

Figure 34. Stress-strain-volume change of 25 mm Quarry, Modified Mohr-Coulomb (MMC) model.

Figure 35. Stress-strain-volume change of 50 mm Quarry, Modified Mohr-Coulomb (MMC) model.

Figure 36. Stress-strain-volume change of 80 mm Quarry, Modified Mohr-Coulomb (MMC) model.

Figure 37. Predicted stress-strain-volume change behavior of Pakal Dul CFRD quarry rockfill material ($\sigma_3 = 1,2$ MPa)

Figure 38. Shear velocity profile for the alluvial deposit.

Figure 39. Reference shear modulus reduction and damping ratio curves

Figure 40. Main vibration modes of the Pakal Dul Dam.

Figure 41. Fourier transform of Chamoli signal and Rayleigh damping.

Figure 42. Fourier transform of Chi-Chi Ila signal and Rayleigh damping

Figure 43. Fourier transform of Uttarkashi signal and Rayleigh damping

Figure 44. Finite element mesh used in the analyses.

Figure 45. Construction settlement - Bidimensional dynamic model.

Figure 46. Rockfill damping ratio - Sensitive analysis.

Figure 47. Acceleration time history Chamoli input motion, 2D model

Figure 48. Acceleration time history Chi-Chi Ila input motion, 2D model

Figure 49. Acceleration time history Uttarkashi input motion, 2D model

Figure 50. Total displacement at the end of the dynamic analysis, 2D analysis.

Figure 51. Crest displacement time history Chamoli input motion, 2D model

Figure 52. Crest displacement time history Chi-Chi Ila input motion, 2D model

Figure 53. Crest displacement time history Uttarkashi input motion, 2D model

Figure 54. Displacement (upstream-downstream direction) for different Strength Reduction factors (SRF).

Figure 55. Evolution of the crest displacement with the Shear Strength Reduction (SRF) - 2D model

Figure 56. Construction settlement - 3D Dynamic model.

Figure 57. Acceleration time history - Rock and alluvial deposit - 3D model

Figure 58. Acceleration time history - Dam crest - 3D mode

Figure 59. Total displacement at the end of the seismic analysis Chamoli signal - 3D model

Figure 60. Permanent crest settlement at the end of the seismic analysis.

Figure 61. Crest displacement time history Chamoli signal - 3D model

Figure 62. Displacement (upstream-downstream direction) for different SRF - 3D model

Figure 63. Evolution of the displacement in the crest and the downstream slope with the SRF - 3D model

LIST OF TABLES

- Table 1. Geometric characteristics of various Concrete Face Rockfill Dams around the world.
- Table 2. Main characteristics of various Concrete Face Rockfill Dams with thick overburden layers (Zhongzhi Fu, 2018)
- Table 3. Material parameters for rockfill material calibrated to quarry material with 80 mm size.
- Table 4. Material properties for curb.
- Table 5. Fib Model Code 2010 recommendations for material properties for nonlinear concrete behavior
- Table 6. Values of strength and moduli for 21 MPa concrete according to Fib Model Code 2010.
- Table 7. Friction coefficient of the various contact interfaces.
- Table 8. Approximate vertical rockfill moduli of the zones of Pakal Dul Dam (see Figure 6)
- Table 9. Main parameters of the Modified Mohr-Coulomb model.
- Table 10. Predicted material parameters of Modified Mohr-Coulomb model Quarry material.
- Table 11. Elastic parameter alluvial layers
- Table 12. Natural periods for the main vibration modes.
- Table 13. Maximum permanent displacement in the Makdisi & Seed analysis. Document No:
0390801-INF-BB-LT3.2-0001 - Static & Dynamic Stability and seismic induced deformations of the CFRD Dam - Report

1. SUMMARY



This report contains the static and dynamic finite element analysis of the Pakal Dul CFRD, including the alluvial deposit in the models as well as the non-linear behavior of concrete together with acceptance criteria following Fib Model Code 2010 (Federation Internationale du Beton, 2010) and Guidelines for Nonlinear Finite Element Analysis of Concrete Structures (RCI, 2017).

The results of the numerical analysis serve as input for the geotechnical and structural designs of the CFRD as well as to validate some analytical approximations. By evaluating several design alternatives and material parameters, various solutions have been implemented, improving the overall behavior of the CFRD for both static and dynamic (seismic) design scenarios.

2. BACKGROUND

Concrete-Face-Rockfill-Dams, or CFRD's, offer many technical and economical advantages over other dam types because they are adaptable to a wide variety of geological conditions. Usually, ideal dam sites for CFRD's offer the possibility of supporting the lower portion of the plinth directly on rock, which is advantageous from the point of view of the deformation of the concrete face under the impoundment of the reservoir. However, many potential sites feature thick overburden layers under the horizontal plinth, known as the articulated plinth, which because of technical or economic restrictions cannot be excavated, thus requiring that the lower plinth be supported on a deformable layer of material (Zhongzhi Fu, 2018). This poses many challenges for the design of the concrete face and articulated plinth, which are analyzed in detail using the finite element model presented herein.

Furthermore, recent incidents involving cracking of the concrete face during first impoundment have raised concerns about the safety of building increasingly taller Concrete Face Concrete Dams. These include the Mohale dam in Lesotho, and Barra Grande and Campos Novos dams in Brazil, the latter being one of the tallest dams of its type in the world (202 m). The type of failure observed in many dams includes evidence of compressive damage, including buckling of the reinforcement and concrete spalling (Modares and Quiroz, 2015).

The design and development of concrete face rockfill dams has historically been based primarily on precedent and empiricism; however these incidents have demonstrated that merely extrapolating current practices to new conditions can lead to serious unforeseen consequences, which may include reservoir dewatering in order to allow for repairs to take place.

Recent advances in computational capabilities, coupled with the development and implementation of rigorous modeling techniques have led to the application of numerical models such as the finite element method to the design and analysis of CFRD's, and indeed other types of dams around the world.

3. INTRODUCTION

This report describes the three-dimensional numerical model of the Pakal Dul CFRD, intended to analyze the behavior of the dam and concrete face during construction and first impoundment, as well as seismic excitation. The methodology has been developed by INGETEC over a decade of experience and has consistently reproduced various aspects of the behavior observed in different dams around the world, including (1) Antamina in Peru, (2) Cethana in Australia, (3) Golillas in Colombia, (4) Campos Novos in Brazil, (5) Barra Grande in Brazil, (6) Cajón in Mexico, (7) Mohale in Lesotho, (8) La Yesca in Mexico, (9) Sogamoso in Colombia, and (10) Quimbo in Colombia. Satisfactory comparisons between measurements and model results, in addition to enriching the methodology, lend weight to it as a rational and robust tool for the analysis of concrete Face Concrete Dams

CFRD's tend to behave well under seismic excitation because the body of the dam is kept dry and the earthquake does not generate pore pressures and the associated degradation of the resistance in the rockfill. Additionally, the reservoir exerts a pressure on the entire surface of the concrete face, which stabilizes the body by increasing its confinement.

However, the effect of seismic events on CFRD is a topic of current research interest, since few dams of this type have been subjected to design loads and the vast majority of them have been built in areas of low seismic activity, so that only a few cases are suitable for detailed dynamic analysis and verification. A notable recent exception is that of the Zipingpu dam located in the Sichuan region in China, with about 156 m in height and 663,8 m in crest length. On May 12, 2008, ground accelerations induced by the 2008 Wenchuan earthquake, the epicenter of which was only 17 km from the dam, reached 0,5 g, considerably exceeding the accelerations at the rock level considered in the design (0,26 g) (Degao Zou, 2013). This allowed for the first time for the evaluation of the behavior of this type of structure under such a high level of acceleration. One of the findings was that the stability of the dam was never compromised. As a consequence of sustaining this acceleration, the dam crest suffered settlements reaching 1 m causing damage to the parapet wall and concrete facing. However, this case shows the capacity of CFRD to resist a considerable seismic acceleration without its stability being compromised. Moreover, with the computational capacity currently available, analyses can be carried out to evaluate the general behavior of this type of dam.

Dynamic behavior of CFRDs is influenced by a series of factors, such as the density and quality of the fill, the geometry of the dam, the shape of the canyon, the characteristics of the joints between slabs and plinth, concrete reinforcement, and the characteristics of the earthquake such as duration, frequency content and amplitude.

This report is divided into the following Chapters:

Chapter 3. Presents the general scope and the contents of this report.

Chapter 4. Describes the finite element static model; which includes the geometry of the dam with its boundary conditions, the constitutive models, the considered interfaces and the construction sequence. The analyses and results of the prediction of the dam behavior using the finite element model

Chapter 5. Presents the methodology, assumptions and results of two and three dimensional finite element models developed in order to assess the behavior of the CFRD to dynamic loading scenarios (behavior of the dam due to the Maximum Credible Earthquake occurrence).

Chapter 6. This Chapter presents the conclusions and recommendations regarding the numerical analyses developed.

Chapter 7. Presents the list of references.

4. STATIC FINITE ELEMENT ANALYSIS: STRESSES AND DEFORMATIONS IN THE CONCRETE FACE

4.1. MECHANISMS INVOLVED IN THE RESPONSE OF THE CONCRETE FACE

Due to their high slenderness, the slabs of the concrete face of a rock fill dam behave essentially like membranes under the action of the hydrostatic load. Hence, the tensile, compressive, and bending stresses that develop in it are primarily due to the deformation of the dam fill; that is, its state is deformation-controlled rather than load-controlled. This implies that the slab deformation is independent of the concrete material properties and reinforcement details, being strongly influenced by rockfill moduli and other geometric aspects.

Additionally, concrete can also expand or contract due to temperature changes, which are usually monitored specifically in order to account for these effects. The design of a concrete face must consider all the mechanisms that contribute to the development of these stresses, including friction and separation between the curb and the concrete face, and the three-dimensional deformation that the concrete face undergoes during construction and filling of the reservoir.

However, due to the scarcity of analytical solutions that include all these mechanisms and until recently, the absence of computational tools capable of considering all mechanisms acting on the slab, the design of concrete faces has been based traditionally on empirical methods and rules of thumb. A reflection of this trend is the determination of the thickness of the concrete slabs which is essentially based on precedent. The thickness of the concrete face has usually been determined based on the reservoir pressure, initially through the formula $t = 0,30 + 0,003H$; in some cases $t = 0,30 + 0,002H$ has been used and even in dams with heights less than 120 m concrete faces have been designed with the formula $t = 0,30 + 0,001H$, where t is the thickness of the slabs and H is the height of the reservoir in meters. Additionally, in the designs of CFRD's, reinforcement amounts of the order of 0,5% have been used, but over time it has decreased to 0,4% and even to 0,3%.

The recent trend to reduce costs in dams of considerable height (> 150 m) includes the elimination of "anti-spalling" reinforcement in compression joints, additional reductions in the thickness of concrete slabs, and in areas of low seismicity the slopes have been increased to $1,30H: 1,0V$ and $1,35H: 1,0V$, even in high-rise dams. In the last decades, there has been a considerable increase in the height of concrete face rockfill dams. This has been possible, considering that after the construction of the Aguamilpa dam (187 m high) there would be no problem in increasing the height of a rockfill dam. However, it must be emphasized that Aguamilpa is a gravel dam, with significantly smaller deformations than are expected in a rockfill dam and that merely extrapolation of existing precedent has sometimes been shown to be inadequate. It is essential that the designs of CFRD's, and especially in the cases where extrapolation is being made on existing precedent, be complemented with numerical tools that can estimate the behavior of the different components, especially the prediction of slab deformations, stresses, and strains.

Even though the slab deformation is primarily controlled by the rockfill, this is only true in the direction perpendicular to the face, and it is important to account for sliding between the two bodies. The load transfer mechanism from the rock to the slab is that of friction at the interface, which depends on the characteristics of the contact. The maximum load that can be transferred by friction depends on the normal pressure acting on the contact and the coefficient of friction that characterizes the roughness of the contact and the materials involved. When the maximum shear stress is exceeded a slip occurs between the two bodies and no greater load is transmitted.

In addition to the stresses in the slab transferred by friction, bending stresses develop in the slabs mainly due to the irregular shape of the foundation behind it. On the other hand, the geometric configuration of the slab, supported on an inclined slope and in some cases on narrow canyons, involves the generation of compressive forces mainly due to the

transfer of loads due to self-weight. In the case of the application of the hydrostatic load, the face undergoes a deformation that involves primarily compression of the central area and tension on towards its perimeter, the latter represented in the opening of the perimeter joints.

In order to consider the effect of the development of the aforementioned stresses, a detailed numerical model must be developed with the ability to incorporate the different mechanisms that generate the stresses induced by movements of the concrete face in response to settlements of the fill by its own weight and by the hydrostatic load of the reservoir. The details of the model are described in the following section. It is important to mention that a numerical analysis of a concrete face rockfill dam can give a general idea and highlight important aspects of its behavior, providing approximate values of the different variables (stresses, strains and deformations), however it would be unrealistic to expect exact results from a numerical model for such a complex system.

4.2. MAIN CHARACTERISTICS OF PAKAL DUL CFRD

Pakal Dul CFRD has a height of 184 m with a proposed 1,40 H : 1,0 V upstream slope and an overall 1,5 H : 1,0 V downstream slope. The concrete face features a height of 148 m from the parapet wall to the toe plinth, a total area of 57100 m² and a 688 m perimeter and consists of 21 reinforced concrete slabs 15 m wide and of variable thickness placed on the extruded concrete curb which in turn is placed on the granular filling of the dam. The concrete face slab reaches laterally towards the abutments or plinth slabs, towards the top with the parapet wall and at the bottom with the articulated plinth. The theoretical thickness of the slab was taken to be 0,30 m at the top and varies uniformly up to 0,73 m.

The hydrostatic load produced by the reservoir is transmitted to the slabs on the concrete face, which follow the deformations of the dam fill and are supported by friction on the contact surface.

The observation of the behavior of rockfill dams has identified two key parameters that are useful for categorizing their behavior: the canyon form factor and the rockfill compressibility. Traditionally the dimensionless factor L / H was used to describe the geometry of the canyon, where L is the length of the crest and H the height of the dam. This type of relationship does not incorporate the shape of the canyon, a variable that has been shown to affect the stresses on the concrete face. In order to carry out a more detailed characterization of the canyon shape, the dimensionless factor A / H^2 has been used, where A is the area of the concrete face and H is the height of the dam. As the canyon becomes narrower, the A / H^2 factor decreases. A dam with an A / H^2 factor of the order of 3,5 or greater can be considered wide.

In order to compare the shape of the canyon and the height of different dams with similar characteristics to the Pakal Dul dam, Figure 1 shows the vertical projection of several concrete faces for different dams made of gravel or rock around the world. The dimensionless A / H^2 factor for the Pakal Dul Hydroelectric Project dam is 2,6, which indicates that the canyon is narrow. Table 1 features the general geometric characteristics of these dams for reference.

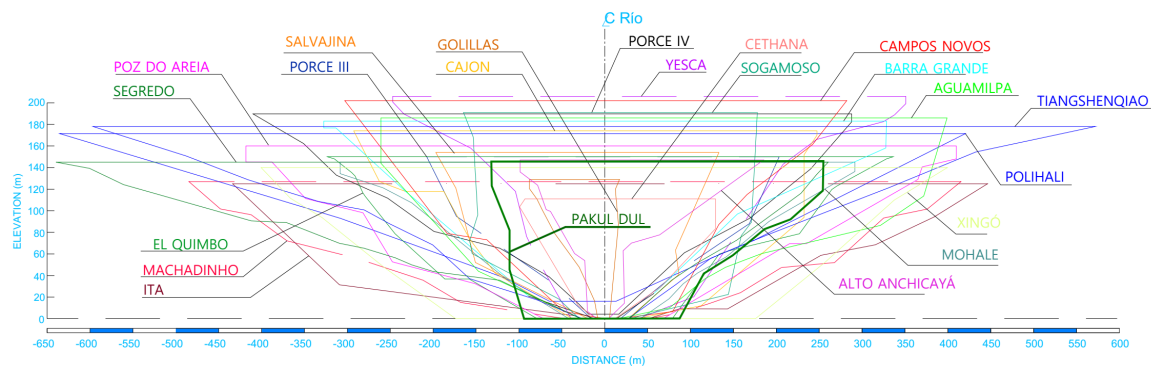


Figure 1. Vertical projections of various concrete faces from dams around the world.

Table 1. Geometric characteristics of various Concrete Face Rockfill Dams around the world.

DAM NAME	COUNTRY	YEAR	HEIGHT (m)	CREST WIDTH (m)	W/H	FACE AREA (m ²)	A/H ²
Cethana	AUSTRALIA	1971	111	222	1,94	25 000	2,03
Alto Anchicayá	COLOMBIA	1974	147	260	1,77	31 000	1,43
Golillas	COLOMBIA	1978	129	105	0,81	17 000	1,02
Areia	BRASIL	1980	160	828	5,18	139 000	5,43
Salvajina	MEXICO	1984	154	330	2,14	63 000	2,66
Aguamilpa	MEXICO	1993	186	660	3,55	130 000	3,75
Xingó	BRAZIL	1994	140	800	5,71	135 000	6,89
Segredo	BRAZIL	1992	145	900	6,21	86 000	4,09
Machadinho	BRAZIL	2002	127	935	7,40	93 000	5,77
Itá	BRASIL	1999	125	880	7,04	110 000	7,04
Tiangshenqiao	CHINA	1997	178	1168	6,56	180 000	5,68
Porce III	COLOMBIA	2011	150	410	1,19	54 000	2,40
Sogamoso	COLOMBIA	2014	191	345	1,81	75 000	2,06
Campos Novos	BRAZIL	2001	202	585	2,90	105 000	2,57
Barra Grande	BRAZIL	2005	185	656	3,55	108 000	3,16
Cajon	MEXICO	2007	174	540	3,10	177 000	5,85
Mohale	LESOTHO	2004	145	600	4,14	145 000	6,90
La Yesca	MEXICO	2012	201	572	2,85	94 000	2,30

4.3. OTHER CFRD'S WITH THICK OVERTURDEN LAYERS UNDER THE TOE PLINTH

Not many Concrete Face Rockfill Dams with thick overburden layers have been built or documented to date. Table 2 shows a list of those that have been found in the literature in comparison with the Pakal Dul dam, which notably is the highest among them. The fact that Pakal Dul dam will be one of the highest CFRD constructed over an alluvial deposit constitutes another element that reaffirms the need to develop numerical analyses including the overburden effects at the CFRD foundation in order to assess the behavior of the dam in terms of induced deformations and stresses.

Table 2. Main characteristics of various Concrete Face Rockfill Dams with thick overburden layers (Zhongzhi Fu, 2018)

Name	Construction Year	Country	Height (m)	Overburden thickness (m)	Cutoff wall	
					Thickness (m)	Height (m)
Pakal Dul	-	India	184	56	1	
Aertash	-	China	164.8	94	1.2	90
Jiudianxia	2008	China	136.5	56	1.2	30
Duonguo	2012	China	112.5	40	1.2	35
Miaojiaba	2011	China	111	48	1.2	41.5
Chahanwusu	2008	China	110	47	1.2	41.8
Nalan	2006	China	109	24	0.8	18
Xieka	2014	China	108.2	100	1.2	86
Laodukou	2009	China	96.8	30	0.8	29.6

4.4. OVERVIEW OF 3D STATIC FE ANALYSIS

The static three-dimensional finite element analysis of the Pakal Dul CFRD is intended to provide an estimate of the deformations and stresses of the dam and concrete face during construction and impoundment, as well as to inform the design of the concrete face and foundation excavation by determining the impact of various alternatives on the resulting stresses and deformations. The model has been developed in Abaqus CAE, and consists of the following components:

- Dam body
- Curb
- Concrete face
- Plinth
- Alluvial Deposit
- Parapet Wall

The following sections describe the process of geometry development, material calibration, boundary conditions and construction sequence considerations as well as results regarding face-slab stresses and deformations, joint openings, among others.

4.5. GEOMETRY

The assembly for the finite element model is shown in Figure 2. In order to represent frictional behavior between the concrete face and plinth, concrete face and curb, as well as between the dam fill and the foundation, separate finite element meshes must be generated in each of these components so as to be able to generate surfaces that may slide and separate from one another if the applied forces so dictate. Each slab in the concrete face is also an independent body, capable of interacting with its neighboring components in like manner.

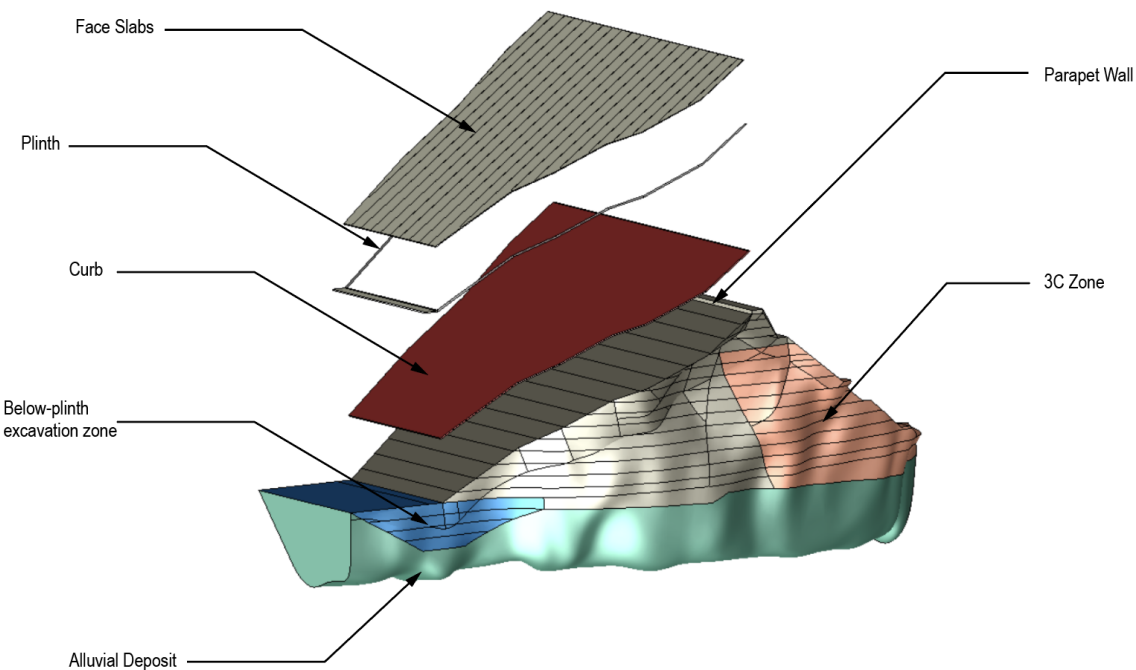


Figure 2. Assembly for finite element model (exploded view).

4.5.1. Face-slab thickness

As described before the thickness of the concrete slab has been modeled implementing a theoretical thickness of the slab to be 0,30 m at the top and varying uniformly up to 73,2 cm as described by the following equation:

$$t = 0,30 + 0,003 H.$$

Equation 1.

Here, H is the depth from the top of the slab to the point in question and t is the concrete slab thickness. Both t and H are given in meters.

B

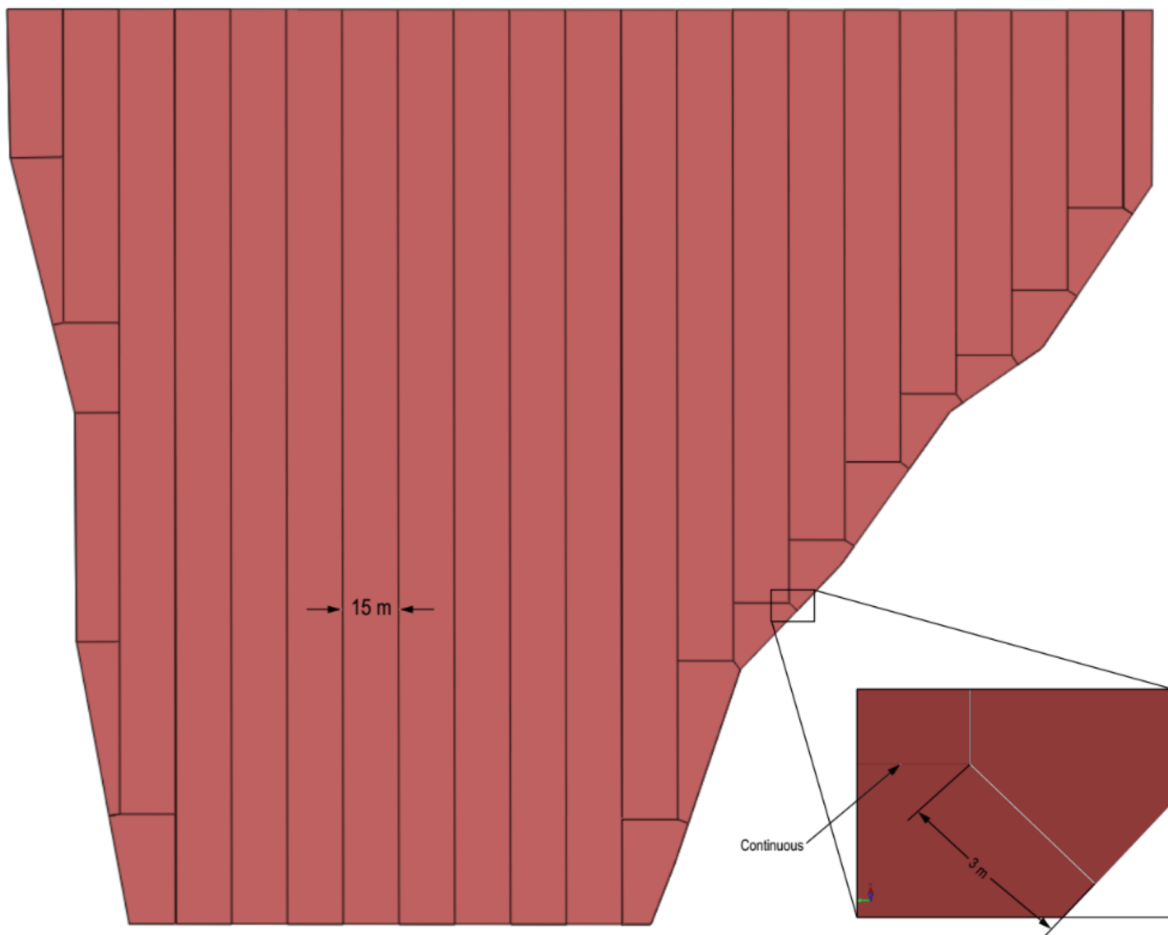


Figure 3. Concrete face geometry for finite element model, consisting of 15 m - wide slabs, with thickness varying according to Equation 1

4.5.2. Finite element mesh

The mesh consists of 118 000 elements and 77 000 nodes. The dam body is meshed with tetrahedra of type C3D4, whereas the concrete face is meshed with improved surface stress visualization elements, which provide accurate stresses on the top an bottom fibers of the slabs since it features integration points on the element faces, as opposed to regular integration elements whose integration points are located inside the elements.

The steel reinforcement is modeled by means of smeared rebar layers carried by surface elements which are embedded in the host solid elements of the slabs.

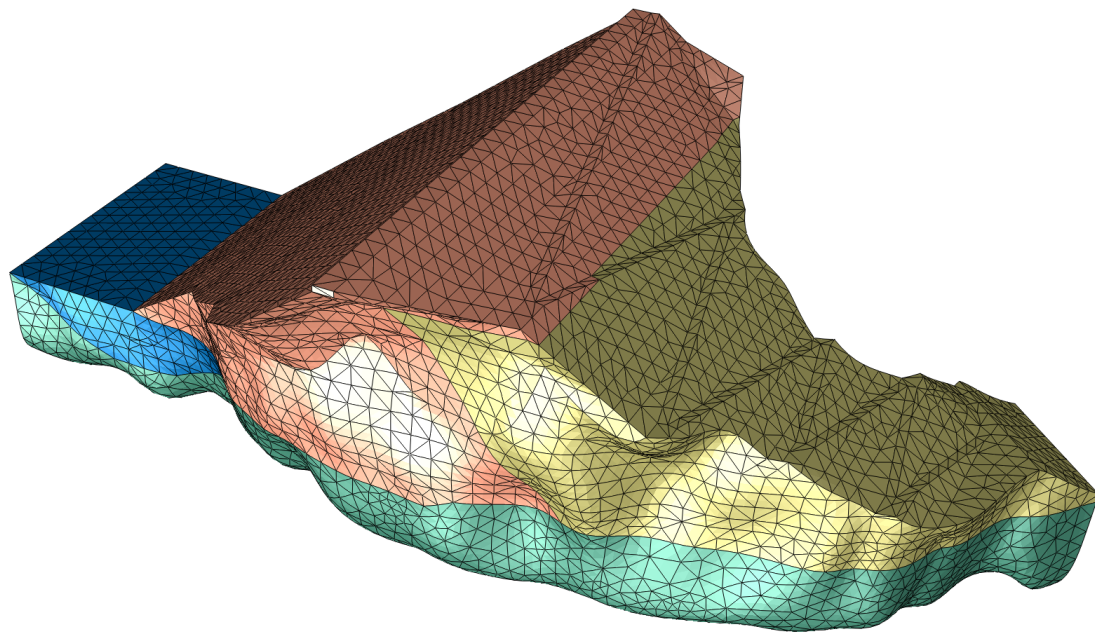


Figure 4. Finite Element Mesh of Pakal Dul CFRD



Figure 5. Finite element mesh of the concrete face

4.6. MATERIALS

B

In order to limit the deformation of the concrete face, the materials that directly support the articulated plinth, as well as the curb (Material 3B) should be properly compacted so as to achieve the required settlements during construction and hence avoid subsequent excessive deformation of the slabs. Figure 6 presents the dam zoning utilized in the numerical model as defined in document 0390801-INF-BB-LT3.2-0003 [GRADING MATERIAL IN DIFFERENT ZONES, GEOMETRY OF CFRD AND ZONING REPORT, INGETEC (2020)].

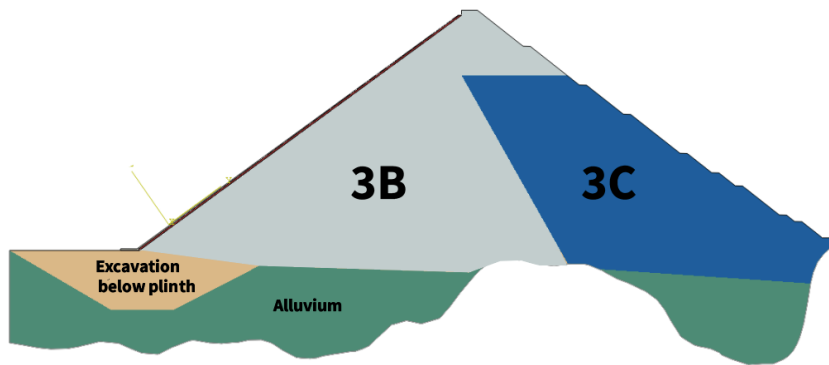


Figure 6. Zonification for Finite Element Analysis

4.6.1. Rockfill materials

The rockfill material is modeled by means of the Modified Drucker Prager/Cap constitutive model available in Abaqus (Simulia, 2020). The model features a yield surface consisting of a shear failure surface where deviatoric stresses induce plastic flow, and a cap surface, where hydrostatic stresses lead to plastic compaction. A typical yield surface can be seen in Figure 7.

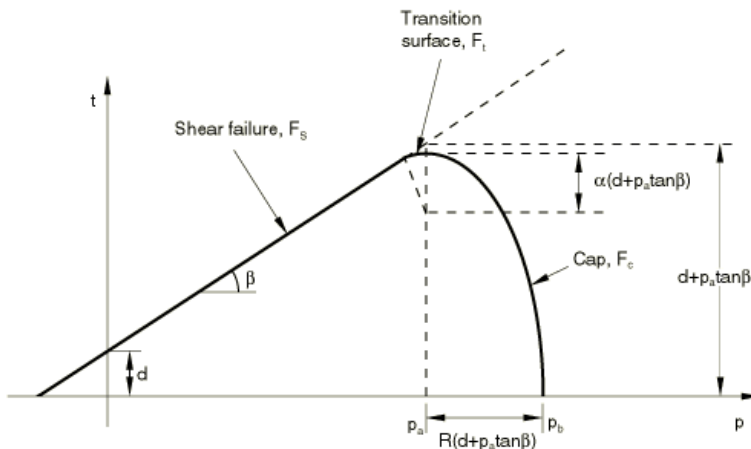


Figure 7. Modified Drucker Prager Cap yield surface. On the vertical axis, t is a measure of deviatoric stress, which reduces to the Von Mises Stress for $K = 1$, where K is the flow stress ratio.

Table 3 presents the material parameters calibrated for the 80 mm size quarry material using laboratory test results provided by CVPP. The results of the calibration process (numerical model and laboratory test results comparison) are presented in Figure 8 to Figure 10.

Table 3. Material parameters for rockfill material calibrated to quarry material with 80 mm size (to be used in zone 3C only)

Property	Value
Density	2,0 ton/m ³
Young's Modulus	35 - 180 MPa
Poisson's Ratio	0,3
Material Cohesion	0,001 MPa
Drucker-Prager Parameter (β)	61 ¹
Cap Eccentricity (R)	0,45
Transition Surface Radius (α)	0

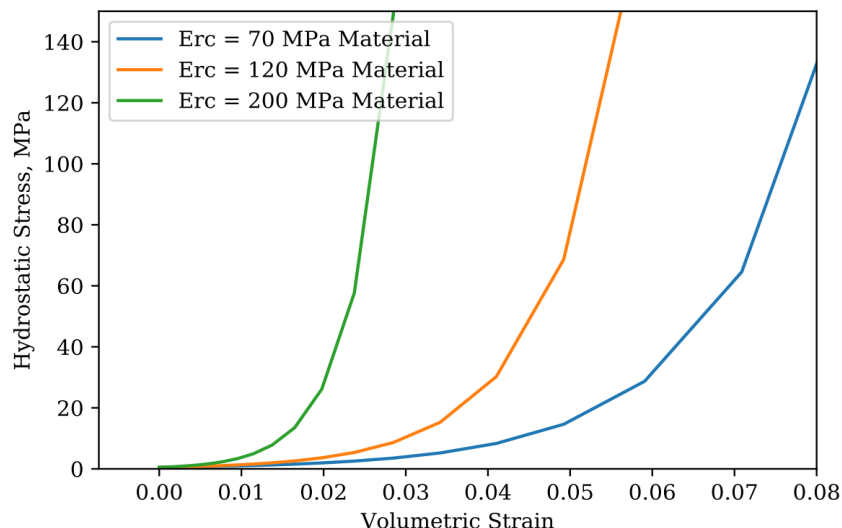


Figure 8. Cap hardening curve for Modified Drucker Prager Cap Model for rockfill material. Material termed $E_{rc} = 70$ MPa corresponds to the best fit to the triaxial test data for the 80 mm Quarry Material shown in . Materials termed $E_{rc} = 120$ MPa and $E_{rc} = 200$ MPa correspond to more compacted materials, necessary to reduce rockfill deformations under impoundment as described in Section 2.9.

Precedent regarding the behavior of rockfills have shown that if the quarried rock to produce the rockfill material is stiff and strong (as the case of Pakal Dul) and gradation, layer thickness and compaction recommendations are followed,

¹ Equivalent to a Mohr-Coulomb friction angle of 44° (Simulia 2020).

construction modulus equal or higher than 120 MPa should be achieved. The fill for the projected excavation at the upstream zone of the CFRD is recommended to have a gradation comprised mainly by alluvial gravels which should result in a construction modulus equal or higher than 200 MPa. Since the actual construction moduli for zones 3B and 3C and the fill for the projected excavation at the upstream zone should correspond to a stiffer material behavior than that observed in the triaxial tests, the values of 70, 120, and 200 MPa constitute conservative estimates and should be validated using the test embankment results.

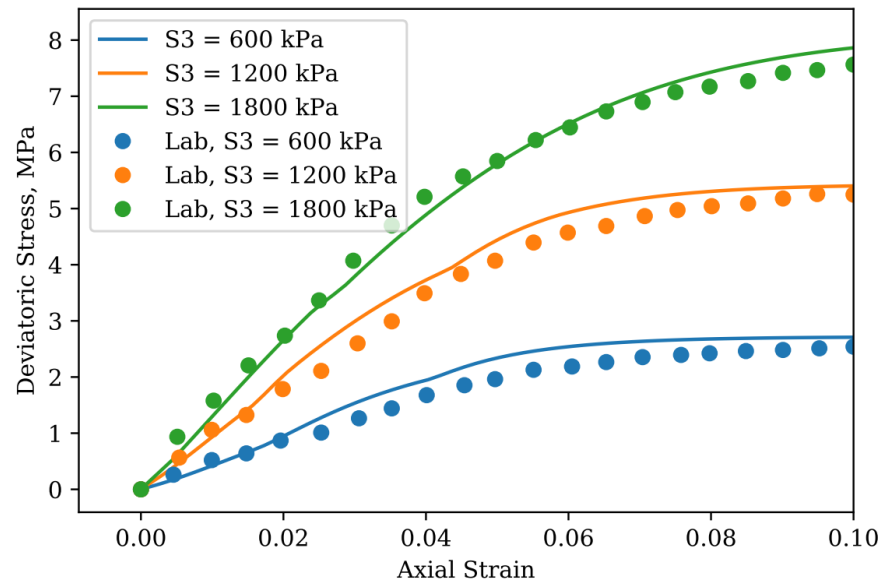


Figure 9. Deviatoric stress in MPa vs axial strain for triaxial tests in comparison with the predictions of the Drucker Prager Cap model.

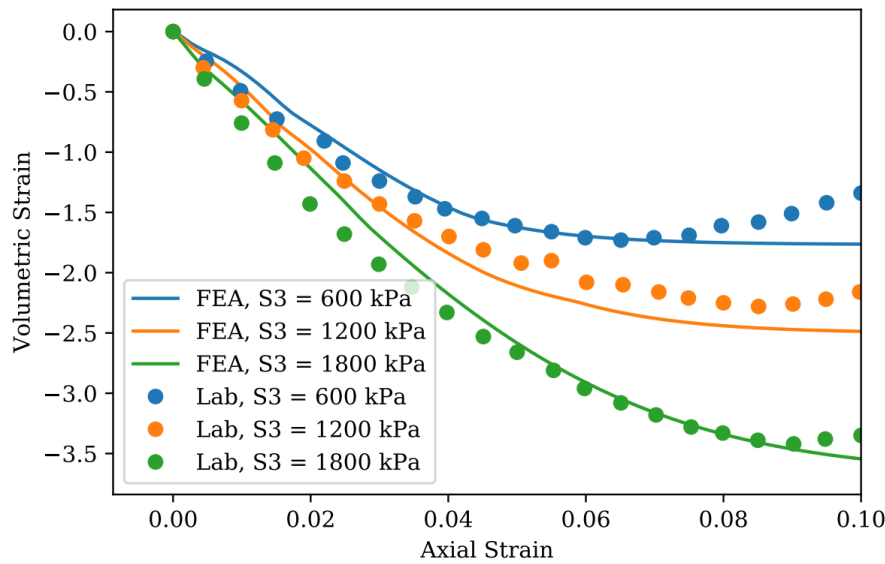


Figure 10. Volumetric strain vs axial strain for triaxial tests comparison with the predictions of the Drucker Prager Cap model for 80 mm quarry material.



It must be noted that while the Geotechnical Parameters Report establishes numerical values for the parameters corresponding to the large scale triaxial tests performed on various particle sizes of quarry material, the finite element analysis has identified the need for stiffer rockfill materials than those tested, both in the zone below the toe plinth as well as the upstream shell (Zone 3B).

4.6.2. Alluvial materials

Alluvial materials will comprise the foundation of the dam rockfill in the central part of the river canyon, due to its disposition and configuration, expected shear strains for these materials during construction and impoundment are projected to be small. Therefore, the alluvial deposit is modeled by means of a linear elastic isotropic constitutive model since its stiffness will remain approximately constant over the expected strain ranges.

Young's modulus for the alluvial deposit has been determined based on the seismic cross section AA located 20 m upstream of the plinth axis (NHPC Limited, 2005) and the MASW geophysical test performed near the plinth (NHPC Limited, 2018).

Based on the geophysical testing results it is concluded that a representative alluvial deposit profile will be comprised by the upper 7 m thick riverborne layer with average shear wave velocity of 450 m/s and a 26 m thick silty sand layer with average shear wave velocity of 350 m/s. Below these two layers a series of very stiff materials classified either as riverborne or silty sands have been encountered.

An average shear wave velocity of 370 m/s has been estimated to characterize the alluvial deposit taking into account the upper two layers; deeper layers not being included in the estimation due to the fact that these exhibit very high stiffness (high shear wave velocities) and therefore the impact in terms of deformability of these layers is not significant to the overall behavior of the dam. Using the average shear wave velocity value of 375 m/s and an unit weight of 1700 kg/m³ a maximum shear modulus of 234 MPa has been calculated. In order to take into account the small strain degradation a 0,65 reduction modulus factor was applied, obtaining a representative shear modulus of 152 MPa for the alluvial deposit, which using isotropic linear elastic constitutive relationships corresponds to a 400 MPa Young's Modulus.

4.6.3. Curb

The curb has an almost negligible impact on the mechanical behavior of the dam, but within the context of the FE model it serves an important role as a geometry that fills the gap between the concrete face and the rockfill, which at the moment of constructing the slab, has deformed from its original configuration due to the sequential placement of layers of material on one another and the resulting deformations at the upstream face. Hence, the curb serves to provide a flat surface upon which the concrete face may rest, developing contact pressures and shear stresses that help establish its equilibrium prior to impoundment.

Table 4. Material properties for curb.

Property	Value
Density	2,3 ton/m ³
Elastic Modulus	8 GPa
Poisson's Ratio	0,30

4.6.4. Concrete

The Structural design of the concrete face specifies a material with characteristic cylinder compressive strength of $f_{ck} = 25$ MPa. The properties required for a nonlinear finite element analysis according to Fib Model Code 2010 (Fib 2010).

Fib Model Code (Fib 2010) provides material parameters for C25 concrete shown in Table 5.

Table 5. Fib Model Code 2010 recommendations for material properties for nonlinear concrete behavior

Parameter (Model Code 2010)	
Characteristic cylinder compressive strength	f_{ck}
Mean compressive strength	$f_{cm} = f_{ck} + \Delta f$
Design compressive strength	$f_{cd} = \alpha_{cc} \frac{f_{ck}}{\gamma_c}$
Minimum reduction factor of compressive strength due to lateral cracking	$\beta_\sigma^{\min} = 0.4; \beta \geq \beta_\sigma^{\min}$ (40% of the strength remains)
Lower-bound characteristic tensile strength	$f_{ctk,min} = 0.7 f_{ctm}$
Mean tensile strength (for ≤ C50)	$f_{ctm} = 0.3 f_{ck}^{2/3}$
Design tensile strength	$f_{ctd} = \frac{f_{ctk,min}}{\gamma_c}$
Fracture energy	$G_F = 73 f_{cm}^{0.18}$
Compressive fracture energy, (Nakamura and Higai, 2001)	$G_C = 250 G_F$
Young's modulus after 28 days	$E_{ci} = E_{c0} \left(\frac{f_{cm}}{10} \right)^{1/3}$
(Initial) Poisson ratio	$\nu = 0.15$
Density plain concrete	$\rho = 2400 \text{ kg/m}^3$
Density reinforced concrete	$\rho = 2500 \text{ kg/m}^3$
Concrete safety coefficient	$\gamma_c = 1.5$
Long term effect coefficient	$0.8 < \alpha_{cc} < 1$

The obtained strength and moduli values for C25 concrete are shown in Table 6 below.

Table 6. Values of strength and moduli for concrete according to Fib Model Code 2010.

Characteristic Cylinder Compressive Strength: (f_ck)	25	MPa
Mean Comp Strength (f_cm)	33	MPa
Mean Comp Strength GRF(f_cm)	21.25	MPa
Mean Tensile Strength (f_ctm)	2.56	MPa
Mean Tensile Strength GRF (f_ctm)	2.3	MPa
Lower-bound characteristic tens. strength (f_ctkmin):	1.8	MPa
Design compressive strength (f_cd):	15.0	MPa
Design Tensile Strength (f_ctd):	1.2	MPa
Initial Elastic modulus after 28 days (E_ci):	32009.0	MPa
Reduced Youngs modulus (E_c):	27208.0	MPa

Concrete damaged plasticity

The nonlinear material behavior of the concrete in the slabs is modeled by means of the Concrete damaged plasticity model in Abaqus.

The model keeps track of internal stiffness degradation through the concept of isotropic damaged elasticity and considers the inelastic behavior of concrete though isotropic tensile and compressive plasticity. The slabs themselves are reinforced with rebar layers that are embedded in the host concrete.

The model considers two failure mechanisms: tensile cracking and compressive crushing.

The elastic modulus is degraded in response to the accumulation of damage, d_t and d_c through

$$E_t = (1 - d_t) E_0$$

$$E_c = (1 - d_c) E_0$$

in tension and compression, respectively.

The stress-strain behavior follows from the scalar damage elasticity equation:

$$\sigma = (1 - d) \mathbf{D}_0^{el} : (\boldsymbol{\varepsilon} - \boldsymbol{\varepsilon}^{pl})$$

The model can be used to describe the cyclic behavior of concrete, although during impoundment the loading is monotonic.

Further details of the theoretical formulation may be found in “Damaged plasticity model for concrete and other quasi-brittle materials” in the Abaqus documentation (Simulia, 2020).

Figure 11 presents the combined tension/compression nonlinear stress-strain behavior adopted for the concrete face implementing Fib Model Code recommendations for C25 concrete for use in the Ultimate Limit State verification through the Global Resistance Factor method. For Serviceability Limit State verification of crack widths, a similar curve is used, only with characteristic values of resistance (Fib, 2020).

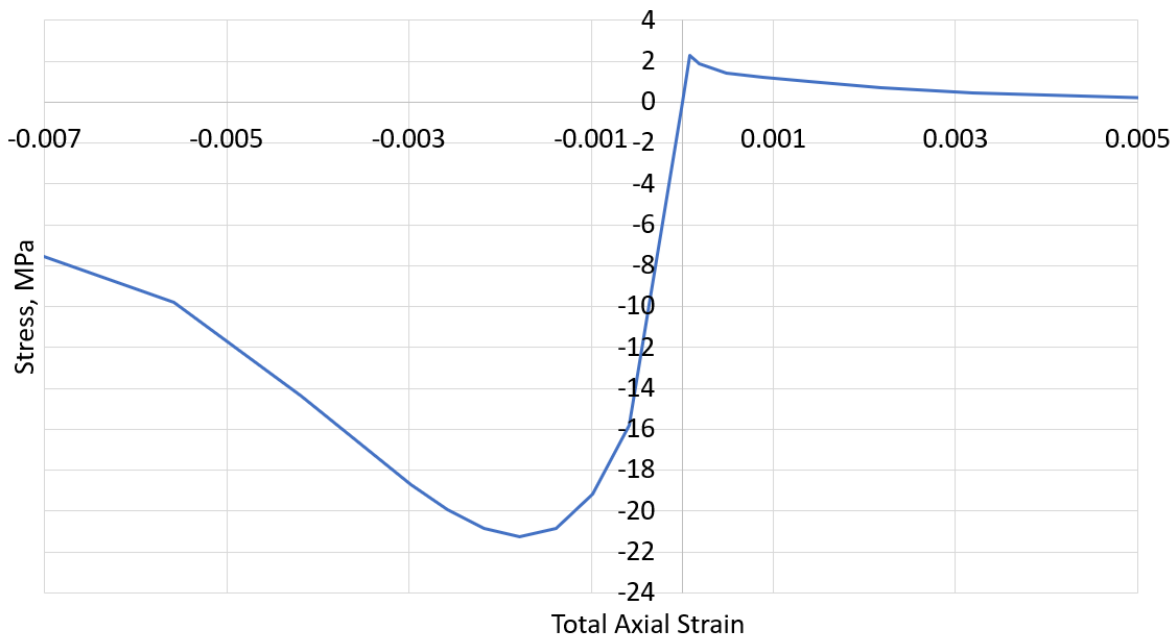


Figure 11. Tension/Compression Behavior for M25 Concrete (see Table 6) using mean GRF resistances.

4.6.5. Reinforcement Steel

Steel with yield stress of 500 MPa is used for concrete reinforcement. Reinforcement steel is incorporated into the finite element model in the slabs by means of embedded element reinforcement in the dam axis and slope (longitudinal) directions. The reinforcement is modeled by means of a smeared technique, designed to take into account the effect of a large number of reinforcement bars, oriented in the appropriate directions and considering the full nonlinear behavior of the steel (Simulia 2020). Using this method, the model does not require the placement of each individual bar, but rather the definition of each reinforcement mesh, consisting of axial and longitudinal bars.



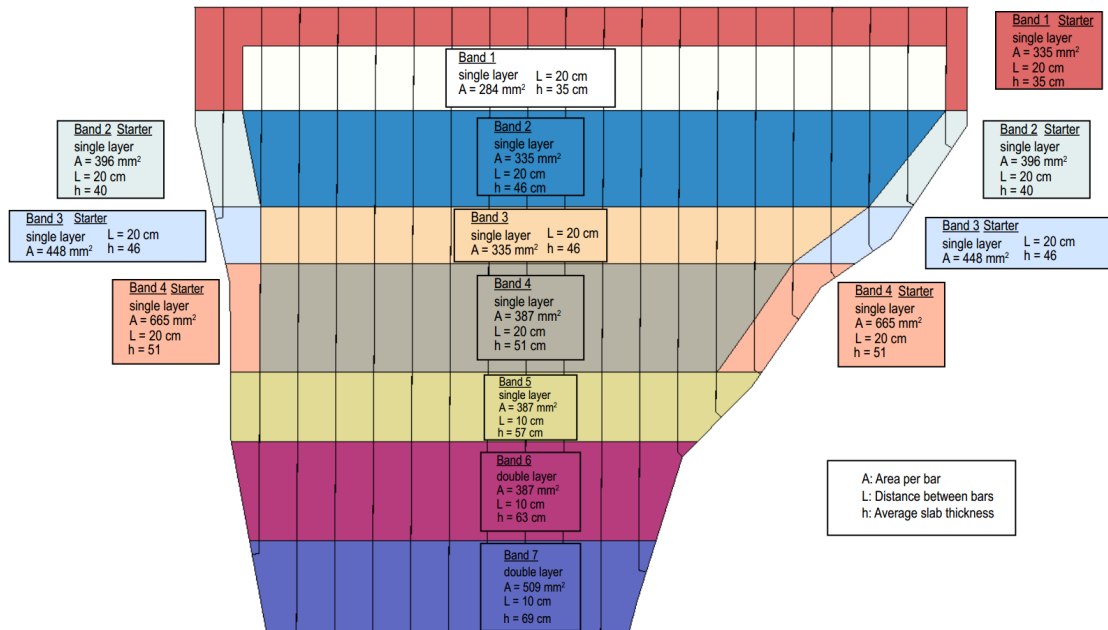


Figure 12. Distribution of reinforcement layers in the slab. Bands 6 and 7 feature two layers of reinforcement, each with nominal cover of 8 cm. In bands 5, 6 and 7, the starting slabs feature the same reinforcement details as each band across the width of the concrete face.



Full details of the reinforcement are included in the Structural Design of Concrete Face Plinth and Parapet Wall Report. Reinforcement steel is included in the behavior of the face slab by means of embedded surface elements which provide reinforcement by means of the smeared reinforcement concept (Simulia 2020).

4.6.6. Foundation

The foundation is assumed rigid below the alluvial deposit, but it is treated as a contact interface, as described in the following section.

4.7. INTERFACES

An important aspect of the behavior of a CFRD is the frictional nature of the contact among the different components of the dam. This aspect of behavior is rarely considered in its full complexity, in part due to the difficulties associated with modeling frictional contact along irregular surfaces. In the Pakal Dul FEA model, full non-linear contact is included among all relevant components in order to describe the stresses, deformations, slip, openings and contact pressures adequately.

Table 7. Friction coefficient of the various contact interfaces.

Frictional contact between concrete slabs	Friction coefficient = 0,50
Frictional contact between slabs and curb	Friction coefficient = 0,85
Frictional contact between slabs and plinth	Friction coefficient = 0,50

Frictional contact between dam and foundation	Friction coefficient = 1,00
---	-----------------------------

The slab joints aren't modeled explicitly. Instead, the contact opening and contact pressure at the interface between slabs is used to identify the regions where joint openings might occur, and those where joints are acting in compression.

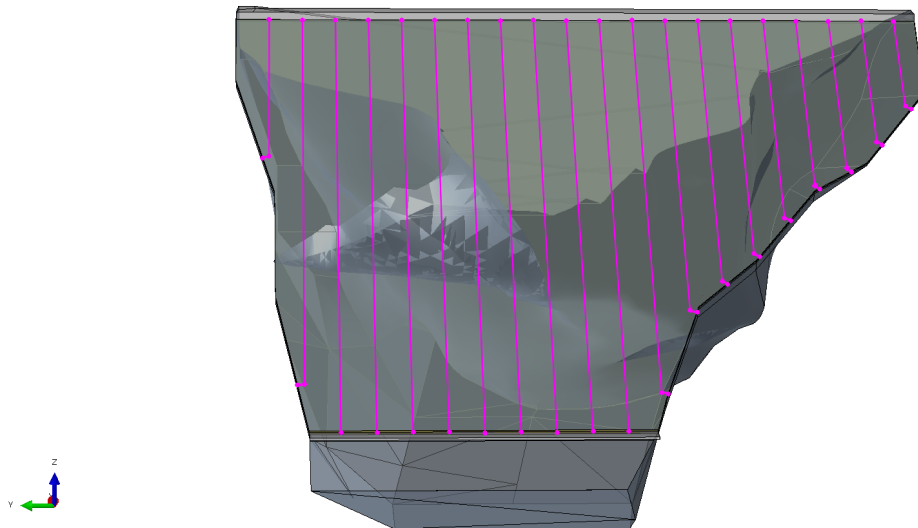


Figure 13. Frictional contact interfaces between concrete face slabs.

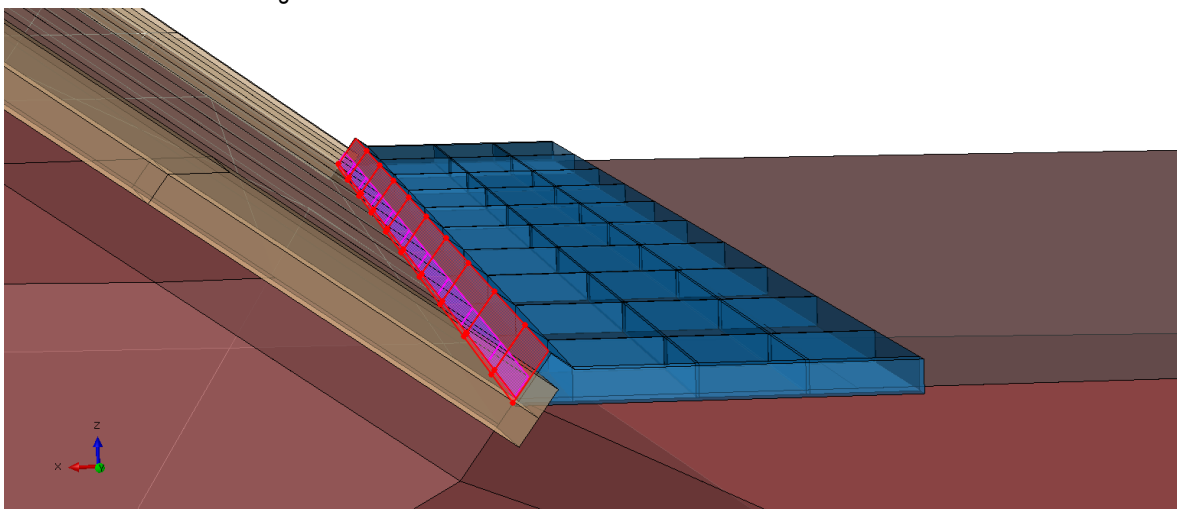


Figure 14. Frictional contact interface between articulated plinth and concrete face.

4.7.1. Compressible joints behavior

In order to model the perimeter joint efficiently and to represent its function of dissipating the contact pressure at the plinth-slab interface, a "soft" pressure-overclosure contact property is adopted in Abaqus whereby a gap of 2 cm is introduced in the geometry, corresponding to the thickness of the wood material. This type of pressure-overclosure

relationship is commonly used to model relatively softer layers of material present on one or both sides of a contact interface (Simulia, 2020).

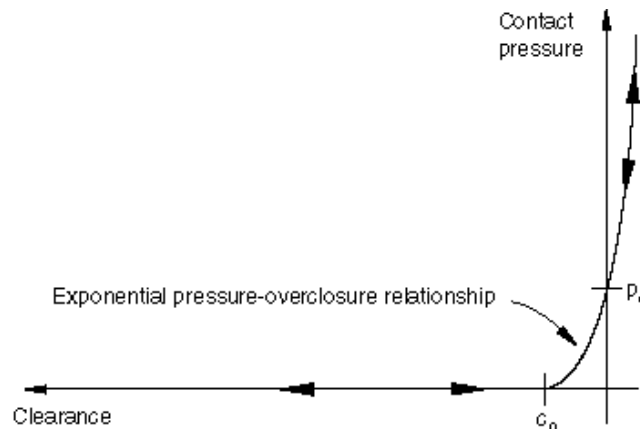


Figure 15. "Softened" pressure-overclosure relationship for considering the effect of a 2 cm layer of wood ($p_0 = 10$ MPa) at the perimeter joint, and rubber ($p_0 = 150$ MPa) for compressible joints

4.8. STAGED CONSTRUCTION AND IMPOUNDMENT

Staged construction is simulated by means of element deactivation and activation in order to approximate the process of sequential placement of rockfill layers. However, because of computational considerations, approximately 10 m-thick layers are added at a time, in a horizontal pattern. It should be noted that this sequence is only for simulation purposes in order to reproduce expected deformation patterns within the dam body, bearing in mind that the dam can not be considered a "wish in place" structure. After the construction of the dam fill, the curb is placed on the upstream face, providing a flat surface for the subsequent placing of the concrete face. The modeled rockfill sequence is considered adequate given the fact that in the simulation the construction of the concrete face is developed in one stage and the deformations and stresses in the concrete slab are mainly associated with the impoundment loads.

4.9. RESULTS AND ANALYSIS OF THREE DIMENSIONAL STATIC ANALYSIS

4.9.1. Settlements and construction moduli

The construction modulus after Fell (2003) is used to provide a means of quantifying the stiffness of the dam under a particular combination of material properties. The modulus at the end-of-construction is defined as:

$$E_{rc} = \frac{f\gamma Hd_1}{\delta_s}$$

Equation 2.

where:

γ is the unit weight of the rockfill

H is the height of the dam below the dam axis

$d_1 = H/2$

δ_s is the deformation of the midpoint of the deforming layer due to the addition of the top half of the rockfill material.

$f = 0,9$ is the stress reduction factor that accounts for the arching effect due to friction with the abutments.

The pattern of settlement at the end of construction can be observed in Figure 14, which given the weight of the rockfill and the dam height, leads to a construction moduli of $E_{rc} = 70$ MPa. It is important to highlight that this value corresponds to an outcome of the numerical model rather than an input such as Young's modulus, since the material behavior is non-linear and is not characterized by a single elastic modulus (see Section 2.5.).

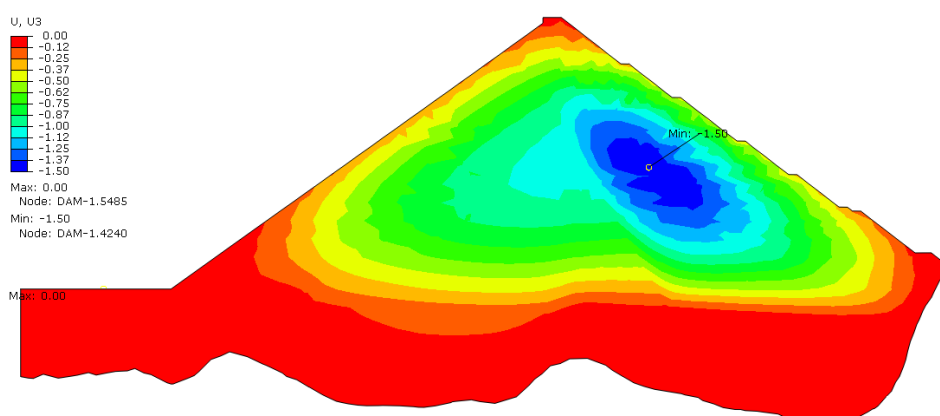


Figure 16. Settlements (m) at the end of construction for rockfill material (Section 2.3.1. Rockfill material), exhibiting a maximum of 1,5 m at an elevation of 1627 m.a.s.l. Section cut through abscisa 0+250.

In the case of Pakal Dul dam the rockfill quarry is expected to provide a high to very high strength rock and both the specifications and the test embankment will be developed in order to ensure a well compacted condition. Combining these premises with a 100 mm d_{50} value for the 3B and 3C zones and Hunter and Fell (2003) empirical correlations a construction moduli between 70 MPa and 350 MPa for medium to high strength rock and very high strength rock respectively. It is observed that the 70 MPa construction moduli value corresponds to a lower bound of the expected

values, therefore, using the result of the calibration based on laboratory test results provides an upper bound solution in terms of displacements and concrete face stresses and is considered a conservative approach.

 It should be noted that both gradation and compaction requirements to be implemented in Pakal Dul CFRD should be adhered to in order to provide a stiff rockfill material. Keeping in mind the zonification specified in Figure 6, and the definition of rockfill modulus of Hunder and Fell (Equation 2), Table 8 shows the approximate construction moduli that should be guaranteed for the specified zones so that the face slab behaves satisfactorily as described in Section 2.9.

Table 8. Approximate vertical rockfill moduli of the zones of Pakal Dul Dam (see Figure 6)

Zone	Modulus
3B	120 MPa
3C	70 MPa
Fill of excavation below plinth	200 MPa

By choosing gravel as the material for the excavation below the toe plinth and ensuring adequate compaction, it is feasible to obtain a vertical modulus of the order of 200 MPa. This well-compacted material is crucial to ensure the adequate behavior of the slab as well as minimizing the deformation of the cutoff wall and its possible interaction with the plinth. This aspect is further discussed in the updated version of the geotechnical zoning report 0390801-INF-BB-LT3.2-0003 - GRADING MATERIAL IN DIFFERENT ZONES, GEOMETRY OF CFRD AND ZONING REPORT.

4.9.2. Deformation of the concrete face under impoundment

 Once the concrete face is placed on the curb, it is supported by friction at the curb-slab interface, as well as being supported by contact with the plinth. After equilibrium of the slab is established, a hydrostatic load is applied to all surfaces of the assembly that are in contact with water, which include the top face of the toe plinth and the top surface of the rockfill upstream of the cutoff-wall. The resulting deformation of the slab can be observed in Figure 17. Maximum slab deformation for this numerical analysis is 45 cm at the lower third of the slab located in the middle of the concrete face. A 45 cm maximum deformation compares reasonably well with the empirical results of Hunter and Fell (2003) for construction moduli between 70 and 120 MPa which provide an estimation of concrete face normal deformations between 20 to 50 cm, taking into account the upstream excavation and the alluvial deposit presence.

Due to anisotropy and zoning related effects the rockfill modulus on first filling (E_{rf}) is higher than the construction (vertical) modulus (E_{rc}). In the case of the simulations the relationship for these two parameters is 1,7.

A 1,7 value is lower than the estimation determined based on Hunter and Fell (2003), which present a range between 1,8 to 3,0. Having a lower rockfill modulus on the first filling results in higher concrete face displacements and stresses, however, a 1,7 moduli relationship does not seem an unreasonable value.

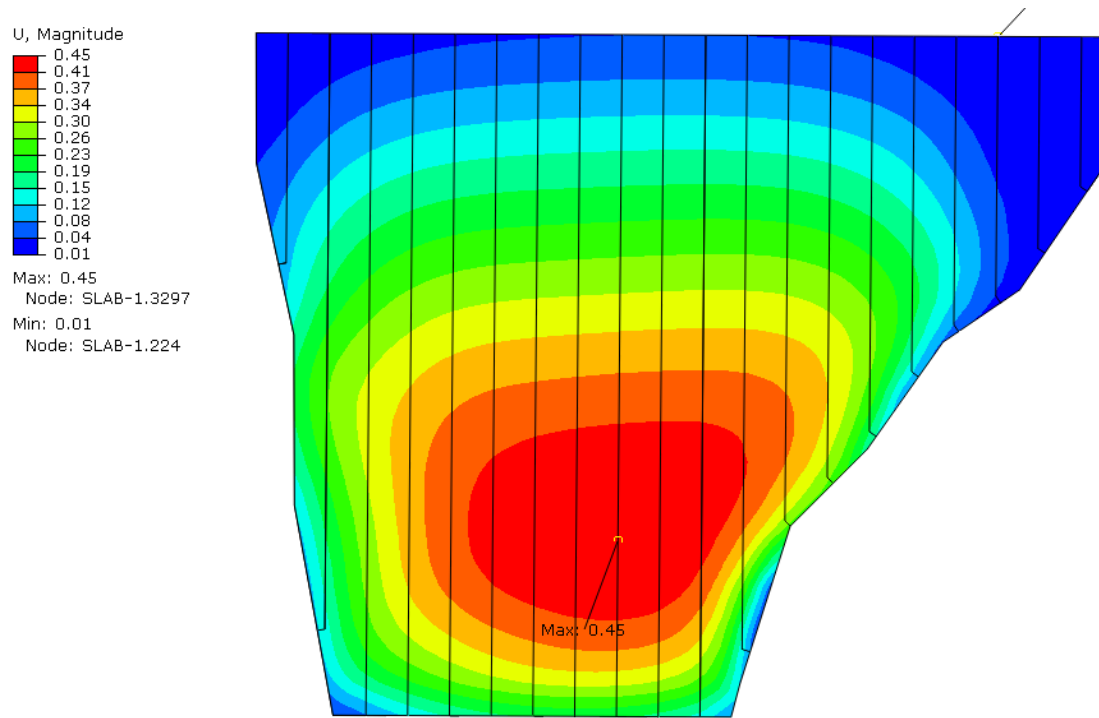


Figure 17. Concrete face deformation (m) under impoundment.

4.9.3. Stresses and strains in the concrete face

The ultimate function of the concrete face is to serve as an impermeable barrier, hence, the design must ensure that under appropriate combination of loads and during the planned operation of the reservoir, the slab continues to be essentially impermeable. Fib Model Code 2010 (Federation Internationale du Beton, 2010) provides guidelines for estimating the crack width under strains for which concrete loses most of its strength due to cracking, as well as recommended limits for watertight structures. For a given strain limit, the design crack width is a function of various parameters, including the reinforcement ratio, the bond strength between concrete and steel, the stress in the steel in cracked regions, among others. The procedure for calculating the design crack width is outlined in Section 4.9.5.

Figure 18 to Figure 21 show stresses in the concrete face under the impoundment of the reservoir for the rockfill deformability previously described and the constitutive model for concrete described in Section 4.6.4. Given the implementation of a non-linear behavior for the concrete featuring strain softening, and loadings which induce inelastic deformations, the acceptance criteria for the concrete face are stipulated in terms of design crack widths and crack width limits. Nevertheless, the stresses are presented for the sake of completeness.

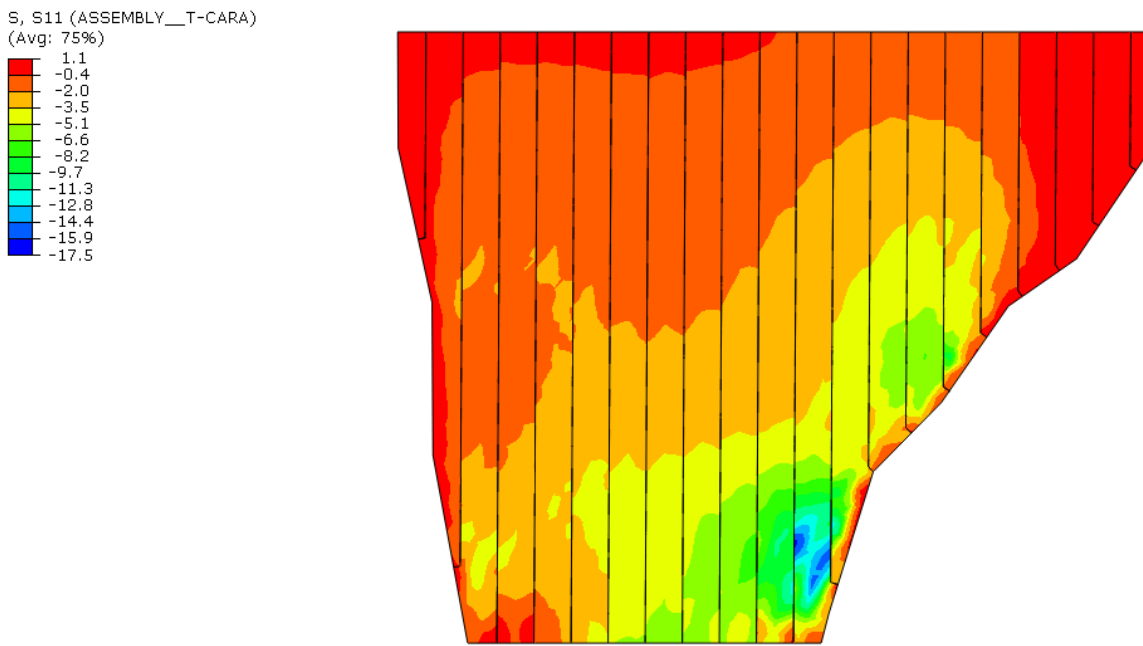


Figure 18. Stresses in the dam axis direction (horizontal), in MPa, on the bottom surface of the slab. Positive/negative values indicate tension/compression.

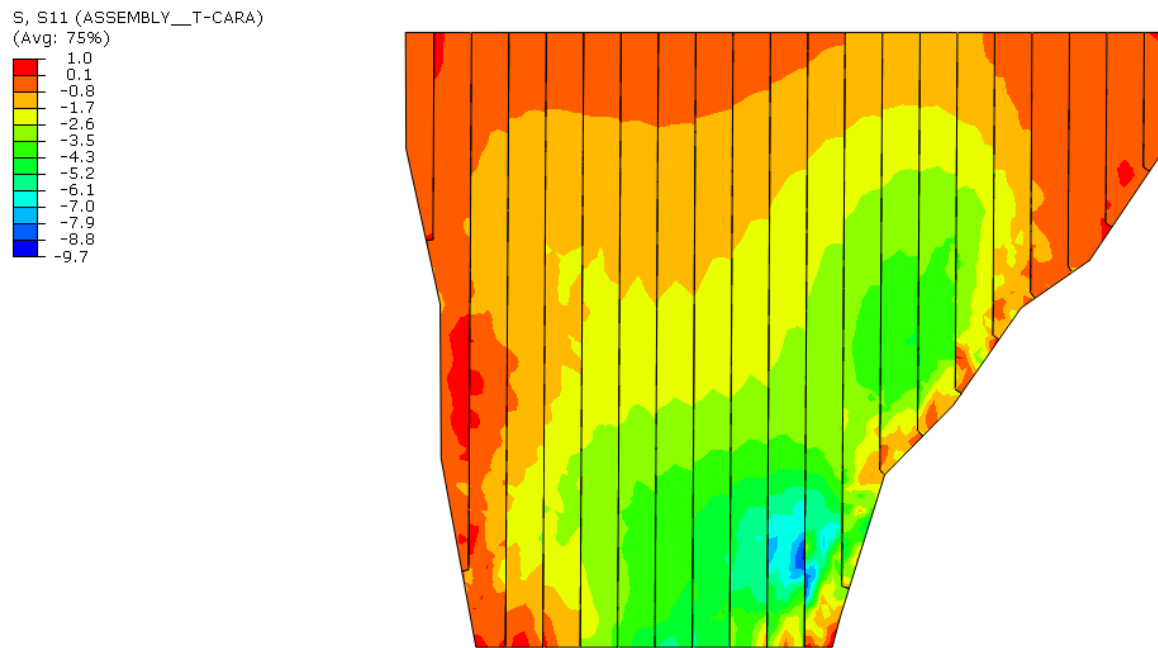


Figure 19. Stresses in the dam axis direction (horizontal), in MPa, on the top surface of the slab. Positive/negative values indicate tension/compression.

S, S22 (ASSEMBLY__T-CARA)
(Avg: 75%)

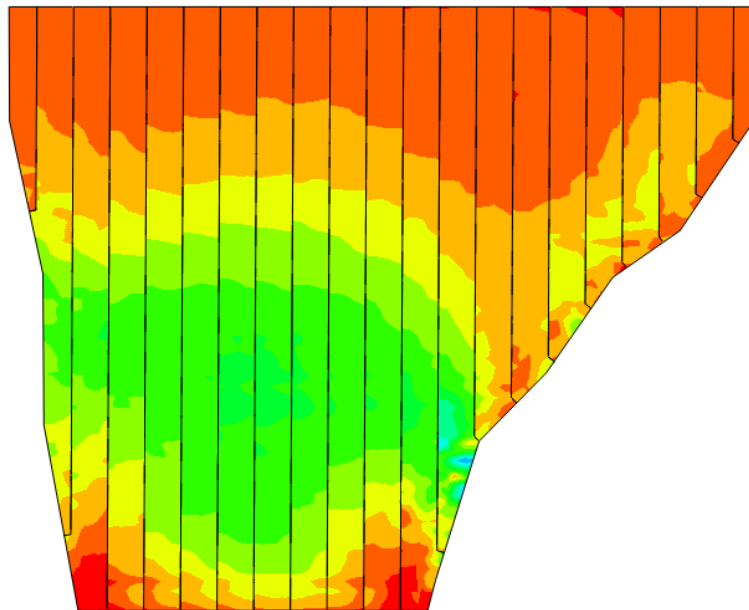
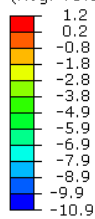


Figure 20. Stresses, in MPa, in the direction of the slope on the bottom surface of the slab. Positive/negative values indicate tension/compression.

S, S22 (ASSEMBLY__T-CARA)
(Avg: 75%)

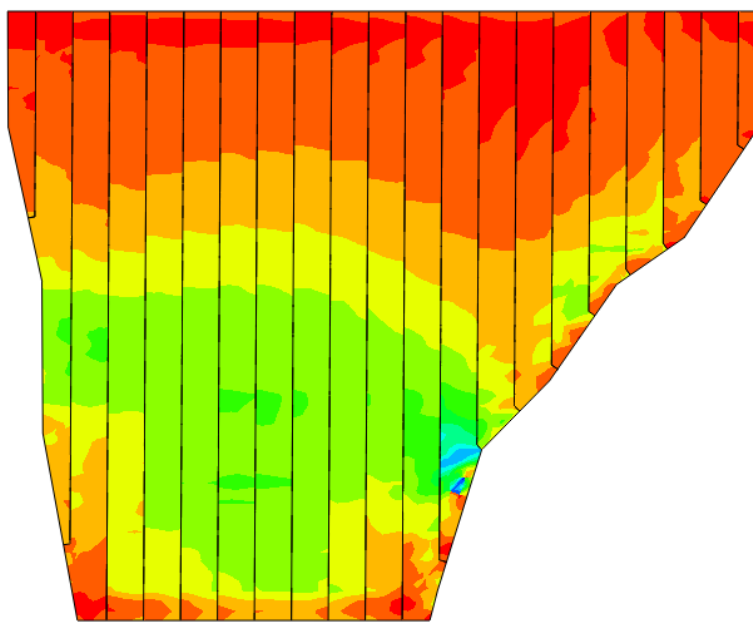
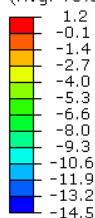
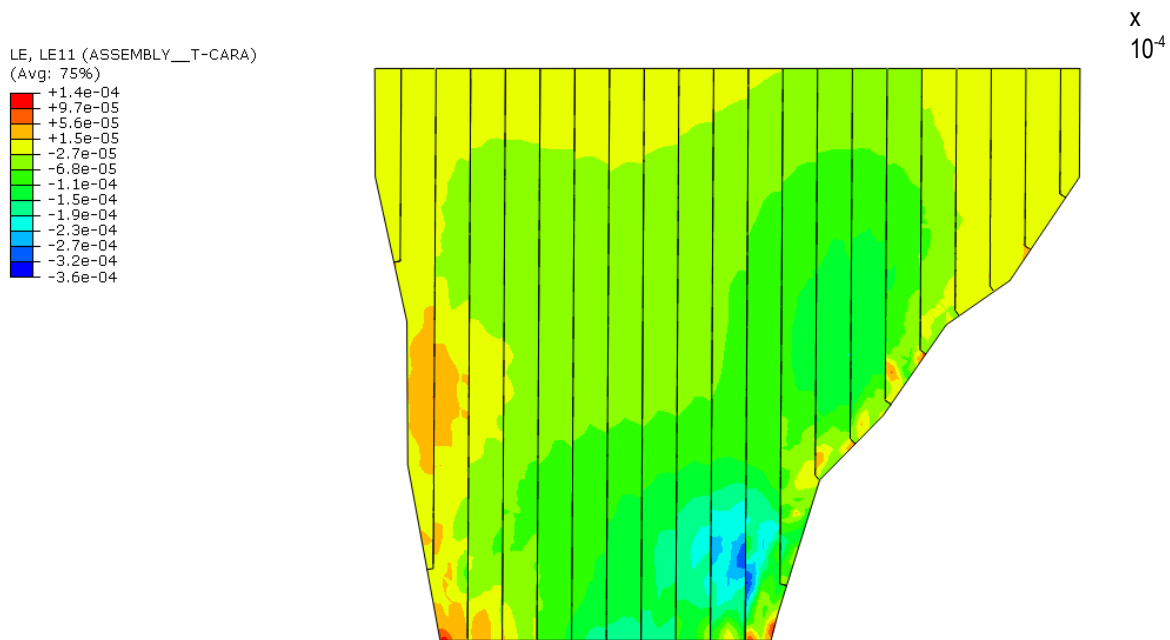


Figure 21. Stresses, in MPa, in the direction of the slope on the top surface of the slab. Positive/negative values indicate tension/compression.

Figure 22 presents the strain patterns in the direction of the dam axis in the concrete face, ranging in the top fiber from -6×10^{-4}



(compression) to 4×10^{-4} (tension), and in the bottom fiber from -4×10^{-4} (compression) to 1×10^{-3} (tension).

Figure 22. Dam axis-wise (total) strains on the bottom surface of the slab under impoundment to 1700 m.a.s.l.

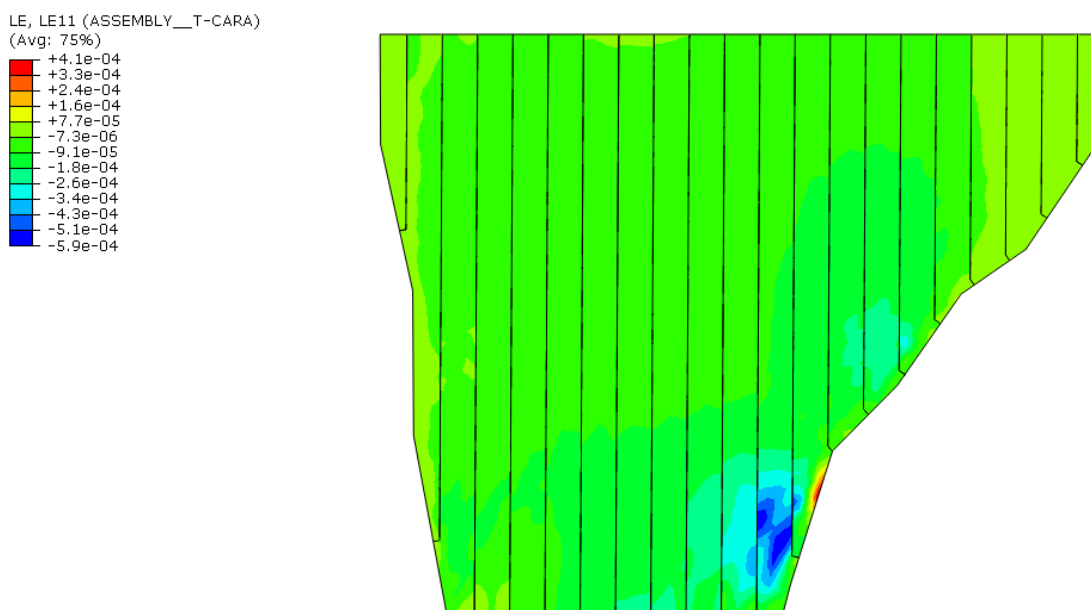
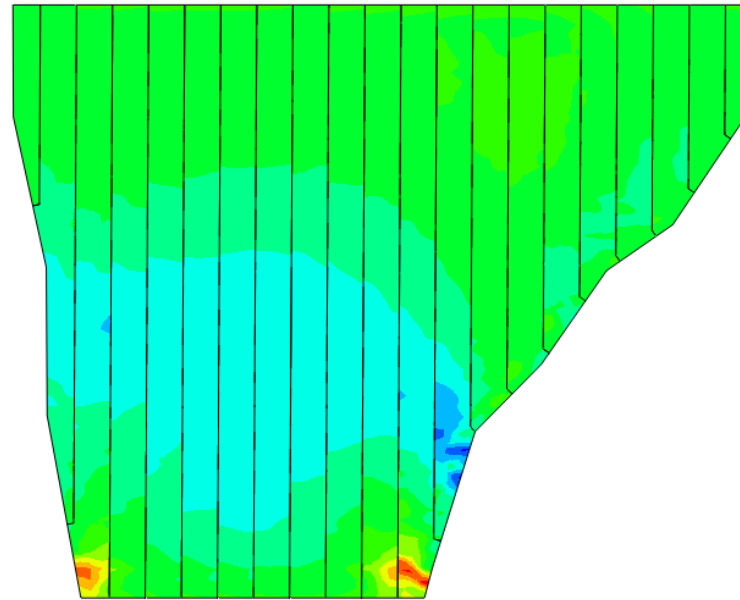
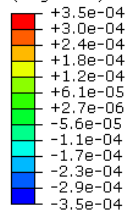


Figure 23. Dam axis-wise (total) strains on the top surface of the slab under impoundment to 1700 m.a.s.l.

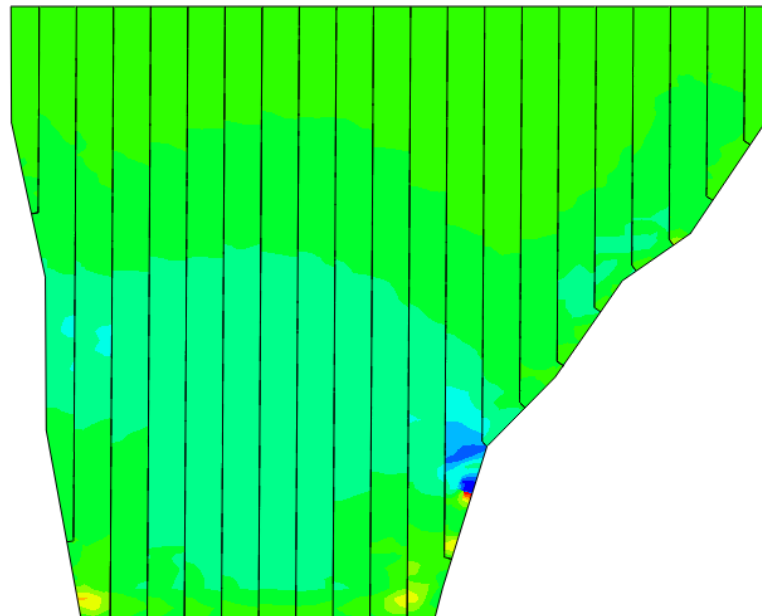
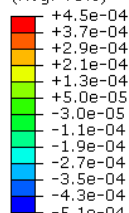
LE, LE22 (ASSEMBLY__T-CARA)
(Avg: 75%)



△ C

Figure 24. Slope-wise strains on the bottom surface of the slab under impoundment to 1700 m.a.s.l.

LE, LE22 (ASSEMBLY__T-CARA)
(Avg: 75%)



△ C

Figure 25. Slope-wise strains on the top surface of the slab under impoundment to 1700 m.a.s.l.

Figure 24 and Figure 25 present the strains in the longitudinal direction of the slabs, ranging, in the top fiber from -5×10^{-4} (compression) to 5×10^{-4} (tension), and in the bottom fiber from -4×10^{-4} (compression) to 4×10^{-4} (tension). These strain values are used to assess the required steel reinforcement in the Structural Design of Concrete Face Report, so as to guarantee an adequate design crack for watertight barriers (as described in numeral 4.9.5) and therefore comply with low-leakage requirements, provided the dam materials comply with the provisions set forth in Section 4.6.1.

4.9.5. Inter-slab and perimeter joint behavior

Figure 26 presents the expected behavior of internal joints, in which joints between slabs 1-2, 2-3, 17-18, 19-20, and 20-21 should correspond to tension joints and the rest of the internal joints are estimated to be primarily in compression. The characterization of concrete face internal joints as either compression or tension joints is an input parameter used in the structural design of the concrete face.

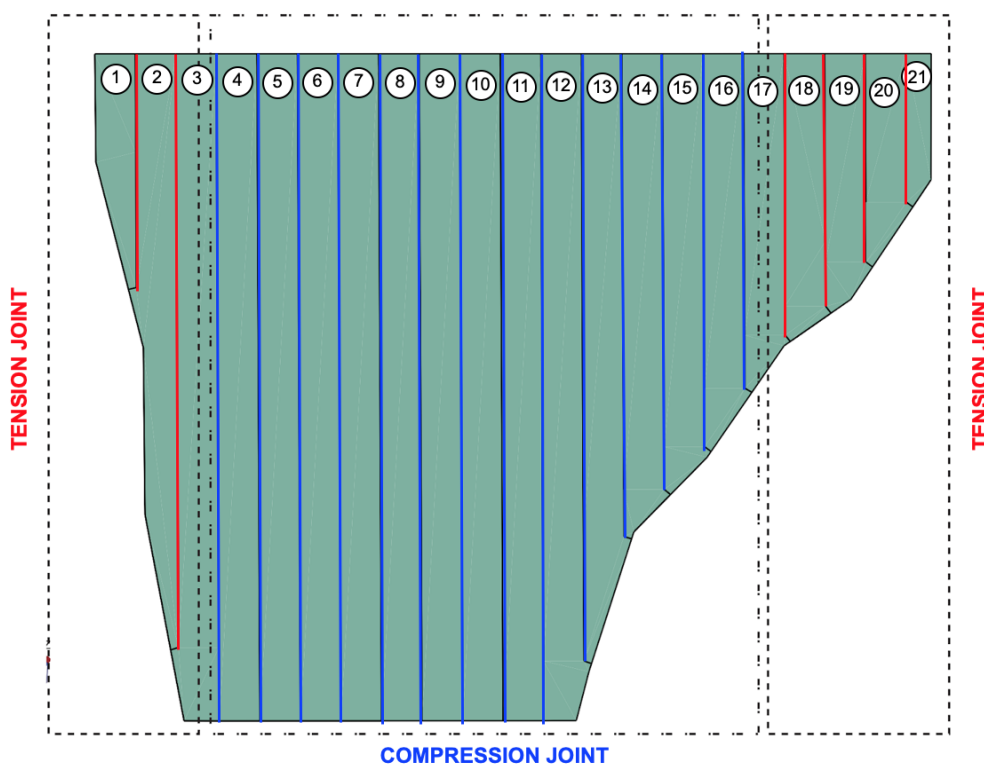


Figure 26. Status of joints in the concrete face. The majority of joints will be under compression, while those with the potential to open are indicated in the Figure.

Additionally, the opening of the perimeter joint in response to the impoundment of the reservoir can be seen in Figure 27 for materials with construction moduli of 120 MPa, 70 MPa, and 200 MPa in zones 3B, 3C and excavation zone, respectively. The opening values for the perimeter joint are estimated to be 20 mm and 10 mm at the left and right abutments, respectively, and 20 mm between toe plinth and the slab; this latter value considering the more rigid material of the excavation zone below the plinth. In order to control settlements induced by the impoundment the design will emphasize that this fill material be composed mainly by gravels so as to achieve a construction modulus in the 200 MPa range. Modulus of this order has been achieved in several dams where an adequate gradation was implemented and thorough construction procedures were used..

The use of this material as a fill for the projected excavation reduces the deformations at the dam toe significantly, limiting bending stresses in the plinth and corner slabs and minimizing the possibility that horizontal displacements of the cut-off wall lead to compression of the perimeter joint at the toe plinth. The obtained displacements of 20 mm at the plinth to concrete face joint can adequately be absorbed by the three joints included in the articulated plinth as long as the deformation of the cutoff wall is kept below 25 mm as specified by INGETEC in the Design Criteria Report. Recommendations regarding the construction and gradation specifications for the upstream excavation fill material will be included in an updated version of the zoning report.

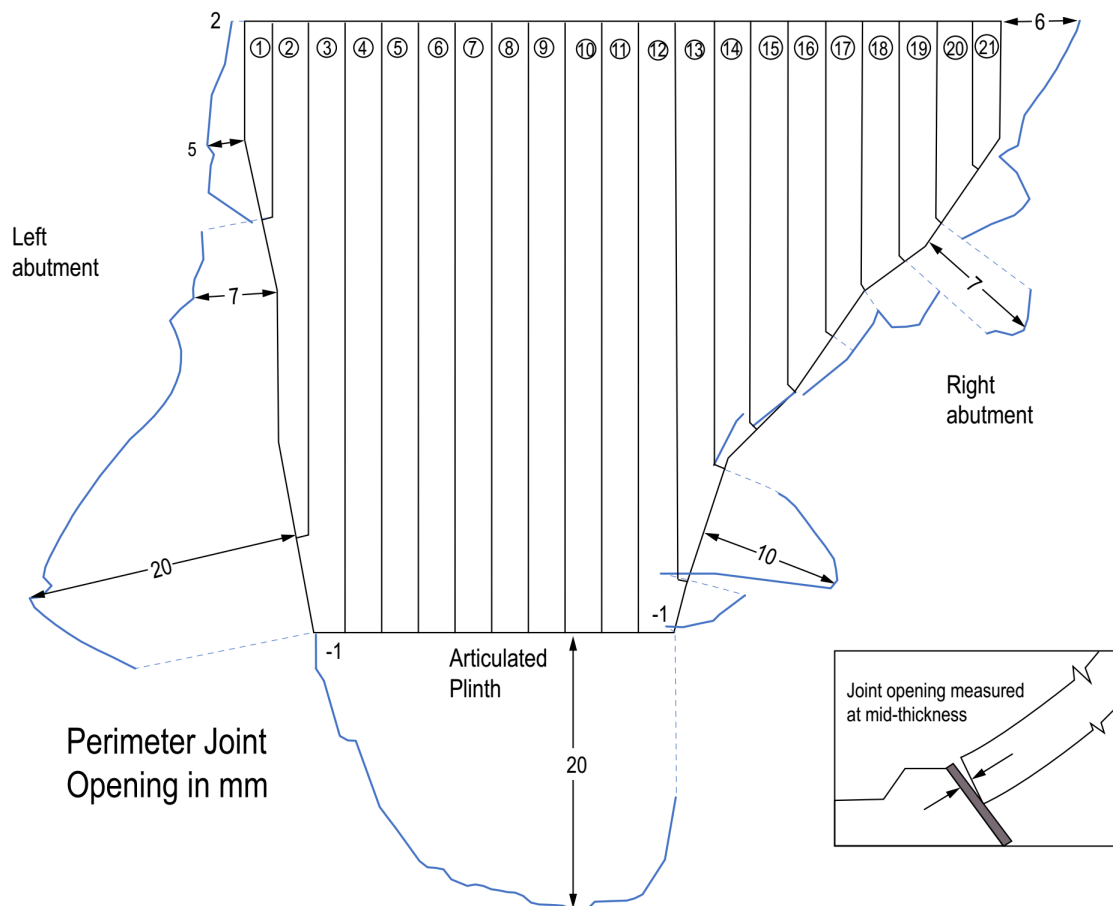


Figure 27. Opening of perimeter joint

4.9.6. Limitation of crack width

One of the main criteria to design the concrete face is to assure that tensile strains or stresses are below the level in which the concrete face cracks are not self-healing and an increase in leakage occurs due to crack width opening.

According to Fib Model Code (Fib 2010), the design crack width has to satisfy the following condition:

$$w_d \leq w_{lim}$$

where:

w_d denotes the design crack width calculated as:

$$w_d = 2 \left[k \cdot c + \frac{f_{ctm} \phi_s}{4\tau_{bms} \rho_{s,ef}} \right] \left(\frac{\sigma_s - \beta \cdot \sigma_{sr}}{E_s} - \eta_r \cdot \varepsilon_{sr} \right)$$

Equation 3.

In Equation 3, a critical input to be obtained from the finite element analysis is the stress in the cracked regions, σ_s , which can be read directly from the analysis at the top and bottom reinforcement fibers presented in Figure 28 to Figure 33, which show stress fields representing “smeared” uniaxial stresses in individual steel bars, despite appearing continuous. Also, individual tension and compression zones include discontinuous steel reinforcement, as required in order to model each slab correctly. The details of numerical modeling methodology and the quantities of steel reinforcement included in each zone of the concrete face are described in Section 4.6.5.

With regard to crack width limitation for fluid-tightness, a limit of $w_{lim} = 0,3$ mm is commonly defined as adequate for maintaining low leakage through concrete, although globally the widest cracks will be below 0,1 mm. Steel reinforcement design is presented as a part of the Structural Design Report [(Document 0390801-INF-SS-LT3.2-0001, INGETEC (2020)] based on the requirements presented in Fib Model Code (Fib 2010).

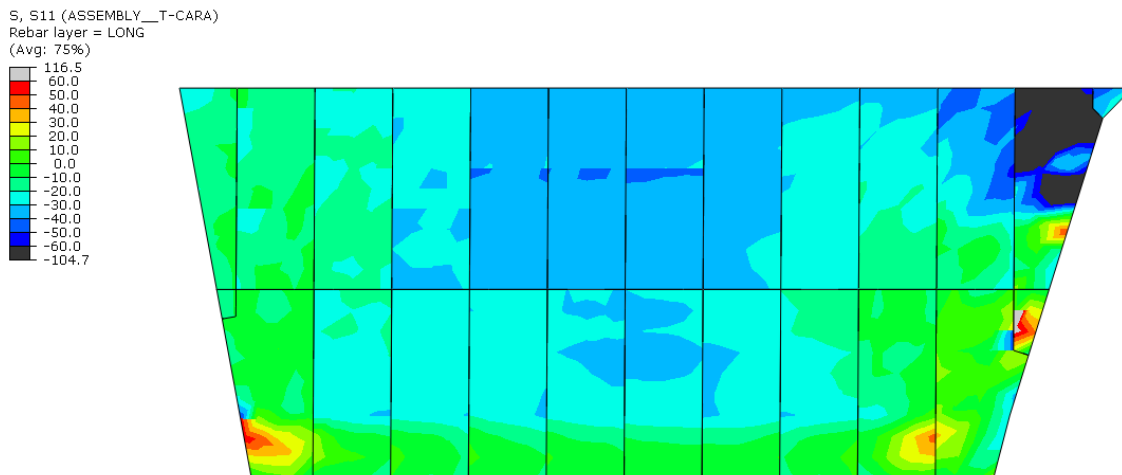


Figure 28. Uniaxial stresses in the top longitudinal reinforcement layer in bands 6 and 7 (EL. 1559 m.a.s.l to EL. 1604 m.a.s.l). The small localized grey zone presents stresses of between 60 and 116 MPa.

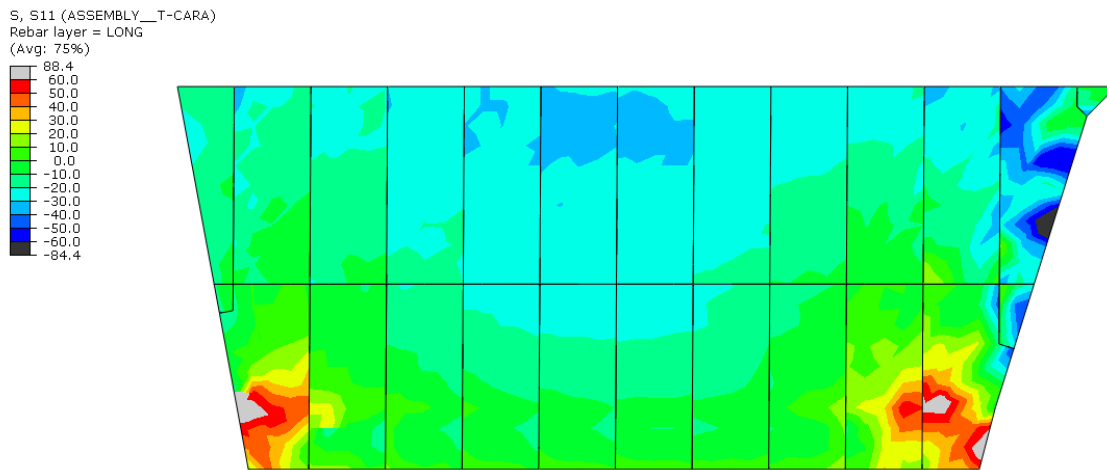


Figure 29. Uniaxial stresses in the bottom longitudinal reinforcement layer in bands 6 and 7 (EL. 1559 m.a.s.l. to EL. 1604 m.a.s.l.). The small localized grey zone presents stresses of between 60 and 88 MPa. The black region represents stresses between -60 and -84 MPa in compression.

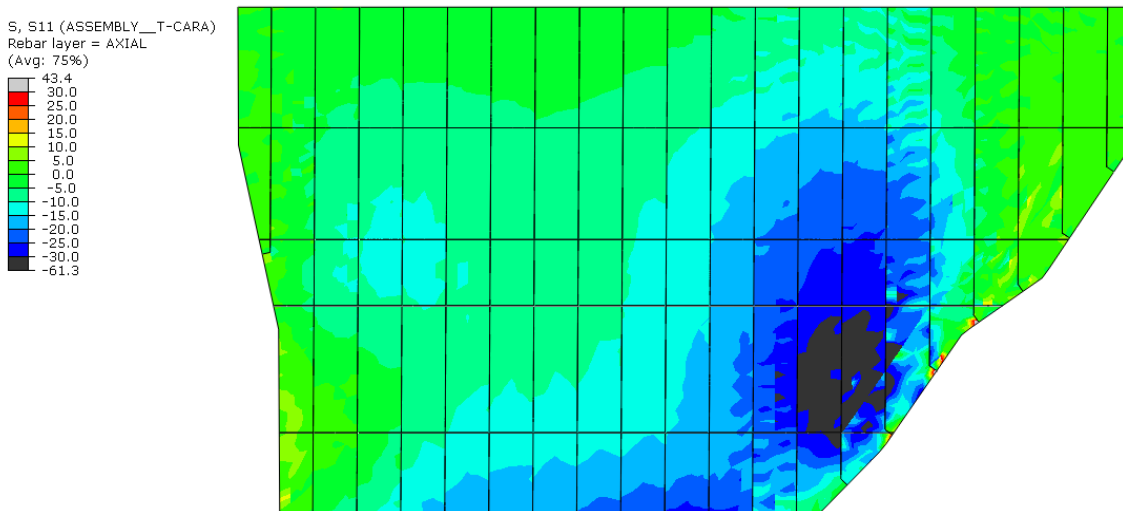


Figure 30. Uniaxial stresses in the bottom longitudinal reinforcement layer in bands 1-5 (EL. 1604 m.a.s.l. to EL. 1704 m.a.s.l.). The black region represents stresses between -30 and -61 MPa in compression.

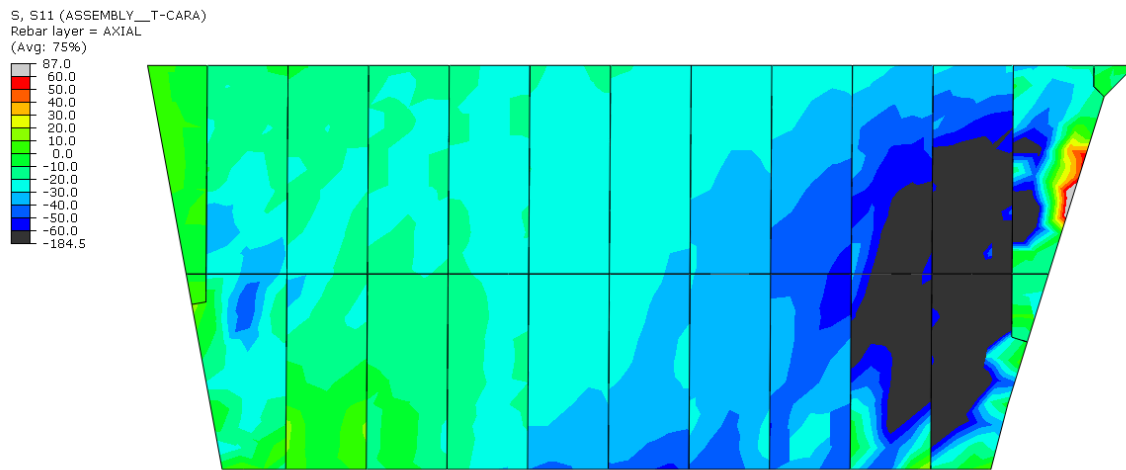


Figure 31. Uniaxial stresses in the top axial reinforcement layer in bands 6-7 (EL. 1559 m.a.s.l. to EL. 1604 m.a.s.l.). The grey zones represent stresses between 60 MPa and 87 MPa while the black region represents stresses of between -60 and -184 MPa in compression.

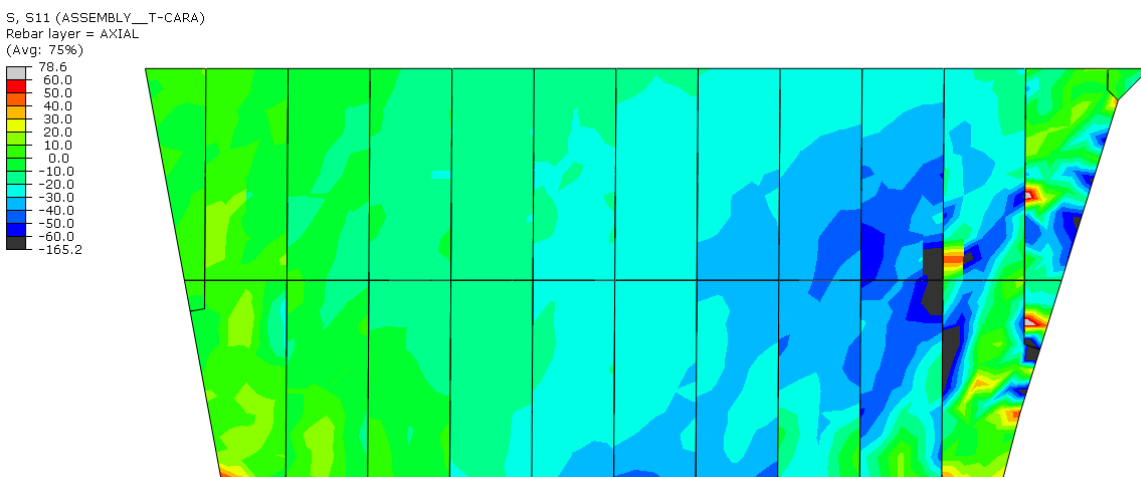


Figure 32. Uniaxial stresses in the bottom axial reinforcement layer in bands 6-7 (EL. 1559 m.a.s.l. to EL. 1604 m.a.s.l.).
 The black zones represent regions of between -60 and -165 MPa in compression.

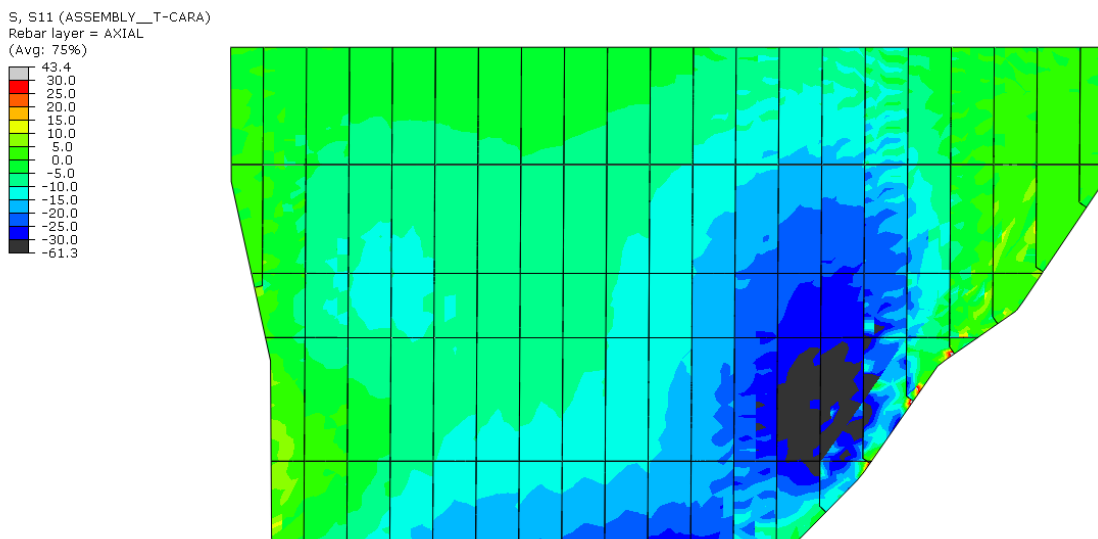


Figure 33. Uniaxial stresses in the single axial reinforcement layer in bands 1-5 (EL.1604 m.a.s.l. to EL 1704 m.a.s.l.).



4.10. RESULTS INTERPRETATION

The Finite Element Method is a valuable addition to the arsenal of tools employed in the analysis and design of Concrete Face Rockfill Dams, helping guide the design of the excavation surfaces, slab thicknesses, joint properties, as well as concrete reinforcement quantities in a more robust way than it was possible some years ago. It can be invaluable in the process of selecting an appropriate level of compaction of rockfill materials, identifying unfavorable geometric features in the excavation surfaces, among other aspects of the behavior of the dam as a whole. The adequate use of the method in the design of concrete structures is greatly aided by the guidelines provided in the Fib Model Code 2010, which has been used extensively in this report in defining the concrete material behavior as well as the reinforcement quantities to guarantee low levels of leakage in regions presenting concrete cracking.

There are aspects of the analysis where the model is likely to provide only a general measure of the stresses that the slabs might be subject to. These could include corner regions where the bending in the dam axis direction might include local stresses that would require a highly localized analysis that is not common practice in the design of such structures.

Long-term behavior, such as creep, has not been considered, since the magnitude of the creep strain rates likely to occur at the Pakal Dul should be rather low.

Parameter calibration for the behavior of rockfills has been developed using laboratory test results provided by CVPP. However, sensitivity analyses have been performed and have uncovered the need for more rigid materials than those tested in the large-scale triaxial tests. Specifically, the construction moduli of zones 3B in upstream shell (120 MPa), 3C in downstream shell (70 MPa), and 3B in the replacement zone below EL 1559 (200 MPa) must be obtained by means of adequate compaction and grading during the test fill. Under these conditions, a maximum settlement estimation of 1.5 m at the middle of the 3C zone and a maximum concrete face deformation (normal to the concrete face) of around 45 cm are obtained.



The low deformation in the slab that results from said rockfill moduli leads to low strains in the reinforcement layers, which together with adequate reinforcement, are associated with small design crack widths (in the 0,3 mm order) according to the Fib Model Code (Fib 2010) helping to validate the geotechnical recommendations and guidelines.

The specified construction moduli must be guaranteed as a result of the test embankment procedure in terms of the maximum settlement obtained in each zone. Furthermore, once the rockfill has been placed, prior to the construction of the face slab, the observed settlements must compare satisfactorily with those of Figure 16 in order for the behavior of the concrete face to be consistent with the results presented herein.

The analysis also identified internal compression and tension joints and provided an estimate of the perimeter joint displacements of 20 mm, 20 mm and 10 mm, for the left abutment, articulated plinth connection and right abutment zones, respectively.

These internal compressible joints will not be required in the case that gradation and compaction standards yield a construction moduli of 120 MPa, 70 MPa, and 200 MPa in zones 3B, 3C and excavation zone respectively, as the resulting behavior of the concrete face will be within serviceability limits.

5. DYNAMIC FINITE ELEMENT ANALYSIS

The dynamic finite element model has been developed with the objective to estimate the fundamental frequencies, the seismic induced deformation and the dynamic stability of the dam. This model was constructed in Midas GTS NX finite element software.

This chapter presents the description of the geometry, the boundary conditions, the calibration of the constitutive models, and the results of the bidimensional and the three-dimensional models. As the concrete face has a negligible effect in the dynamic stability and the seismic induced deformation, this feature was not included in this model.

5.1. GEOMETRY

The dynamic model includes both the rockfill material and the foundation materials. Foundation materials include the bedrock, the silty sand and the river borne soil deposits. Figure 34 shows the solid elements implemented to model these materials. Foundation geometry and stratigraphy were constructed based on the geological sections provided by CVPP and the plinth excavation defined by INGETEC (2020).

It is important to note that the different surfaces were created with cubic Non-Uniform Rational B-Spline (NURBS) surfaces, in order to capture the terrain's details and create a smooth transition, which reduces the number of edges and provides a more uniform mesh.

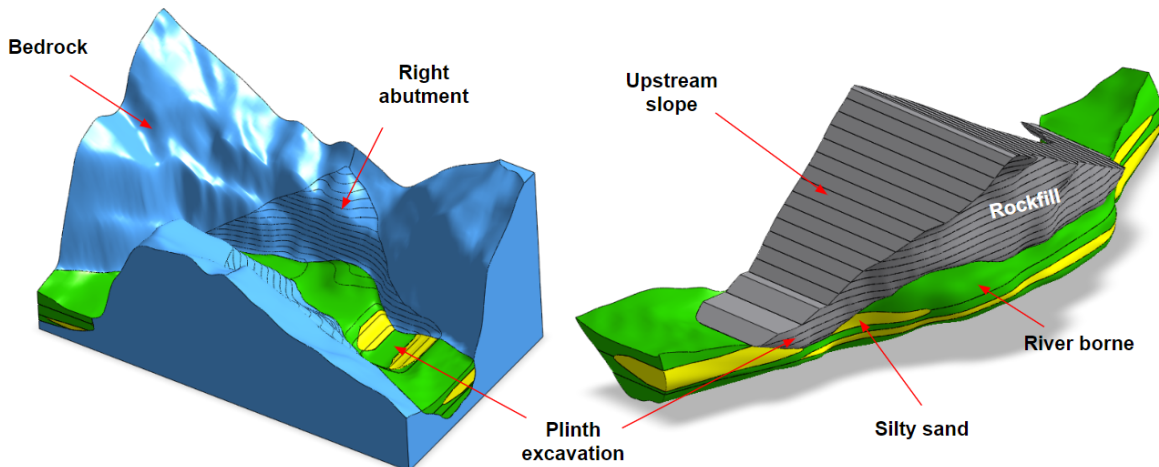


Figure 34. Dynamic model geometry

Figure 35 illustrates the discretization of the three dimensional geometry with linear tetrahedral elements, which includes 63 670 elements for the bedrock, 49 698 elements for the alluvial deposit, and 76 941 elements for rockfill material. The element size was selected in each material according to the wave propagation velocity and the time step of the seismic signal, ensuring the accuracy of the model.

On the model's sides, absorbent elements were included, which allow to eliminate the boundary effect caused by reflection waves. These elements use viscous dampers according to the Lysmer and Kuhlemeyer formulation (Lysmer, 1969).

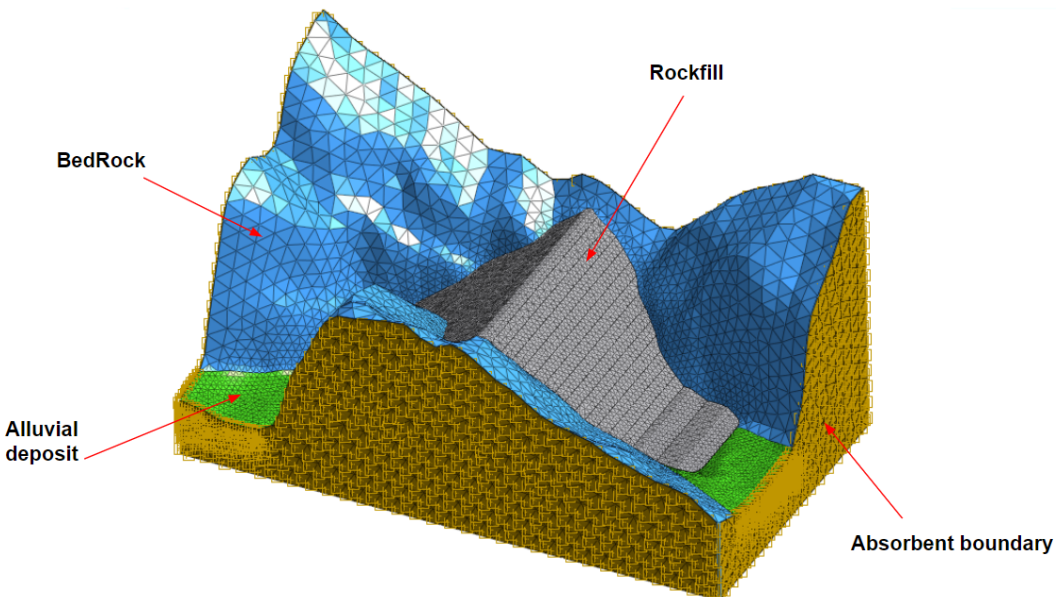


Figure 35. Dynamic model - Mesh

Figure 36 presents the mesh of the alluvial deposit and the rockfill material. As shown in this Figure, the rockfill material was divided into 19 horizontal layers in order to simulate the construction process, and the alluvial deposit was divided into five layers according to their composition (silty sand or river borne) and their shear wave velocity. The selected shear wave velocity profile and the characterization of these materials are presented in Section 3.2.2.

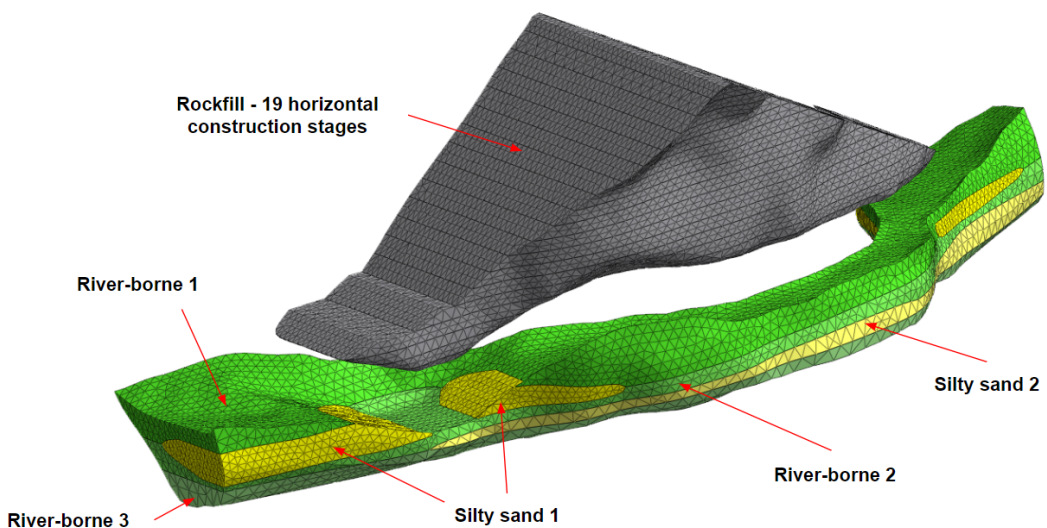


Figure 36. Mesh detail - Alluvial deposit and rockfill

5.2. MATERIALS

Although for static analysis is very common to implement an hypoelastic material behavior (i.e. hyperbolic model developed by Duncan and Chang to describe rockfill behavior), in the case of the dynamic developed for Pakal Dul CFRD the Modified Mohr-Coulomb was used in order to solve the representation of plastic behavior and permanent displacement calculations limitations of hypoelastic models, which are considered key components to properly model the behavior of rockfill materials under dynamic loading. The Modified Mohr-Coulomb model is an elastoplastic model with multiple yield surfaces, which can simulate the behavior of this material more accurately and consider the seismic permanent deformations.

On the other hand, the river-borne and the silty sand layers were modeled with a linear elastic model, using Young's modulus in the range of small strain.

In contrast to the Modified Drucker Prager/Cap model used in the static model developed in Abaqus, the fact that the Modified Mohr-Coulomb model includes different loading/unloading moduli makes it more suitable for handling the irreversible cyclic deformations expected during a seismic event. The ready availability of this material model in Midas-GTS NX is the primary reason for the development of the dynamic models in Midas whereas the static models, which includes the concrete face and hence that requires a more robust treatment of interfacial contact was developed in Abaqus/CAE.

5.2.1. Rockfill material

The behavior of the rockfill material was captured with the Modified Mohr-Coulomb (MMC) model, also known as the Hardening Soil model. This is an advanced elasto-plastic model which includes two types of hardening; Shear hardening to model irreversible strain due to primary deviatoric loading (See Figure 37), and compression hardening to model irreversible plastic strain owing to primary compression.

The MMC describes a hyperbolic stress-strain relationship in axial compression in a similar way to the hyperbolic Duncan-Chang model. However, in the case of the MMC, material behavior is described based on the plasticity theory, achieving a better representation of the volumetric strain.

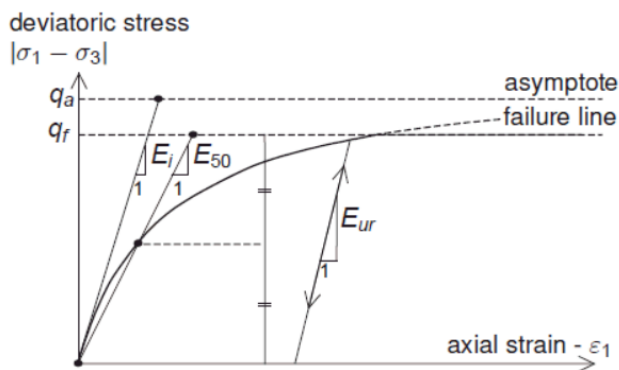


Figure 37. Strain-stress relationship in a triaxial compression test with the modified Mohr-Coulomb model
Source: Midas GTS NX (2019), Analysis reference manual.

As depicted in Figure 37, the MMC model uses three types of reference stiffness moduli to calculate the total strains, differentiating between virgin loading and unloading/reloading. The main parameters of the MMC model are summarized in Table 9.

Table 9. Main parameters of the Modified Mohr-Coulomb model.

Parameter	Description
E_{50}^{ref}	Secant stiffness in triaxial test
E_{eod}^{ref}	Tangential stiffness in oedometric test
E_{ur}^{ref}	Elastic modulus at unloading
R_f	Failure ratio
p^{ref}	Reference pressure
m	Power for stress-level dependency of stiffness
φ'	Effective friction angle
c'	Effective cohesion

Rockfill's parameters for this constitutive model were calculated based on the triaxial results of the quarry material. The initial parameter estimation was developed using the theoretical expression and then adjusting the MMC parameters through triaxial test simulation (element test) to improve the prediction. Figure 38 to Figure 40 show the triaxial results and the numerical prediction with the calibrated parameter of the MMC model. It is important to note that the triaxial test with a confining pressure of 1,8 MPa was not included in the calibration, because this stress level is not representative for Pakal Dul CFRD. It should be noted that the calibration focuses on reproducing material behavior for the expected strain range under seismic motion (axial strains up to 6%).

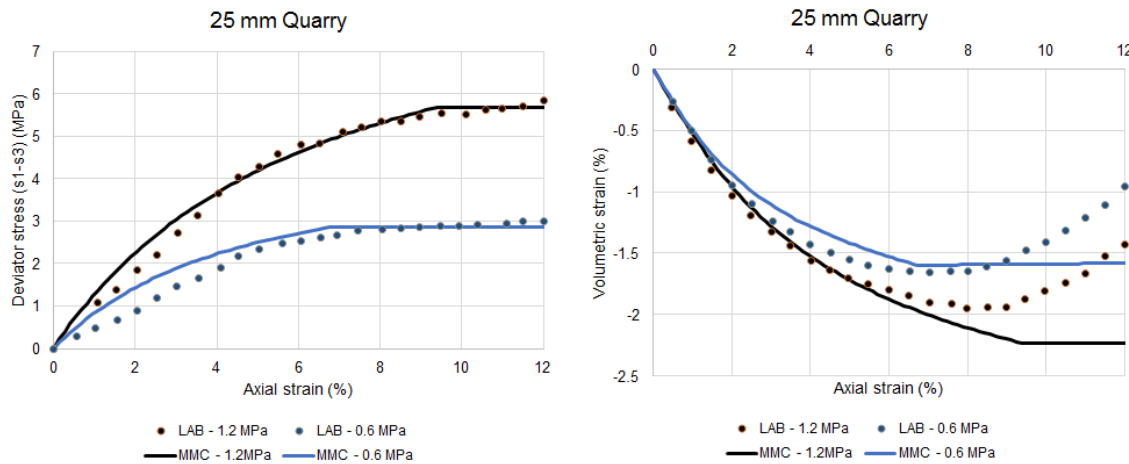


Figure 38. Stress-strain-volume change of 25 mm Quarry, Modified Mohr-Coulomb (MMC) model.

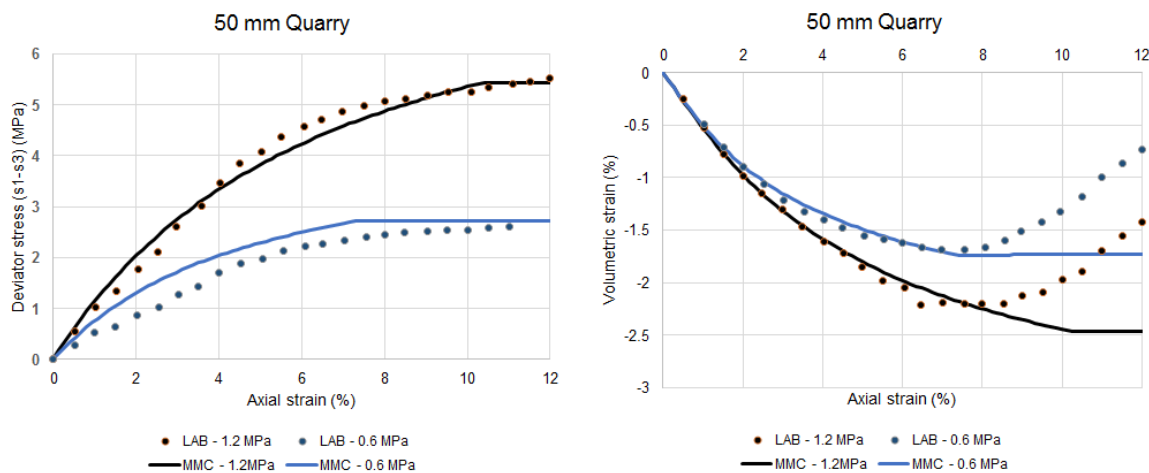


Figure 39. Stress-strain-volume change of 50 mm Quarry, Modified Mohr-Coulomb (MMC) model.

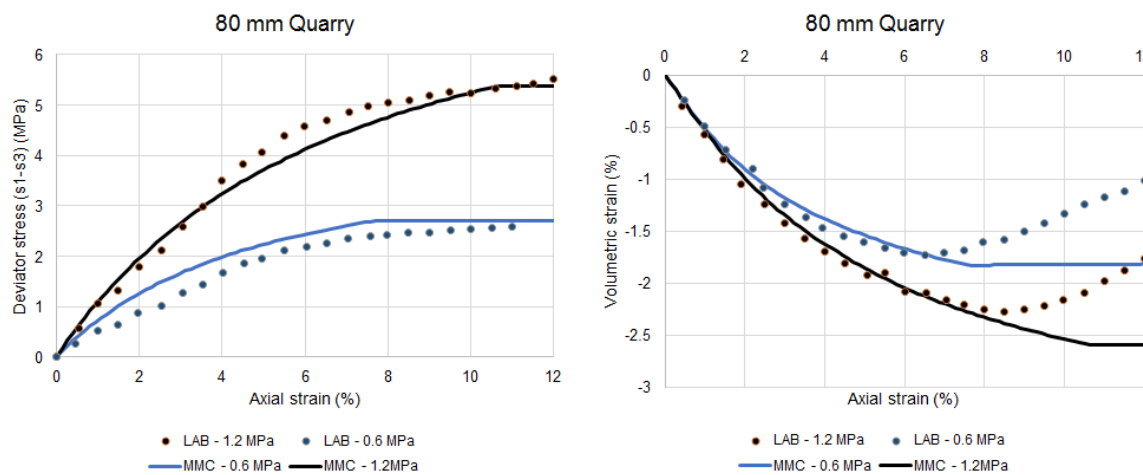


Figure 40. Stress-strain-volume change of 80 mm Quarry, Modified Mohr-Coulomb (MMC) model.

In order to reproduce the expected behavior for the rockfill real gradation (maximum particle size of 600 mm) a parameter analysis was developed to understand the maximum particle size impact on the behavior of the available rockfill material

Table 10 summarizes the estimated MMC parameters for the rockfill prototypes and the real rockfill (maximum particle size of 600 mm). The stiffness modulus and the friction angle for the latter were calculated using a simple power correlation, which is consistent with the Weibull's theory on rock aggregates (Weibull W., 1939), the empirical evidences of the size effect in the breaking particles (Oldecop, 2013), and the scaling law used on similar works (Zhou X., 2019; Honkanadavar N.P., 2016).

Table 10. Predicted material parameters of Modified Mohr-Coulomb model Quarry material.

Parameter	Quarry 25 mm	Quarry 50 mm	Quarry 80 mm	Quarry 600 mm (real rockfill)
E_{50}^{ref}	61 MPa	54 MPa	52 MPa	39 MPa
E_{oed}^{ref}	49 MPa	43 MPa	41 MPa	30 MPa
E_{ur}^{ref}	183 MPa	162 MPa	156 MPa	116 MPa
R_f	0,88	0,88	0,88	0,88
P_{ref}	100 kPa	100 kPa	100 kPa	100 kPa
m	0,5	0,5	0,5	0,5
ϕ'	44,6°	43,8°	43,7°	42,0°

Ψ'	5°	5°	5°	5°
c'	5 kPa	5 kPa	5 kPa	5 kPa

As presented in Table 10, the quarry material exhibits a greater compressibility and lower shear resistance for bigger particle size, which is due to a high rate of increase in the breakage factor with the increase in particle size. This behavior is displayed in Figure 41, which presents the predicted stress-strain-volume change behavior for the quarry prototypes and the real rockfill (600 mm) at a particular confining pressure.

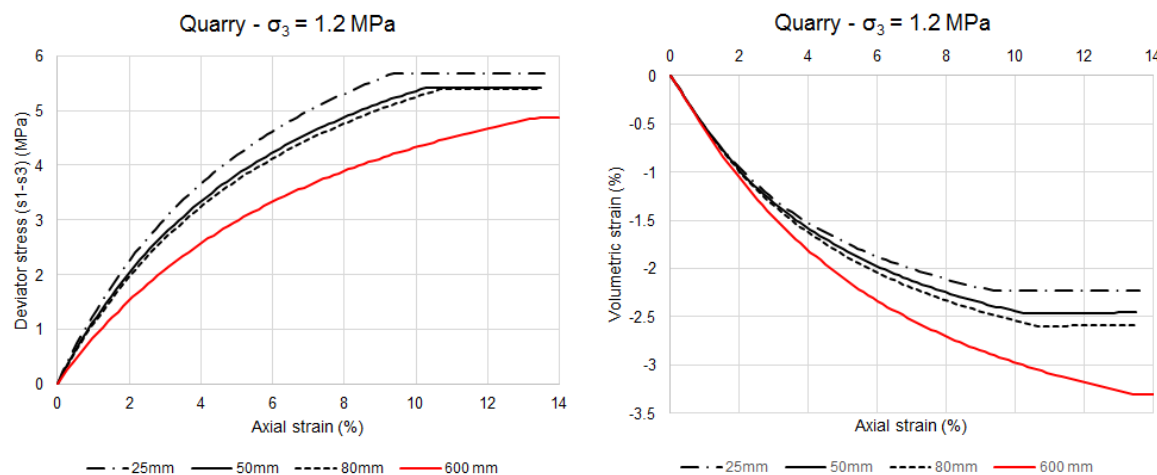


Figure 41. Predicted stress-strain-volume change behavior of Pakal Dul CFRD quarry rockfill material ($\sigma_3 = 1.2$ MPa)

It is important to clarify that the rockfill parameters used on the dynamic finite element model and presented in Table 9 differ from the rockfill parameters presented in document no- 0390801-INF-BB-LT3.2-0002. 0002 - Geotechnical parameters of Dam report, because the former corresponds to a Modified Mohr Coulomb model, whereas the latter corresponds to a Duncan Chang model.

5.2.2. Alluvial deposit

The isotropic linear elastic constitutive model was used to capture the dynamic behavior of the silty sand and the river borne layer. The Young's modulus for each of the five layers shown in Figure 36 was calculated based on the elastic relationship between shear modulus and shear velocity for a homogeneous medium and the modulus degradation was estimated based on wave propagation analyses and the use of shear modulus degradation curves.

According to the seismic cross section AA located 20 m upstream of the plinth axis (NHPC Limited, 2005) and the MASW geophysical test performed near the plinth (NHPC Limited, 2018), the shear wave velocity of the alluvial deposit range from about 300 m/s to 1200 m/s. Based on this geophysical survey and the stratigraphical description obtained at the drilled boreholes, the shear velocity profile at the plinth axis shown in Figure 42 was defined.

The shear velocity values for each layer are the product of the interpretation of the geophysical test and a sensitivity analysis carried out, in order to select the Vs values that produce the highest acceleration on the bidimensional model.

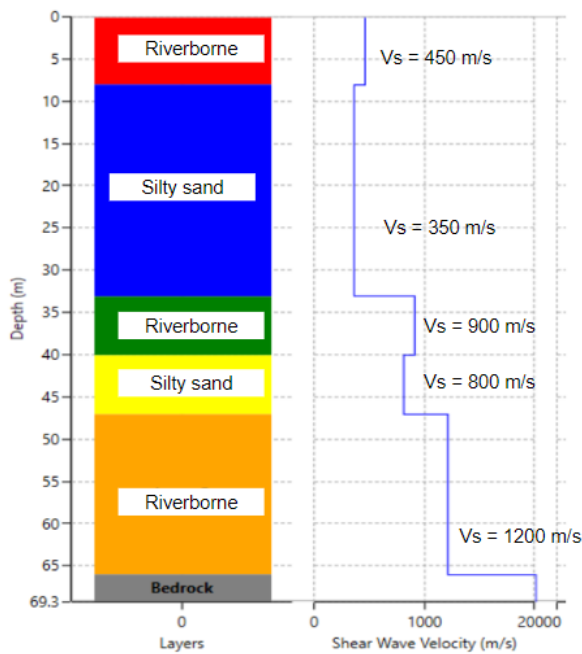


Figure 42. Shear velocity profile for the alluvial deposit.

In order to select the appropriate Young's modulus and damping ratio for each layer, a one-dimensional wave propagation analysis was performed on the software DEEPSOIL (Hashash, 2016). This analysis was carried out for the Chamoli seismic signal [input motions are described in 0390801-INF-BB-LT3.2-0001 document (INGETEC, 2020)], taking into account that this input motion produces the highest displacement in the Makdisi and Seed (Makdisi, 1979) analysis presented in the Static & Dynamic Stability and Seismic Induced Deformations of the CFRD Dam Report (INGETEC, 2020). The reference shear modulus reduction curves and damping ratio curves used for this analysis are shown in Figure 43.

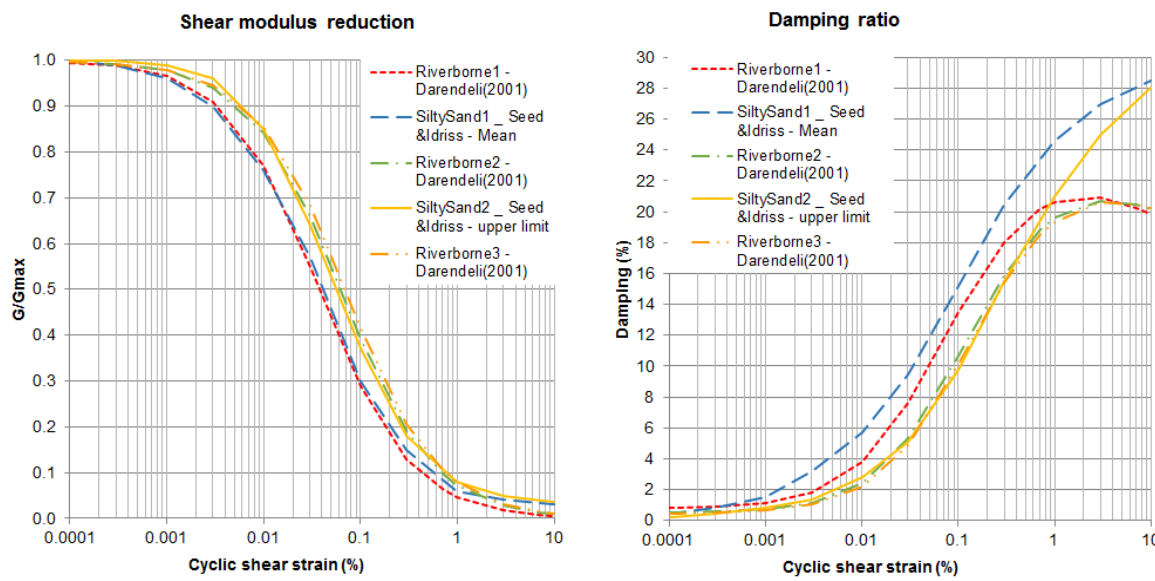


Figure 43. Reference shear modulus reduction and damping ratio curves

Table 11 summarizes the calculated Young's modulus and damping ratio for the alluvial layers. These values were estimated selecting from the reference curves the damping ratio and shear modulus reduction ratio (G/G_{max}) for 65% of the maximum shear strain obtained in the one-dimensional wave propagation analysis.

Table 11. Elastic parameter alluvial layers

Parameter	River borne 1	Silty sand 1	River borne 2	Silty sand 2	River borne 3
V_s (m/s)	450	350	900	800	1200
ν	0,3	0,3	0,3	0,3	0,3
ρ (kg/m ³)	1700	1700	1700	1700	1700
G_0 (MPa)	344	208	1377	1024	2448
G/G_0	0,81	0,22	0,85	0,80	0,89
G (MPa)	280	46	1117	824	2184
E (MPa)	729	119	3060	2143	5679
ξ (%)	3	18	2	3	2

The Young's modulus presented in Table 11 correspond to small to medium strain range moduli estimated based on the shear wave velocity profile and the performed one-dimensional wave propagation analysis. Therefore, these values differ from the Young's moduli presented in document No- 0390801-INF-BB-LT3.2-0002. 0002 - Geotechnical parameters of Dam report, which correspond to large strain moduli estimated using SPT N60 values.

5.2.3. Bedrock

In order to have parallel faces on the model boundaries and to include the absorbent elements, a bedrock material was included. The behavior of this material was described using an isotropic linear elastic model with a Young's modulus of 10 GPa and a damping ratio of 2%. These parameters allow to represent rock impedance without introducing significant changes in both the frequency content and the amplitude of the input motions.

5.3. MODAL ANALYSIS

As a first step in the dynamic analysis of the Pakal Dul CFRD, a modal analysis was performed to identify the dam's principal vibration modes and fundamental period. Figure 44 shows the total deformation for the first four vibration modes and Table 12 summarizes the natural periods of the first five vibration modes.

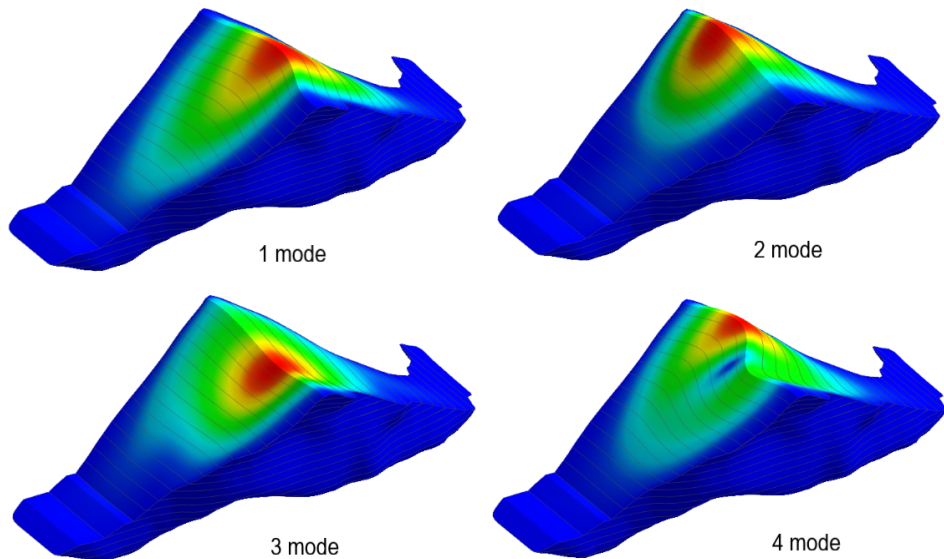


Figure 44. Main vibration modes of the Pakal Dul Dam.

Table 12. Natural periods for the main vibration modes.

Vibration mode	Period (s)
1°	2,08
2°	1,71
3°	1,62
4°	1,53

5°	1,45
----	------

5.4. DAMPING

Rayleigh damping was considered to model the energy dissipation in the numerical model. This method is a very convenient way of accounting for damping in the numerical model, because it provides damping that is approximately frequency independent over a defined range of frequencies.

Rayleigh damping is viscous damping which is proportional to a linear combination of mass and stiffness. The damping matrix \mathbf{C} is given by the following equation.

$$\mathbf{C} = \alpha \mathbf{M} + \beta \mathbf{K}$$

Equation 4. Rayleigh damping

where, \mathbf{M} is the mass matrix, \mathbf{K} is the stiffness matrix, and α and β are the Rayleigh damping parameters.

Rayleigh damping parameters α and β represent the mass and stiffness proportional damping coefficients. These parameters can be calculated using the Equation 5, which uses two reference vibration modes with their corresponding frequency (ω_1 y ω_2) and damping ratios (ξ_1 y ξ_2).

$$\alpha = \xi_1 \frac{2\omega_1 \omega_2}{\omega_1 + \omega_2}$$

$$\beta = \xi_2 \frac{2}{\omega_1 + \omega_2}$$

Equation 5. Rayleigh parameters

The two reference vibration modes allow to define an operational domain in which the achieved damping has the value of the damping ratios (ξ_1 y ξ_2). The selection of the frequencies ω_1 and ω_2 should take into account the fundamental vibration modes of the structure and the predominant frequencies of the seismic signal, avoiding the overdamping of the signal.

Based on the modal analysis presented in the section above, it was estimated that the Pakal Dul dam fundamental period is around 2,0 seconds. On the other hand, the predominant frequencies of the Uttarkashi-Ghatwari, Chi-Chi Ila and Chamoli seismic input motions (INGETEC, 2020) were evaluated through the Fourier transform.

Figure 45 to Figure 47 show the Fourier transform of the three considered seismic signals, and the variation of the damping ratio with frequency. This damping was defined for a range of frequencies between 0,5 Hz (2,0 s) and 2,0 Hz (0,5 s), and the same damping ratio for the two reference frequencies ($\xi_1 = \xi_2$). As shown in these figures, the selected frequencies ensure a damping ratio ξ_1 for the predominant frequencies of the seismic signals.

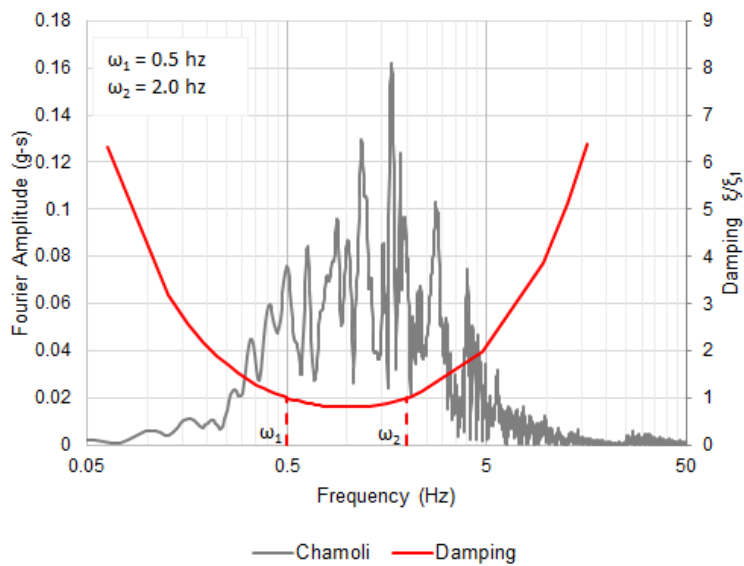


Figure 45. Fourier transform of Chamoli signal and Rayleigh damping.

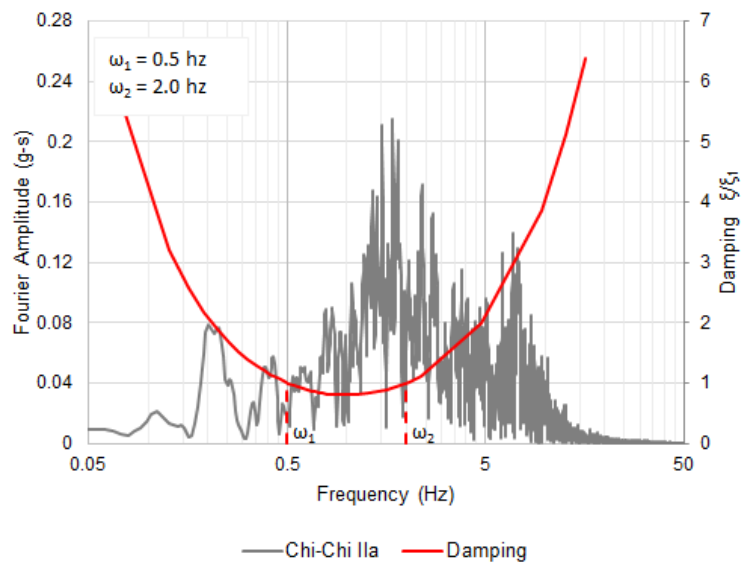


Figure 46. Fourier transform of Chi-Chi Ila signal and Rayleigh damping

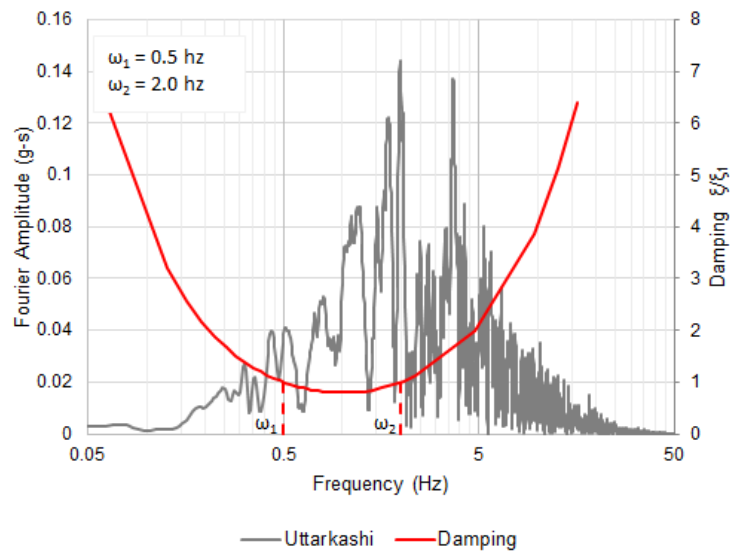


Figure 47. Fourier transform of Uttarkashi signal and Rayleigh damping

5.5. BIDIMENSIONAL (2D) MODEL

Due to the complexity of the three-dimensional dynamic model, a bi-dimensional numerical model was developed first using the dam's maximum section. The objective of this model is to investigate the seismic behavior of the dam for the three seismic signals that produced the highest displacement in the Makdisi and Seed technique (Makdisi, 1979); Uttarkashi-Ghatwari, Chi-Chi Ila and Chamoli (see Table 13), and to select the critical seismic signal for the three-dimensional analysis.

Table 13. Maximum permanent displacement in the Makdisi & Seed analysis. Document No: 0390801-INF-BB-LT3.2-0001
 - Static & Dynamic Stability and seismic induced deformations of the CFRD Dam - Report

SEISMIC SIGNAL	U_{\max} (cm)	SEISMIC SIGNAL	U_{\max} (cm)
CHAMOLI	60,4	TABAS_DAYHOOK (1997)	0,0
CHI-CHIILA067	19,2	LOMAPRIETA_SANTACRUZ (1985)	0,0
UTTARKASHI_GHATWARI (2005)	1,2	CAPEMEND_SHL090	0,0
ROORKEE	1,0	TOKACHI_HKD113	0,0
CHI-CHITCU088 (2007)	0,0		

The finite element mesh of 1627 elements and 1730 nodes is shown in Figure 48. As depicted in the figure, the alluvial deposit of this model was divided into the same five layers, but the bedrock layer was not included because the absorbent

boundaries are applied in the aluvial sides. On the bottom of the model, pinned boundary conditions were included to constraint the displacements.

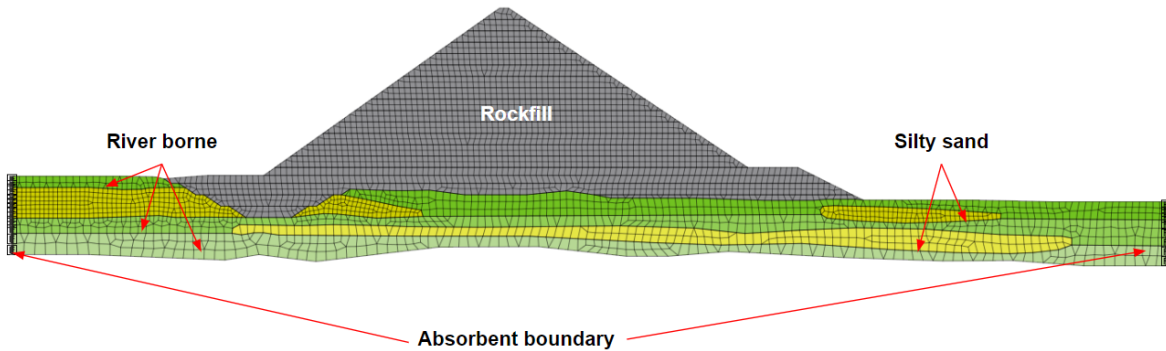


Figure 48. Finite element mesh used in the analyses.

In order to represent correctly the initial stress-strain conditions are required as a first step to model the construction process. The construction process was modeled by activating the rockfill material in a horizontal pattern sequence of 10 m thick layers, and the simulation of the reservoir impoundment through a hydrostatic pressure on the upstream slope. Figure 49 presents the construction settlements, showing a maximum vertical displacement in the middle of the dam of 1,66 m.

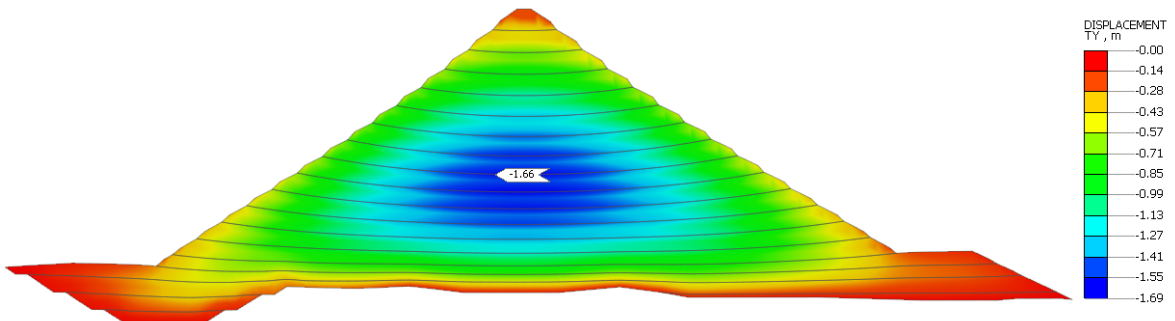


Figure 49. Construction settlement - Bidimensional dynamic model.

In addition to the hydrostatic pressure, the hydrodynamic effect of the reservoir was considered through the Westergaard added mass technique (Westergaard, 1931). This method uses a parabolic approximation for the additional pressure due to earthquake motion. Because the hydrodynamic forces act in both directions, this pressure is regarded as an added mass.

In this numerical model the Generalized Westergaard formulation proposed by Zangar (Bureau of Reclamation, 2011) was used, which takes into account the hydrodynamic pressure on inclined faces.

5.5.1. Rockfill damping calibration

In order to select the appropriate damping ratio for the rockfill material a sensitivity analysis was developed by using the Chamoli seismic input motion and assessing the dam behavior for different rockfill damping ratios.

On the basis of the results of each dynamic analysis, it was verified if the 65% of the maximum cyclic shear strain ($0,65\gamma_{max}$) in most elements of the central zone of the dam were close to the cyclic shear strain associated to the damping ratio of the analysis, according to the reference rockfill damping ratio curve.

Figure 50 shows the results of the sensitive analysis for a damping ratio of 8% and 12%. As shown in this Figure, the reference cyclic shear strain for a damping ratio of 12% is close to the cyclic shear strain from the dynamic analysis results. Consequently, and given the fact that the strains in the three-dimensional model will be lower, a damping ratio of 12% was used to adequately represent the damping in the numerical model.

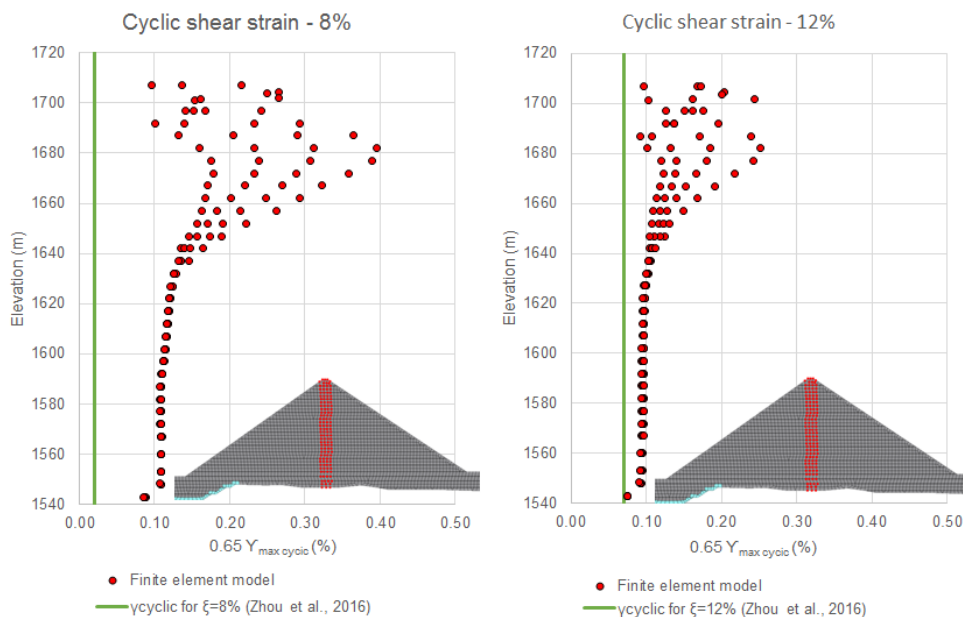


Figure 50. Rockfill damping ratio - Sensitive analysis.

5.5.2. Accelerations

Figure 51 plots the acceleration history for the Chamoli record at the dam crest and the dam bottom in the mid-section. As shown in this Figure the peak acceleration at the crest is $3,38 \text{ m/s}^2$, which corresponds to an amplification factor of 1,20.

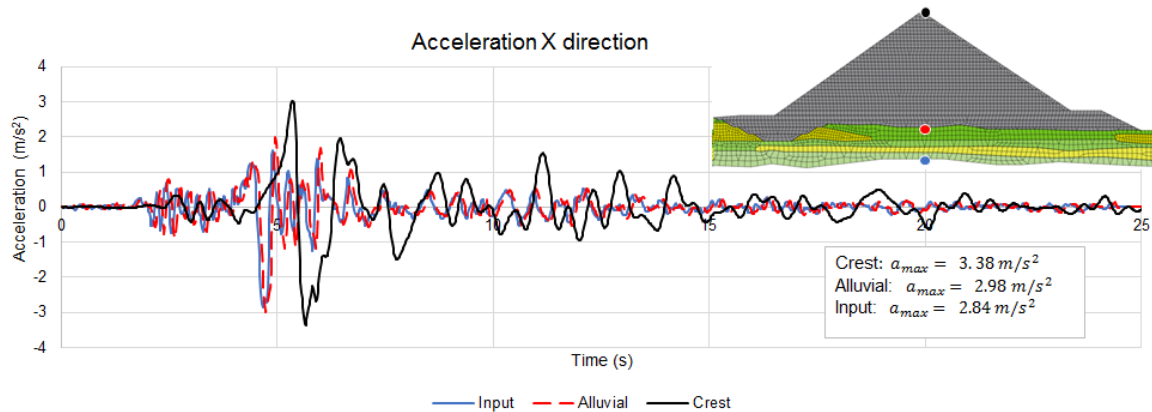


Figure 51. Acceleration time history Chamoli input motion, 2D model

The dam crest and dam bottom acceleration time histories for the Chi-Chi Ila input motion are given in Figure 52. The amplification factor for this record is around 1,13, with a peak acceleration at the crest of $3.25 m/s^2$.

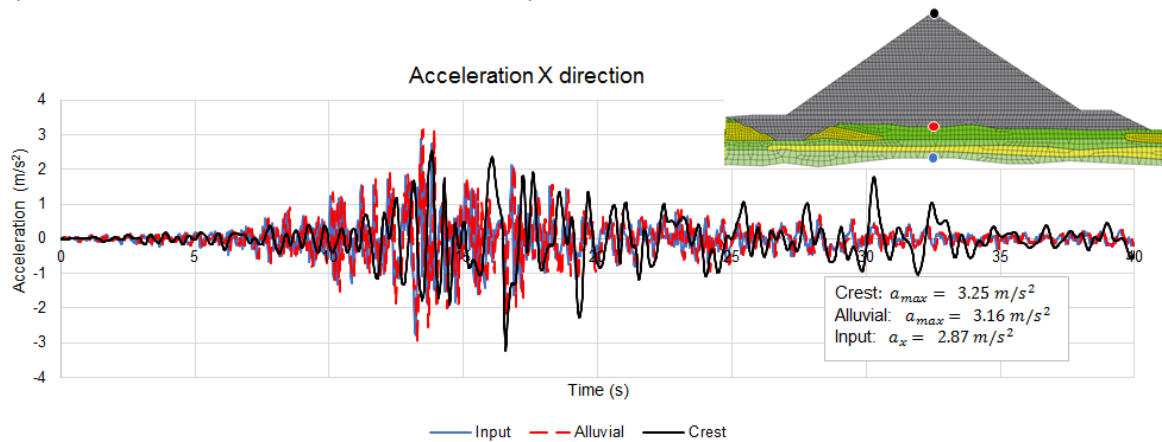


Figure 52. Acceleration time history Chi-Chi Ila input motion, 2D model

The amplification factor at the crest for the Uttarkashi input motion is 1,3, which is in the same order of magnitude as the amplification factor for the other records. Figure 55 shows the acceleration history for this seismic signal at the dam crest and the dam bottom in the mid-section.

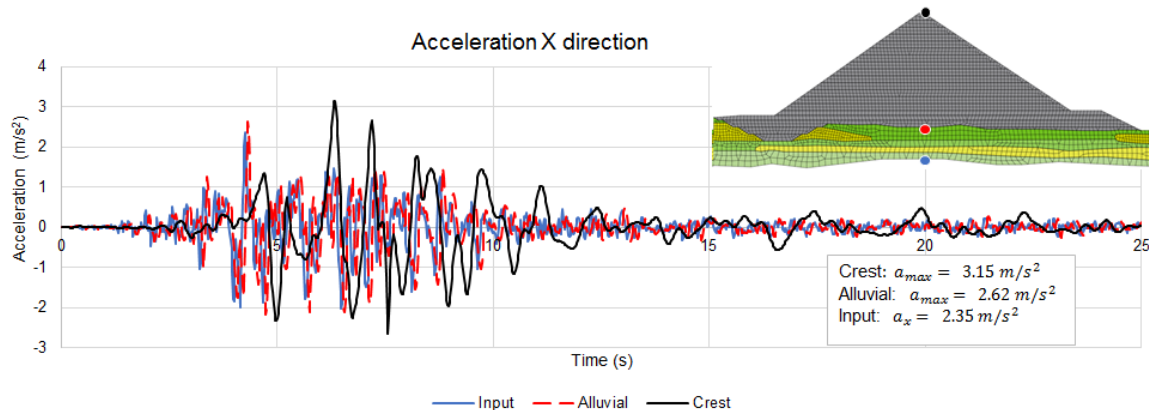


Figure 53. Acceleration time history Uttarkashi input motion, 2D model



Although the IT Roorkee input motion produces a displacement of only 1,0 cm using the Makdisi and Seed technique. This signal was analyzed, in order to have a comparison with the input approved by the National Committee on seismic design parameter (NCSDP). Figure 54 shows the acceleration time history for the IT Roorkee, as depicted in this figure, the amplification factor at the crest is 1,19, which is in the same order of magnitude of the other three signals analyzed.

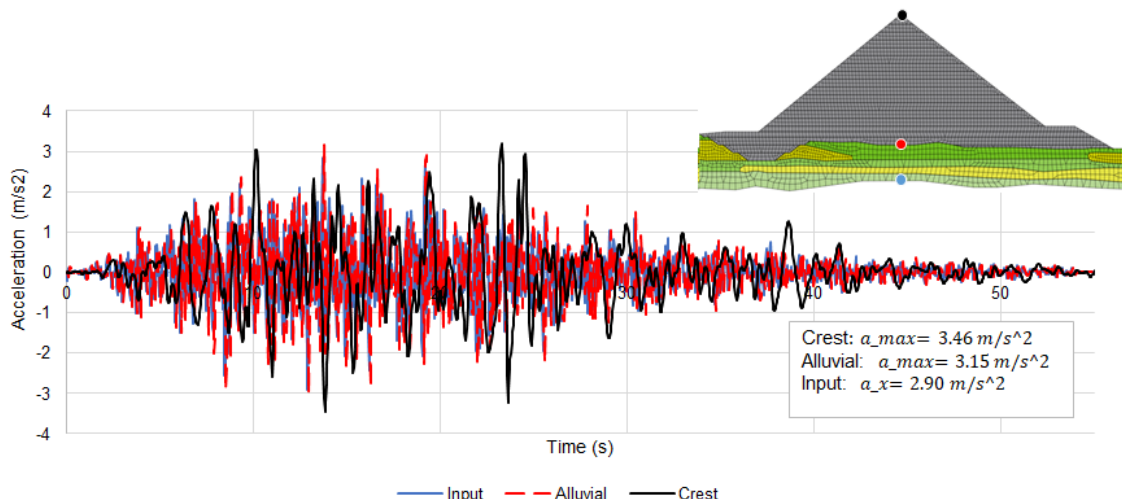


Figure 54. Acceleration time history IT Roorkee input motion - 2D model

5.5.3. Permanent deformation due to earthquake

Figure 55 shows the total displacement at the end of the dynamic analysis for the three input records considered. As depicted in this Figure the total displacement including construction, impoundment and seismic deformation at the crest is in the 0,7 m to 0,9 m range.

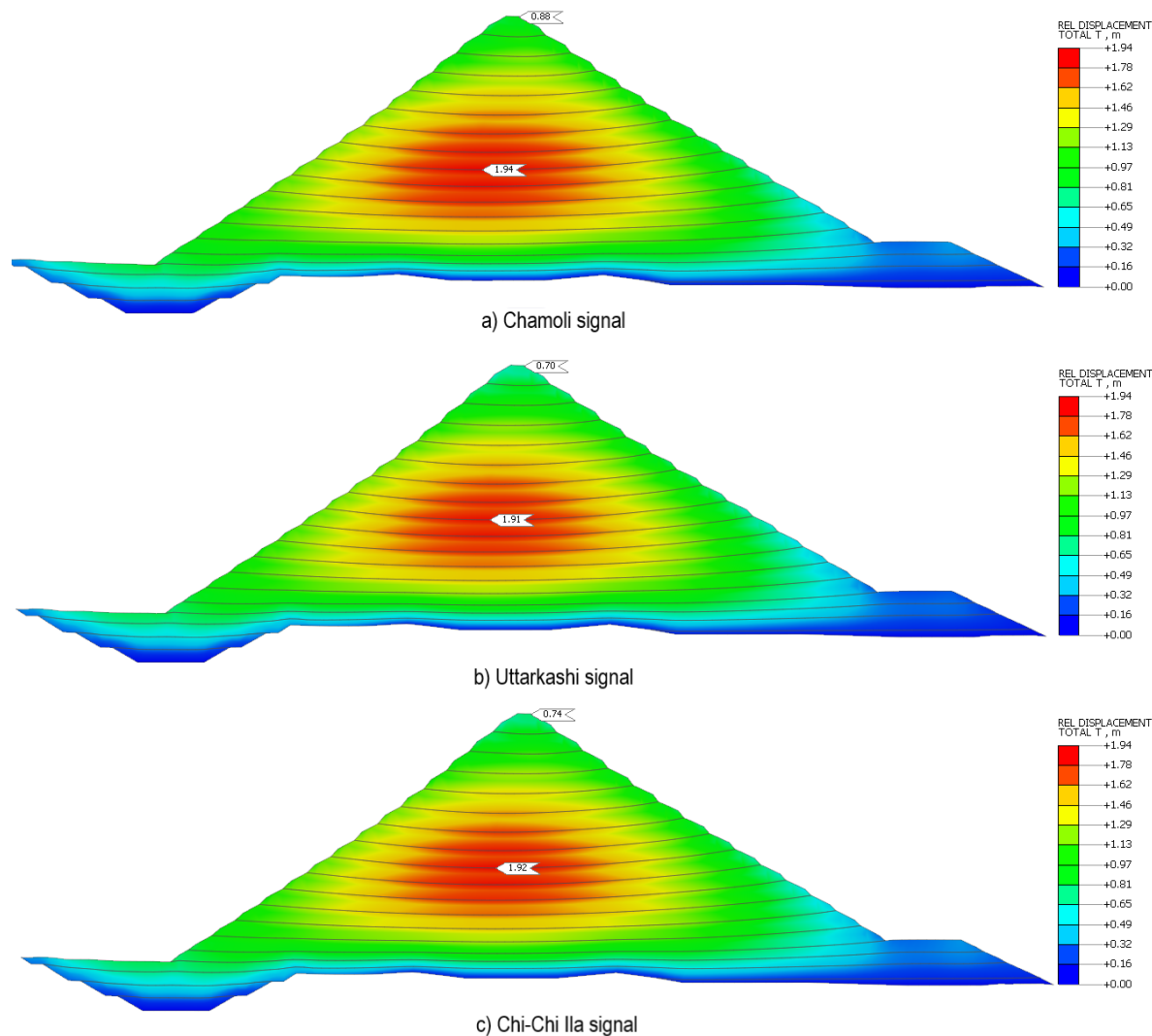


Figure 55. Total displacement at the end of the dynamic analysis, 2D analysis.

In order to evaluate the deformation only during the earthquake event, the crest displacement time histories for the Chamoli, Chi-Chi Ila and Uttarkashi seismic signals are presented in Figure 56, Figure 57 and Figure 58, respectively.

The crest settlement due to earthquake in these results varies between 33 cm and 49 cm, while the total seismic displacement is in the 39 cm to 62 cm range, presenting the highest displacement for the Chamoli record. This is explained by the fact that this seismic signal has a frequency content closer to the dam's natural frequency.

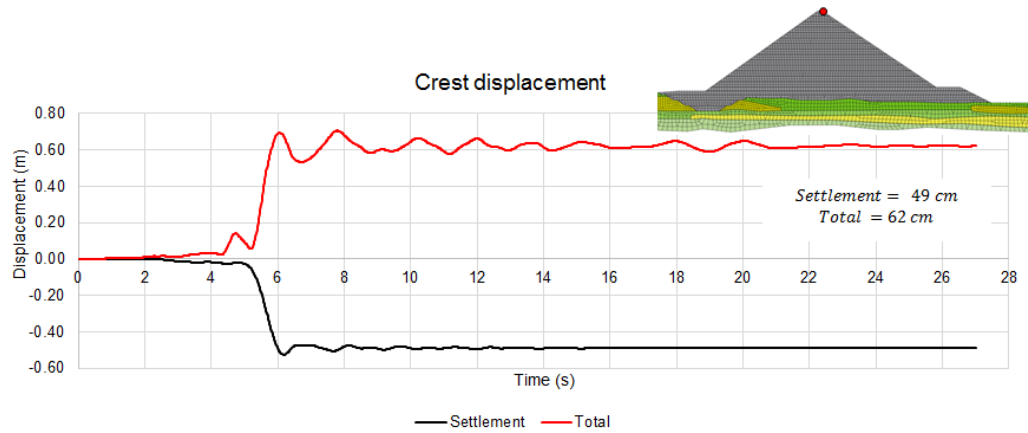


Figure 56. Crest displacement time history Chamoli input motion, 2D model

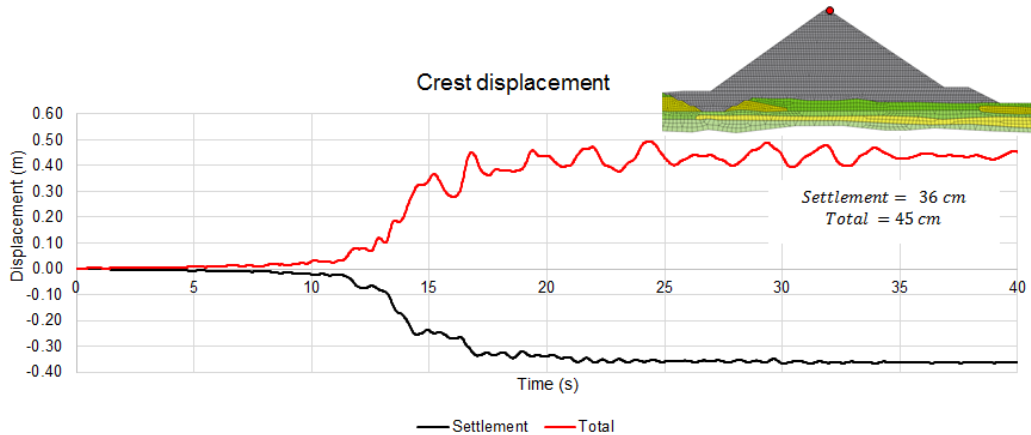


Figure 57. Crest displacement time history Chi-Chi Ila input motion, 2D model

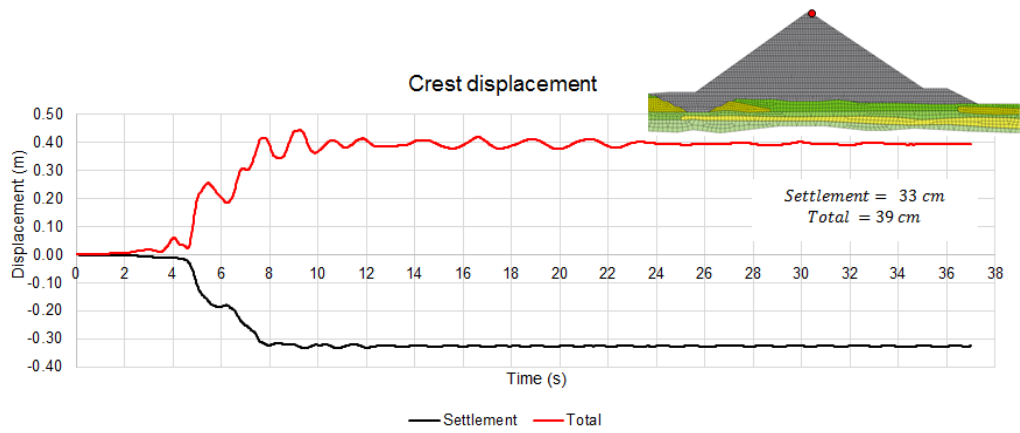


Figure 58. Crest displacement time history Uttarkashi input motion, 2D model



By way of comparison, the crest displacement time history for the IT Roorkee input motion is presented in Figure 59. The crest settlement due to the earthquake of this seismic signal is 55 cm, while the total displacement is 70 cm. These values are slightly higher than the deformation estimated with the Chamoli signal, which is a result of the high frequency content and the long duration of this signal that means more total cycles.

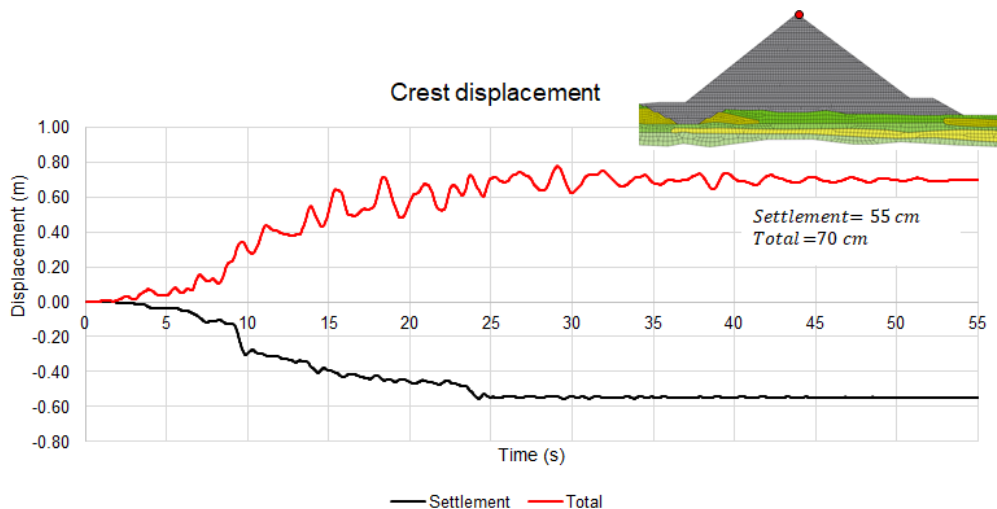


Figure 59. Crest displacement time history IT Roorkee input motion - 2D model

The results of the dynamic model for the synthetic IT Roorkee signal are less representative of the possible movements that the Pakal Dul Dam can experience under the design earthquake than those of Chamoli, Chi-Chi Ila, or Uttarkashi. This is because the strong motion duration of this signal is almost twice that estimated with the relationship developed by Theofanopoulos & Watabe (1989) using the magnitude and the distance-to-site of the Maximum Credible Earthquake (8.0 magnitude and an epicentral distance of 15 km) and because this synthetic signal has a high frequency content that is not in agreement with real records for the same conditions.

5.5.4. Dynamic stability from two dimensional analysis

Based on the dynamic simulations there is no evidence of dynamic instability, such as significant permanent displacement on the downstream slope or deformation time history curves with continuous increasing trend during the dynamic action. Therefore, it can be concluded that the bidimensional numerical model of the Pakal Dul dam presents a factor of safety greater than 1,0 for the designed earthquake.

In order to quantify the safety factor under dynamic condition, the Dynamic Strength Reduction Method was applied (Xinrong Liu, 2017; Zhang H., 2018). This method is based on the principle of the static strength reduction method and consists of the following basic ideas: 1) Reduce the shear strength parameter c' and $\tan(\phi)$ into $c'/$ SRF and $\tan(\phi)/$ SRF. 2) Perform a dynamic analysis including the construction processes and impoundment. 3) Judge whether the dam is in the critical state according to the instability criteria. 4) When the dam reaches the limit equilibrium state under a certain Strength Reduction Factor (SRF), the value of SRF represents the safety factor under dynamic condition.

The key point in this method is to assess the possibility of instabilities on the dam body. Under static conditions, the instability state is mainly defined by means of the convergence criteria, which cannot be applied in this case, because

there is no concept of convergence for the dynamic analysis. Therefore, the dam deformation characteristics are used as the basis for a judging criterion in the dynamic stability.

Two instability criteria were adopted. 1) The mutation of the seismic permanent displacement of a feature point, e.g. the dam's crest, which can be seen establishing the relation between the seismic permanent displacement and the strength reduction factor. 2) Crest displacements higher than 1,0 m, are not considered admissible due to the loss of freeboard.

Figure 60 shows the displacement on the upstream-downstream direction of the Chamoli signal for different Strength Reduction Factors (SRF). As shown in these contour plots, there is a progressive growth in the displacements at the downstream slope with the SRF, and an important change in the deformation between a SRF of 1,4 and 1,5.

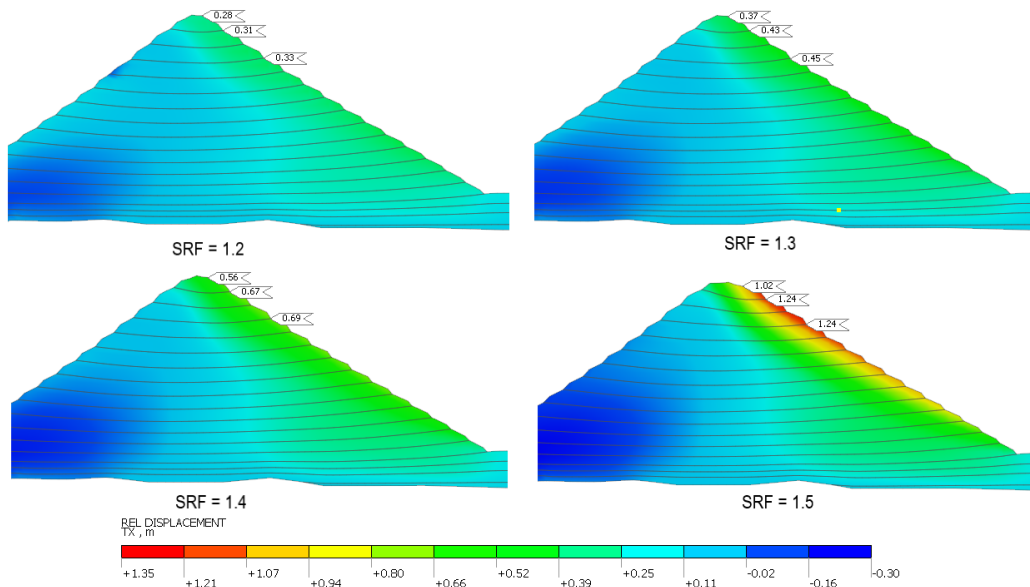


Figure 60. Displacement (upstream-downstream direction) for different Strength Reduction factors (SRF).

Intending to quantify the factor of safety under dynamic condition, the evolution of the seismic permanent deformation at the crest with the SRF was plotted in Figure 61. From these results and the stability criteria adopted, it can be estimated that the factor of safety of the Pakal Dul CFRD for the maximum credible earthquake is around 1,3, which complies with the recommendations of ICOLD (2004) and the Bureau of Indian Standards (1975).

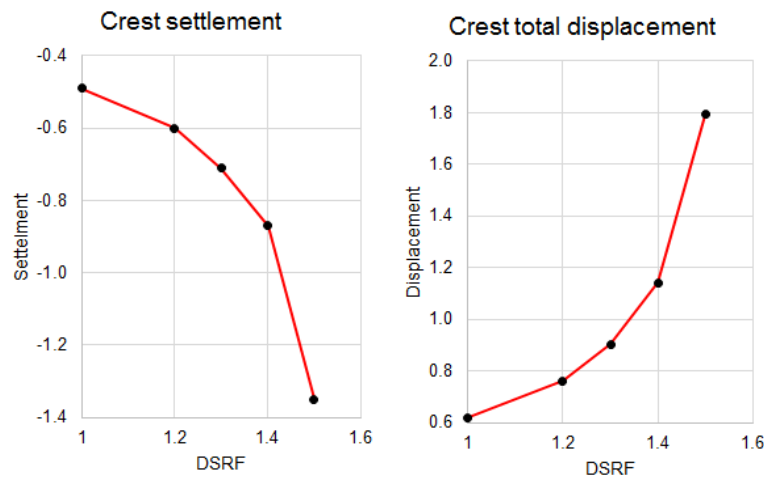


Figure 61. Evolution of the crest displacement with the Shear Strength Reduction (SRF) - 2D model

The method used to quantify the safety factor under dynamic condition provides more accurate results than other methods, such as the pseudo-static method, which does not consider the effect in the frequency content of the signal, or the dynamic time-history method, in which the safety factor is defined as the ratio of shear force and shear stress at any point in time, when the system is not necessarily in the limit equilibrium state, being inconsistent with the premise of a limit equilibrium analysis.

5.6. THREE-DIMENSIONAL (3D) MODEL

The dynamic three-dimensional analysis of the Pakal Dul CFRD was performed based on the calibrated parameters from the bidimensional model, and the geometry and finite element mesh described on Section 3.1. This model included the same features of the bidimensional model, such as the simulation of the construction process, the hydrostatic pressure in the impoundment step, and the hydrodynamic effect of the reservoir through the added mass technique.

Figure 62 shows the settlement at the end of the construction process. In contrast with the bidimensional results, the maximum construction settlement is 1,3 m. With this value and the vertical effective stress in that point, the estimated construction moduli is around 90 MPa, which is in the range of construction moduli expected for the materials and compaction and gradation standards to be implemented in Pakal Dul CFRD.

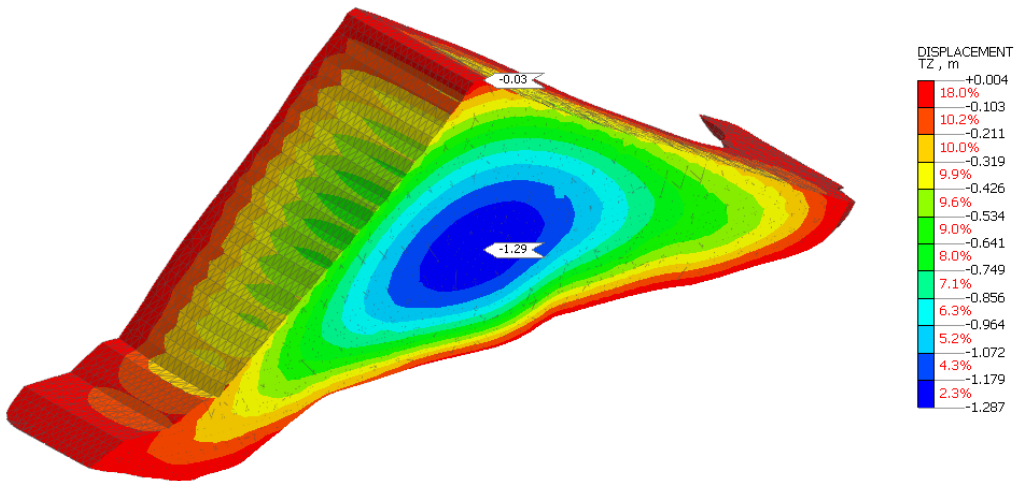


Figure 62. Construction settlement - 3D Dynamic model.

Because the higher displacements on the bidimensional model were obtained for the Chamoli seismic input motion. This record was considered as the critical input motion on the three-dimensional analysis.

5.6.1. Acceleration

Figure 63 shows the acceleration time history of the Chamoli record at the alluvial bottom and dam bottom. As depicted in this Figure, there is a small amplification of the signal through the bedrock that can be considered negligible. On the other hand, the peak acceleration at the dam bottom is 4.02 m/s^2 .

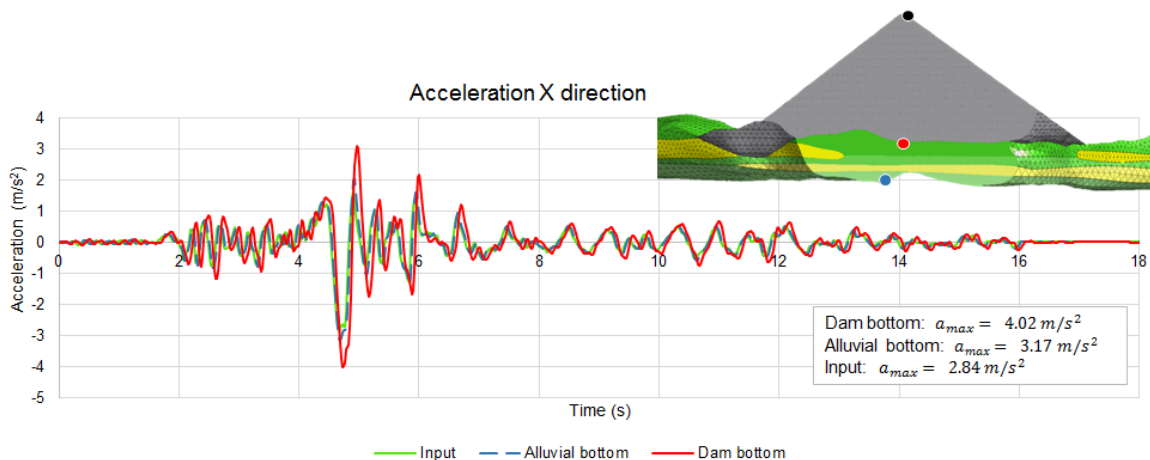


Figure 63. Acceleration time history Chamoli input motion - Rock and alluvial deposit - 3D model

The acceleration time history at the dam crest for this seismic signal is presented in Figure 64. The peak acceleration at the crest is 4.22 m/s^2 , which corresponds to an amplification factor of 1.5. The difference in the amplification factor between the bidimensional and three-dimensional model is attributed to the wave focusing effect associated with the

narrow canyon of the Pakal Dul CFRD and the difference of fundamental periods between for the 3D dam geometry and the maximum dam section.

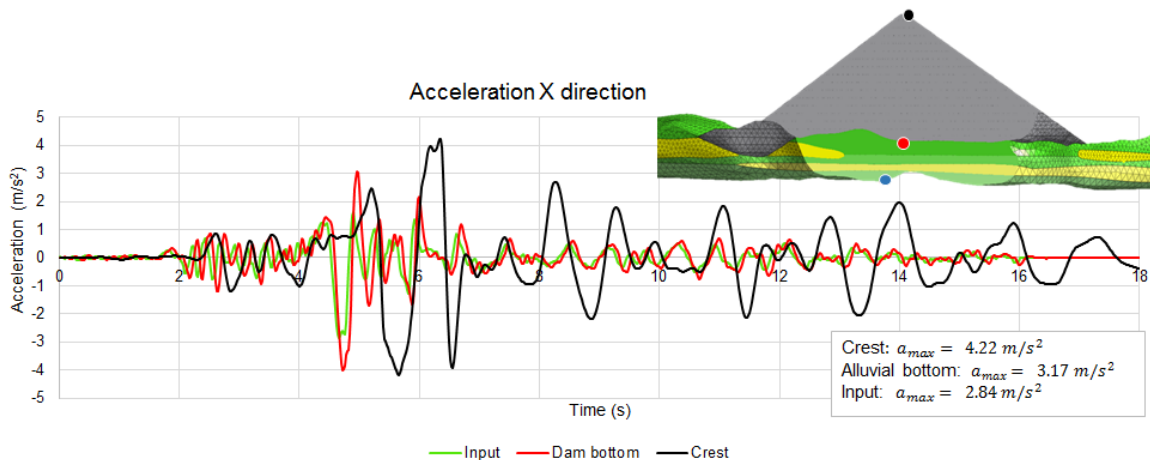


Figure 64. Acceleration time history Chamoli input motion - Dam crest - 3D mode

Unlike the bidimensional results, the acceleration at the crest in the three-dimensional analysis presents higher acceleration peaks after 8 seconds. This behavior is associated with the amplification of the low amplitude peaks found after 8 seconds, which have frequency content similar to the dam's natural frequency. In the bidimensional model, there is no amplification at this point, because the plane strain condition changes the dam's natural frequency to a lower value.



To compare with the results of the Chamoli signal, the acceleration time history of the IT Roorkee record at the dam bottom and the dam crest are depicted in Figure 65. The amplification factor for this input motion is 1,70, with a maximum acceleration value of 5.00 m/s^2 . Similarly, the crest acceleration for this input motion is higher in the 3D model than the bidimensional model, because the dam's natural frequency in the 3D condition is closer to the signal predominant frequency.

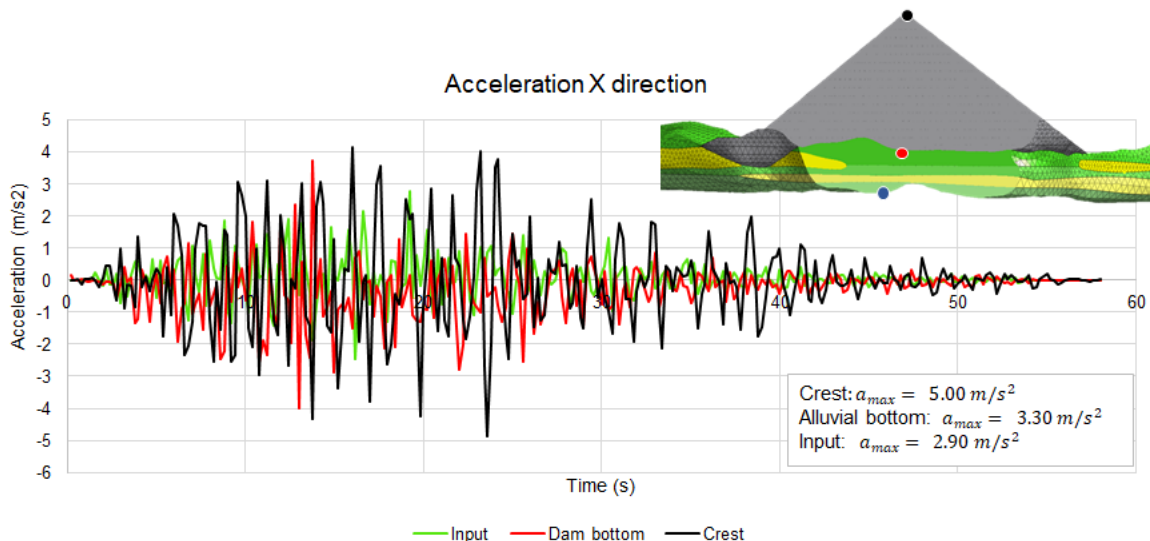


Figure 65. Acceleration time history IT Roorkee input motion - Dam crest - 3D model

5.6.2. Permanent deformation due to earthquake

Figure 66 shows the total displacement at the end of the dynamic analysis for the Chamoli record. As shown in this figure the maximum total displacement including construction, impoundment and seismic deformation at the crest is 0,85 m. This displacement is slightly lower than the displacement predicted on the bidimensional model, which is explained by lower displacements during the construction steps and impoundment, due to the arching effect produced in the abutments., however, the difference is considered not significant.

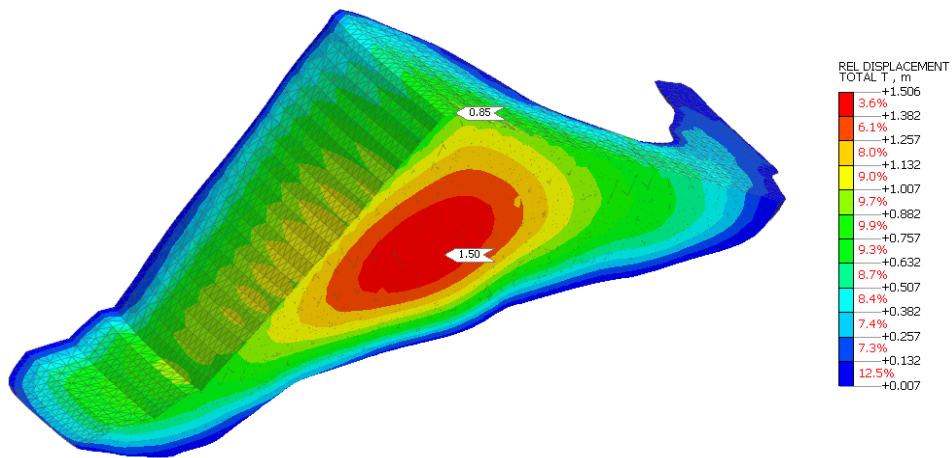


Figure 66. Total displacement at the end of the seismic analysis Chamoli signal - 3D model

As shown in Figure 66, the displacement along the crest varies considerably between the abutments and the mid-section. In order to see this behavior more clearly, the permanent settlement along the crest is presented in Figure 33, where it is observed that the settlement varies between a negligible value in the abutments to a maximum value of 50 cm.

It can be seen that the maximum vertical displacement is not in the maximum section and the settlement along the crest depends considerably on the abutment morphology, highlighting the importance of taking into account the abutment real geometry as considered in this model.

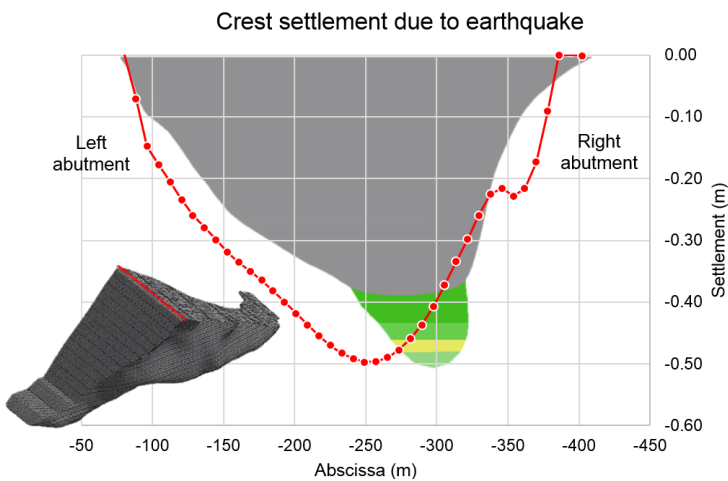


Figure 67. Permanent crest settlement at the end of the seismic analysis.

The seismic displacement time history for the crest point with maximum displacement is presented in Figure 68. As shown in this figure the permanent seismic settlement for the Chamoli record is 50 cm, while the permanent seismic total displacement is 69 cm. These values are slightly higher than predicted in the bidimensional model, which is due to the higher acceleration values obtained in the three-dimensional model.



Figure 68. Crest displacement time history Chamoli signal - 3D model



Figure 69 shows the seismic displacement time history at the point of maximum displacement in the crest for the IT Roorkee input motion that serves as a comparison with the previous result. The permanent seismic settlement for this record is 64 cm, which is almost 30% more settlement than the value estimated with the Chamoli signal. However, the total displacement estimated with this synthetic signal is practically the same value obtained with the Chamoli seismic signal, which indicates that the Chamoli motion produces a higher displacement in the downstream direction and therefore the Pakal Dul Dam is more prone to dynamic instability with this record.

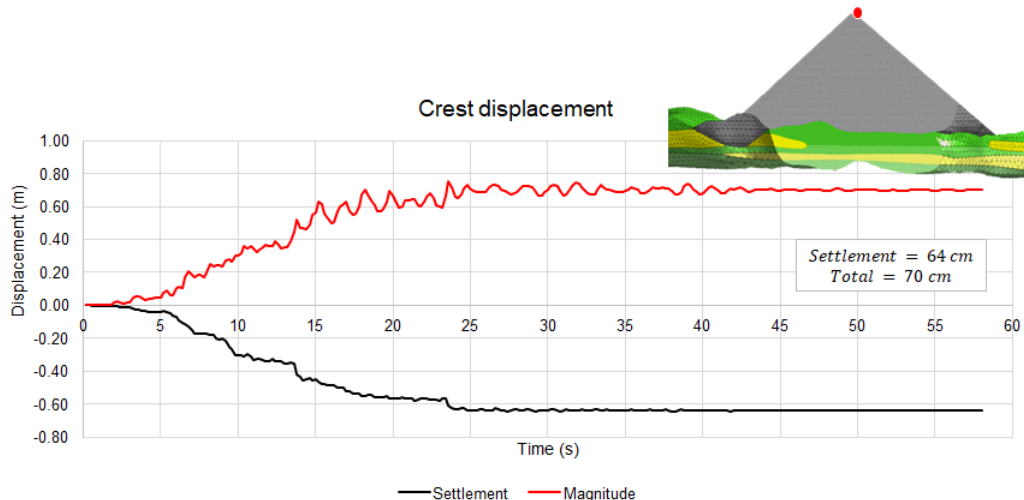


Figure 69. Crest displacement time history IT Roorkee signal - 3D model

In conclusion, based on the results of the bidimensional and three-dimensional model, it is expected that the Pakal Dul dam undergoes seismic permanent settlement between 50 and 64 cm and seismic permanent total displacement of approximately 70 cm.

These values are in agreement with the estimated displacement using the Makdisi (Makdisi, 1979) and Seed technique (40 cm to 60 cm), the Earthquake Severity index (64 cm) and the Swaisgood Methodology (39 cm), presented in the Static & Dynamic Stability and Seismic Induced Deformations of the CFRD Dam Report (INGETEC, 2020). Moreover, recent evidence of similar rockfill dams subject to strong ground shaking indicates similar displacements. For instance, Zipingpu dam experienced about 0.74 m of crest settlement during the 2008 earthquake (Wieland M., 2010).

5.6.3. Dynamic stability from three dimensional analysis

As with the bidimensional results, the results of the three-dimensional model for the Chamoli signal does not show evidence of dynamic instability. Besides, the three-dimensional configuration is found to be more stable, due to the change in direction of the Marasudar river and the arching effect produced by the narrow canyon.

Despite this, the dynamic stability of the three-dimensional model was checked using the Dynamic Strength Reduction Method and the same instability criteria as defined in Section 3.5.4.

Figure 70 shows the displacement on the upstream-downstream direction for the Chamoli signal and different Strength Reduction Factors (SRF). As shown in this Figure, there is an increasing trend for the downstream slope displacement as a function of the SRF.

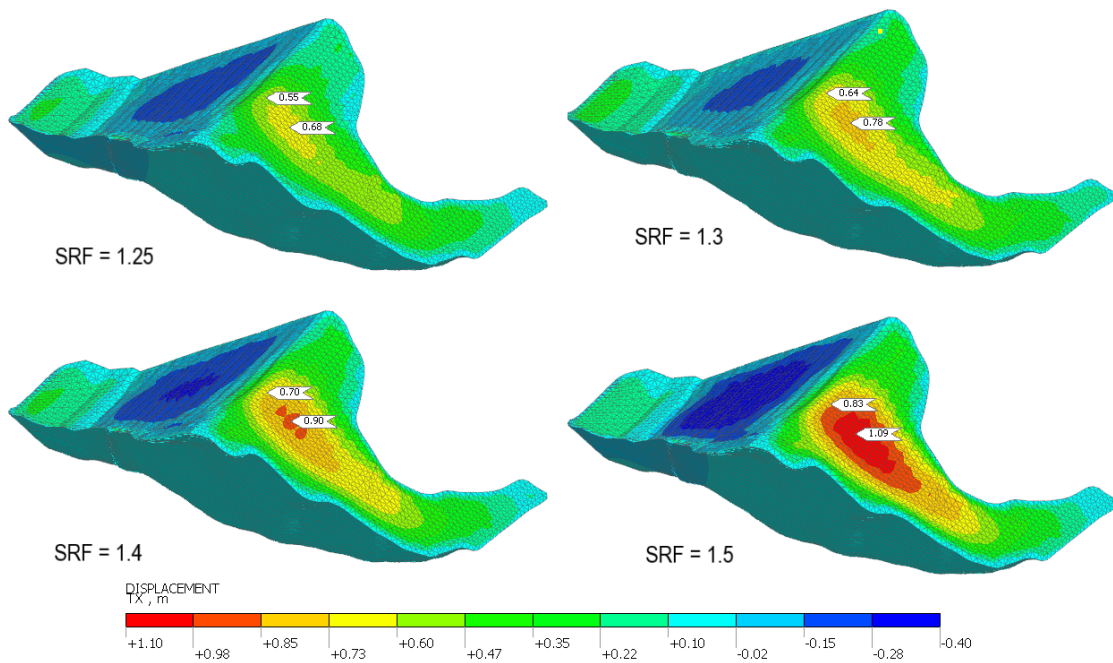


Figure 70. Displacement (upstream-downstream direction) for different SRF - 3D model

In order to quantify the factor of safety under dynamic condition, the evolution of the seismic permanent deformation for the two points shown in Figure 71 was analyzed. Even though the displacement curves present a behavior relatively close to a linear approximation, a factor of safety of around 1.3 is defined, based on the criterion of crest displacements higher than 1.0 m.

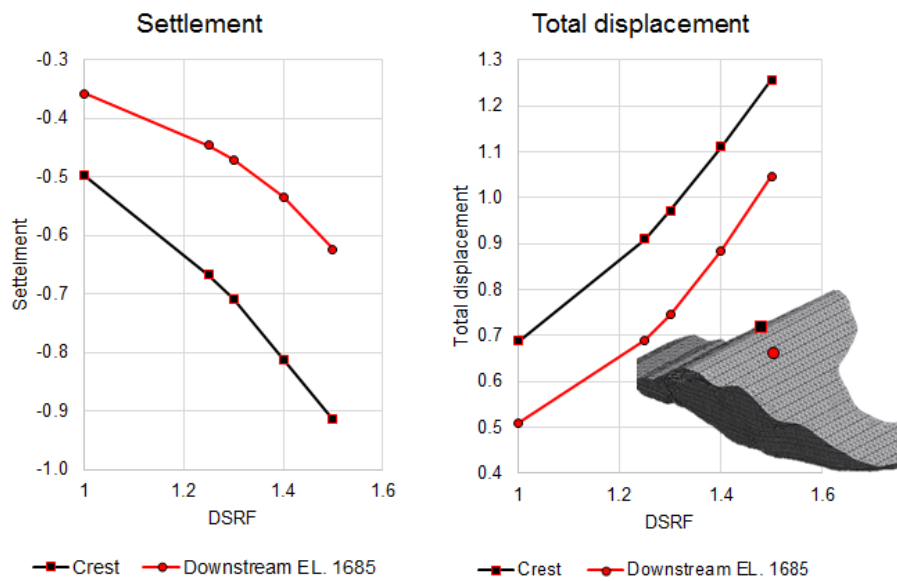


Figure 71. Evolution of the displacement in the crest and the downstream slope with the SRF - 3D model

The trend of the displacement curve shown in Figure 71 supports the hypothesis that the three-dimensional geometry of the Pakal Dul dam should have equal or larger factor of safety than the 2D analyses, due to the use of the critical cross section of the dam for 2D analyses.

Based on the 2D and 3D finite element dynamic analysis results is expected that Pakal Dul CFRD will have an adequate behavior under strong motions shaking (i.e. MCE seismic design scenario) as it complies with the stability criteria defined by ICOLD (2004) and the Bureau of Indian Standards (1975).

6. CONCLUSIONS

6.1. STATIC FINITE ELEMENT ANALYSIS

- Parameter calibration based on laboratory test results provided by CVPP resulted in a static numerical model that can be characterized by a 70 MPa construction moduli which is acceptable for the construction of Zone 3C. However, a stiffer material is recommended for construction of Zone 3B, where around 120 MPa is desirable in order to limit deformation of the face slab.
- Numerical analyses results have shown that in order to improve the overall behavior of the dam, in particular, the concrete face and the articulated plinth, is strongly recommended that the projected excavation at the upstream zone of the dam be filled with a material comprised mainly of gravel which due to its stiffness limit deformations at the concrete face-articulated plinth connection and the possibility that concrete face displacements induce loads in the upper part of the cutoff wall. The articulated plinth includes three joints in the dam axis direction in order to accommodate the displacements that occur at the upstream dam toe. Recommendations regarding the fill of this excavation will be provided in an updated version of the dam zoning report.
- Based on the numerical analyses results, a maximum settlement of the dam is expected to be between 1,0 m to 1,5 m is estimated (1,5 m corresponding to the 70 MPa numerical simulation for Zone 3C and 120 MPa for Zone 3B). This maximum settlement should occur at a middle depth of the maximum height of Zone C. Settlement patterns are influenced by dam zoning, in particular the distribution of Zones 3B and 3C throughout the dam body.
- Maximum concrete face displacements (normal to the concrete slab plan) are estimated to be close to 45 cm. An important effect of the alluvial material and rockfill material due to excavation at the upstream toe have been identified for both the concrete slab and perimeter joint between the concrete slab and the articulated plinth connection. This effect has been assessed in the numerical modeling.
- Perimeter joint displacements between 10 to 20 mm have been estimated. In order to achieve these values is strongly required to provide the high stiffness of the upstream excavation fill during the test embankment. Based on the obtained results, test embankment results will constitute a crucial input to validate or adjust the specification for the dam body fills. The 200 MPa construction modulus that was used to model the behaviour of the fill for the excavation projected at the upstream zone of the CFRD is considered to be a representative and achievable parameter if recommendations regarding gradation (mainly gravels) and construction processes are followed. It should be highlighted that the test embankment results are paramount to assure adequate compaction, strength and stiffness of all the materials that comprise the CFRD body in particular zones 3B and 3C, and the fill projected at the upstream zone of the CFRD.
- Strain patterns for the impoundment scenario with the reservoir at 1700 m.a.s.l. have been estimated, and the values obtained are the inputs for the structural design of the concrete face and reinforcement steel. Maximum strains have been identified in the lower third of the concrete face, where appropriate reinforcement will be designated in order to limit cracking to below 0,3 mm. Steel reinforcement design is presented in the Report 0390801-INF-SS-LT3.2-0001 *Structural Design of Concrete Face, Plinth and Parapet Wall* (INGETEC, 2020).
- Individual internal joints between slabs of the face slab have been identified as being primarily opening or closing, serving to inform the structural joint design.

6.2. DYNAMIC FINITE ELEMENT ANALYSIS

- The behavior of the rockfill material was captured with the Modified Mohr-Coulomb (MMC) model, also known as the Hardening Soil model. In contrast with the Drucker Prager/Cap model used in static analysis, the MMC model includes different loading/unloading moduli and therefore it is more suitable for handling the irreversible cyclic deformations expected during a seismic event.
- In comparison with classic dynamic models that use nonlinear hysteretic models or hypoelastic models, this numerical model can reproduce permanent seismic deformation more accurately, by the adoption of an elastoplastic model with hardening and stress-dependent stiffness modulus. This feature plays a central role in a dynamic finite element analysis, because it is well known that a strong ground shaking can induce dynamic deformations on rockfill dams, due to rockfill compaction.
- The three-dimensional results of the Chamoli signal show a peak acceleration at the crest of $4,22 \text{ m/s}^2$, which corresponds to an amplification factor of close to 1,5. This amplification is attributed to the amplification through the alluvial deposit and the wave focussing effect associated with the narrow canyon of the Pakal Dul dam. According to Jansen's unpublished plot, titled "Measured ratios (amplification) of crest and base acceleration at embankments dams in response to earthquakes", the obtained amplification factor is in agreement with the measured acceleration at other dams for the same peak ground acceleration.
- Based on the results of the finite element model, it is expected that the Pakal Dul dam undergoes seismic permanent settlement between 50 and 64 cm and seismic permanent total displacement of approximately 70 cm. These values are in line with the estimated displacement using the Makdisi and Seed technique, the Earthquake Severity index, the Swaisgood Methodology, and the recent evidence of similar rockfill dams subject to strong ground shaking.
- Although the finite element analysis showed considerable seismic permanent displacement, there was no evidence of dynamic instability, such as significant permanent displacement on the downstream slope or deformation time history curves with continuous growth trend during the dynamic action. Besides, the three-dimensional configuration was found more stable, due to the change in direction of the Marasudar river and the arching effect produced by the narrow canyon.
- A factor of safety under dynamic condition of around 1,3 was estimated for the Pakal Dul dam, based on the results of the Dynamic Strength Reduction Method and considering crest displacement higher than 1,0 m as inadmissible due to the loss of freeboard. Therefore, it can be concluded that the Pakal Dul dam for the operation condition under the defined maximum credible earthquake is stable and it complies with the stability criteria defined by ICOLD (2004) and the Bureau of Indian Standards (1975).





7. REFERENCES

- Advanced Technology and Engineering Services. (2004). Laboratory tests conducted on rock samples from Pakal Dul Hydroelectric Project (J and K).
- Advanced Technology and Engineering Services. (2008). Laboratory tests conducted on rock samples from Pakal Dul Hydroelectric Project (J and K).
- Bureau of Reclamation (2011). Seismic induced load on Spillway Gates Phase I - Literature review. Report DSO-11-06.
- Central Soil and Material Research Station (2019). Report on large size triaxial shear test on blasted rockfill material DDR04 quarry from Pakal Dul H.E. Project, Kishtwar, J&K. Report No. 04/RF/RSD/CSMRS/E/08/2019.
- Darendeli, M. B. (2001). Development of a New Family of Normalized Modulus Reduction and Material Damping Curves, Department of Civil, Architectural and Environmental Engineering, The University of Texas, Austin, Texas.
- Federation Internationale du Beton. (2010). Fib Model Code for Concrete Structures.
- Fell, R., MacGregor P., Sapledon D., Bell G. (2005). Geotechnical Engineering of Dams. Taylor & Francis Group.
- Hashash, Y. (2016). DEEPSOIL 6.1, User Manual.
- Honkanadavar N.P., S. K. (2016). Modeling the triaxial behavior of riverbed and blasted quarried rockfill materials using hardening soil model. Journal of Rock Mechanics and Geotechnical Engineering.
- Hunter, G., and Fell, R. (2002). The deformation behavior of rockfill. The University of New South Wales, School of Civil and Environmental Engineering.
- ICOLD, (2004). Concrete Face Rockfill Dams – Concepts for Design and Construction. Committee on Materials for Fill Dams.
- ICOLD (2010). Concrete Face Rockfill Dams. Bulletin 141. Commission Internationale des Grands Barrages. Paris.
- INGETEC (2019). Design Criteria. Rev.1. Pakal Dul, CFRD Design Consultancy
- INGETEC (2020). Geotechnical parameters of the dam. Pakal Dul, CFRD Design Consultancy.
- INGETEC (2020). Static & Dynamic stability and seismic induced deformation of the CFRD dam. Pakal Dul, CFRD Design Consultancy
- INGETEC (2020). Structural design of concrete face, plinth and parapet wall, Report 0390801-INF-SS-LT3.2-0001. Pakal Dul, CFRD Design Consultancy.
- Lysmer, J. (1969). Finite Dynamic model for infinite media. Journal of the Engineering Mechanics Division.
- Makdisi, F., and Seed, H. (1979). Simplified procedure for estimating dam and embankment earthquake-induced deformations. Journal of Geotechnical Engineering 104(7): 849–867.

Modares M. and Quiroz J.E. (2015) Structural analysis framework for concrete-faced Rockfill Dams. *Int J Geomech* 16(1):04015024

NHPC Limited (2005). Geophysical investigation involving seismic refraction profiling at the dam site and TRT area along with ultrasonic testing core samples Pakal Dul (Drangdhuran) hydroelectric project (J and K). Geophysical report no. NH/GEOPHY/99.

NHPC Limited (2018). Geophysical seismic refraction and MASW investigation for geotechnical evaluation, Pakal Dul Project, J and K. Geophysical report no. NH/GEOPHY/180.

Oldecop, L. A. (2013). Rockfill mechanics. Advances in Unsaturated Soils, (pág.). London: Taylor & Francis Group.

Rijkswaterstaat Centre for Infrastructure (2017). Guidelines for the Nonlinear Finite Element Analysis of Concrete Structures). Doc.nr.: RTD 1016-1:2017, Version: 2.1. 15 June 2017

Seed, H. B. and Idriss, I. M. (1970). Soil moduli and damping factors for dynamic response analyses. Report No. EERD 70-10, Earthquake Engineering Research Center, University of California, Berkeley, California, 40p

Swaisgood, J. (2003). Embankment dam deformations caused by earthquakes. Pacific Conference on Earthquake Engineering.

Theofanapulus, N.A. and Watabe, M. (1989). A new definition of strong motion duration and comparison with other definitions. *Structural Engineering/Earthquake Engineering*, Vol 6, No. 1.

Weibull W. (1939). A statistical theory of the strength of materials. *Proc. R. Swed. Inst. Eng. Res.*

Westergaard, H. M. (1931). Water Pressures on Dams during Earthquakes. *ASCE Transactions*.

Wieland M. (2010). CFRD's in highly seismic regions. *Water power magazine*.

Xinrong Liu, Y. L. (2017). Numerical analysis of evaluation methods and influencing factors for dynamic stability of bedding rock slope. *Journal of Vibroengineering*.

Zhang H., L. S. (2018). Research on Method of Dynamic Stability Analysis for Slopes of Earth and Rockfill Dam Basing on the P-Z Model. *Tehnicki Vjesnik*.

Zhou X., G. M. (2019). Grain size and time effect on the deformation of rockfill dams: a case study on the Shuibuya CFRD. *Géotechnique*.